1-1-2014

Regulation and Kinase Activity of the Trk Family of Receptor Tyrosine Kinases

Stephen Charles Artim
University of Pennsylvania, sartim@gmail.com

Regulation and Kinase Activity of the Trk Family of Receptor Tyrosine Kinases

Abstract
The tropomyosin-related kinase (Trk) family consists of three receptor tyrosine kinases (RTKs) called TrkA, TrkB, and TrkC. These RTKs are regulated by the neurotrophins, a class of secreted growth factors responsible for the development and function of neurons. Given the high homology between the Trks and their use of overlapping signaling pathways, the key question to be addressed is how the activation of the different Trks can lead to distinct cellular outcomes. To this end, I first sought to determine the mechanism of autoregulation for the Trk tyrosine kinase domain (TKD). The Trk TKDs are members of the insulin receptor kinase (IRK) superfamily and recent data suggest that the IRK family displays a wide array of autoinhibitory mechanisms. To determine where TrkA and the closely related Ror2 TKD (from an unconventional Wnt receptor) lie in this spectrum, we determined the crystal structures of the kinase domains of these RTKs. In both cases, the conformation of the activation loop resembles the IRK activation loop conformation, with subtle but notable differences in the case of Ror2. These findings aid in understanding the range of autoinhibitory mechanisms of the IRK family, in addition to providing a foundation for deciphering consequences of TKD mutations in this family. I also observed crystallographic dimers of the inactive TrkA TKD that resemble those seen for other RTK TKDs - which may aid in understanding the reported pre-formed inactive TrkA dimers observed in cells. To understand the molecular basis for differences in signaling specificity of the Trk receptors, I investigated whether the TrkA and TrkB TKDs differ in their intrinsic kinase activities. I show that the TrkA TKD autophosphorylates itself faster than its TrkB counterpart. However, this difference of autophosphorylation is not due to a difference in kinase activity per se. Rather, my data indicate that the difference in autophosphorylation may arise because of self-association of the TrkA TKD that does not occur with TrkB. My work sheds light on potential differences between TrkA and TrkB signaling, as well as providing a quantitative understanding of Trk TKD activation, which is useful for effective and selective inhibitor design.

Degree Type
Dissertation

Degree Name
Doctor of Philosophy (PhD)

Graduate Group
Biochemistry & Molecular Biophysics

First Advisor
Mark A. Lemmon

Keywords
Autophosphorylation, Kinase structure, Neurotrophin Receptors, Receptor Tyrosine Kinase, TrkA, TrkB

REGULATION AND KINASE ACTIVITY OF THE TRK FAMILY OF RECEPTOR TYROSINE KINASES

Stephen C. Artim

A DISSERTATION

in

Biochemistry and Molecular Biophysics

Presented to the Faculties of the University of Pennsylvania

in

Partial Fulfillment of the Requirements for the

Degree of Doctor of Philosophy

2014

Supervisor of Dissertation

_____

Mark A. Lemmon

Professor and Chair, Department of Biochemistry and Biophysics

Graduate Group Chairperson

_____

Kathryn M. Ferguson, Associate Professor of Physiology

Dissertation Committee

Michael Atchison, Professor of Animal Biology

Ben Garcia, Associate Professor of Biochemistry and Biophysics

Virginia Lee, Professor in Alzheimer's Research in Department of Pathology and Lab Medicine

Ronen Marmorstein, Professor of Biochemistry and Biophysics

David Speicher, Professor and Director in Computational and Systems Biology, The Wistar Institute

Todd Strochlic, Assistant Professor of Biochemistry and Molecular Biology, Drexel University

REGULATION AND KINASE ACTIVITY OF THE TRK FAMILY OF RECEPTOR TYROSINE

KINASES

ACKNOWLEDGMENT

I would like to first thank my mentor, Mark Lemmon, for all of his support, dedication and guidance throughout my graduate school years. He has taught me many skills for which I am grateful.

I thank my thesis committee for all of their wonderful insight and suggestions.

I also thank all members of the Lemmon laboratory, past and present, for their support and for fostering a fun, intellectual, and motivated laboratory environment. They include Nick Bessman, Katarina Moravcevic, Jon Kenniston, Diego Alvarado, Daryl Klein, Fumin Shi, Neo Wu, Kelsey Speer, Matt Rapp, Jin Park, Sung Hee Choi, Jason Moore, Jeannine Mendrola, Dan Freed, Camilla Oxely, and Pamela Burgess-Jones. I would also like to thank members of the Ferguson and Van Duyne laboratories, past and present, for their helpful discussions.

A special thank you to all of my friends and family who continue to support me. I thank my wife Ashley, my mother and father, two brothers and family for their love and support, and for believing in me.

I thank all of the teachers that have helped me to be where I am today. Many of them did what they could with the very few resources available, but their tenacity and care for their students was always evident. I am grateful for what they have done for me.

I thank the University of Pennsylvania VMD/PhD program, especially Michael Atchison and the rest of the executive committee.

ABSTRACT

REGULATION AND KINASE ACTIVITY OF THE TRK FAMILY OF RECEPTOR TYROSINE KINASES

Stephen C. Artim

Mark A. Lemmon

The tropomyosin-related kinase (Trk) family consists of three receptor tyrosine kinases (RTKs) called TrkA, TrkB, and TrkC. These RTKs are regulated by the neurotrophins, a class of secreted growth factors responsible for the development and function of neurons. Given the high homology between the Trks and their use of overlapping signaling pathways, the key question to be addressed is how the activation of the different Trks can lead to distinct cellular outcomes. To this end, I first sought to determine the mechanism of autoregulation for the Trk tyrosine kinase domain (TKD). The Trk TKDs are members of the insulin receptor kinase (IRK) superfamily and recent data suggest that the IRK family displays a wide array of autoinhibitory mechanisms. To determine where TrkA and the closely related Ror2 TKD (from an unconventional Wnt receptor) lie in this spectrum, we determined the crystal structures of the kinase domains of these RTKs. In both cases, the conformation of the activation loop resembles the IRK activation loop conformation, with subtle but notable differences in the case of Ror2. These findings aid in understanding the range of autoinhibitory mechanisms of the IRK family, in addition to providing a foundation for deciphering consequences of TKD mutations in this family. I also observed crystallographic dimers of the inactive TrkA TKD that resemble those seen for other RTK TKDs – which may aid in understanding the reported pre-formed inactive TrkA dimers observed in cells. To understand the molecular basis for differences in signaling specificity of the Trk receptors, I investigated whether

the TrkA and TrkB TKDs differ in their intrinsic kinase activities. I show that the TrkA TKD autophosphorylates itself faster than its TrkB counterpart. However, this difference of autophosphorylation is not due to a difference in kinase activity *per se.* Rather, my data indicate that the difference in autophosphorylation may arise because of self-association of the TrkA TKD that does not occur with TrkB. My work sheds light on potential differences between TrkA and TrkB signaling, as well as providing a quantitative understanding of Trk TKD activation, which is useful for effective and selective inhibitor design.

TABLE OF CONTENTS

LIST OF TABLES

LIST OF ILLUSTRATIONS

Chapter 1:

Introduction

1.1 Cellular communication mediated by Receptor Tyrosine Kinases (RTKs)

The ability of cells to interpret extracellular clues and respond accordingly either by proliferating, migrating, or differentiating is crucial for maintaining homeostasis. A major advance in understanding how cells communicate with surrounding cells and the environment occurred in the 1950s when Rita Levi-Montalcini and Stanley Cohen discovered the first soluble growth factor from mouse salivary-gland extracts and snake venom (Cohen and Levi-Montalcini, 1957; Levi-Montalcini, 1952; Levi-Montalcini and Cohen, 1960). This growth factor was termed nerve growth factor (NGF), since applying NGF to cells resulted in neurite outgrowth. However, understanding of how the cells recognize NGF and respond accordingly remained elusive. In the early 1960s, Cohen then discovered another growth factor termed epidermal growth factor (EGF) (Cohen, 1962; 1965), but how NGF and EGF dictated the cellular response remained a mystery.

In 1978, Cohen and co-workers demonstrated the existence of a specific receptor for EGF (the EGF receptor or EGFR) and showed that, upon binding of EGF, there was an increase of cellular phosphorylation (Carpenter et al., 1978). Twenty years earlier, Gene Kennedy had described the first protein kinase by discovering that a liver enzyme catalyzed the phosphorylation of a protein, casein (Burnett and Kennedy, 1954). Subsequently, Fischer and Krebs discovered that phosphorylase kinase catalyzes the transfer of a gamma phosphate from ATP to a serine side-chain in phosphorylase b, (Fischer and Krebs, 1955; Fischer et al., 1959; Krebs and Fischer, 1956). Also during this time, phosphatases were identified as enzymes that remove phosphates from proteins. These discoveries in the 1970s and 1980s solidified the idea that the reversible modifications of phosphorylation and dephosphorylating catalyzed by kinases and

phosphatases represent a wide and significant mechanism utilized to modify protein function (Cohen, 2002).

Many of the initial studies showed that phosphorylation only occurs on serine or threonine residues. However, the discovery that the Rous sarcoma viral protein kinase, v-src, was responsible for transformation (Collett and Erikson, 1978) led Tony Hunter to discover that v-src phosphorylated proteins on tyrosine residues (Hunter and Sefton, 1980). These studies also showed that deregulated tyrosine kinase activity is involved in tumorigenesis (Gschwind et al., 2004; Hunter and Eckhart, 2004).

In the 1980s, data from various groups working on EGFR (Ushiro and Cohen, 1980), insulin receptor (IR) (Kasuga et al., 1982), and platelet-derived growth factor receptor (PDGFR) (Ek et al., 1982) demonstrated that growth factors bind and activate receptors with intrinsic tyrosine kinase activity. Surprisingly, the major substrates for phosphorylation by RTKs were shown to be the RTKs themselves (Cohen, 2002). In the late 1980s, Tony Pawson discovered the existence of src homology-2 (or SH2) domains as non-catalytic domains crucial for modulating signaling effects of tyrosine kinases. He and others then showed that SH2 domains recognize specific phosphorylated tyrosines on RTKs and other signaling proteins (Anderson et al., 1990; Sadowski et al., 1986). Upon ligand binding, autophosphorylation of dimeric RTKs creates tyrosine phosphorylated motifs recognized by SH2 domains and protein tyrosine binding (PTB) domains. During the 1990s, various studies culminated in a mechanistic link between RTKs and signaling cascades such as the small GTPase Ras – mitogen activated kinase (MAPK) pathway, ultimately leading to gene transcription that results in an array of cellular responses depending on the RTK and ligand (Cohen, 2002; Gschwind et al., 2004). These discoveries revealed that RTKs transmit extracellular information to the

interior of the cell by initiating a kinase-dependent signaling cascade that ultimately leads to a cellular response according to the extracellular stimulus.

Also in the 1990s, the receptor for NGF was determined to be Trk, a tyrosine kinase originally identified as tropomyosin-related kinase (trk), discovered previously in colon cancer (Kaplan et al., 1991a; 1991b; Klein et al., 1991a). It was later revealed that the trk oncogene was a fusion protein of dimerizing domains of non-muscle tropomyosin and the tyrosine kinase domain (TKD) of the TrkA receptor (Greco et al., 2010). Other neurotrophin ligands and receptors have been discovered and now the Trk RTK family consists of three members: TrkA, TrkB, and TrkC (Barbacid, 1994).

The RTK family in humans is now known to comprise 58 members that fall into 20 different families. Most RTKs play key roles in crucial cellular processes such as proliferation and differentiation, cell migration, cell-cycle control, cell survival and metabolism (Gschwind et al., 2004; Lemmon and Schlessinger, 2010).

1.2. Role of the Trk family in the nervous system

The Trk family of neurotrophin receptors is crucial for the development and maintenance of the nervous system. The family consists of three members, TrkA (NTRK1), TrkB (NTRK2) and TrkC (NTRK3). Neurotrophin ligands primarily bind to specific receptors – nerve growth factor (NGF) to TrkA, brain-derived neurotrophic factor (BDNF) and neurotrophin-4/5 (NT4) to TrkB, and neurotrophin-3 (NT3) to TrkC (Brodeur et al., 2009).

Evolutionarily, RTK appearance is thought to coincide with the transition to multicellularity, allowing complex interactions to occur between cells and their

environments (Casaletto and McClatchey, 2012; King, 2004). Indeed, homologues of most RTKs exist in *Drosophila* and in *C. elegans* (Sopko and Perrimon, 2013). However, Trk signaling has been considered a vertebrate innovation due to the lack of evidence of Trk receptors in many invertebrate species including *Drosophila* and *C. elegans* (Benito-Gutierrez et al., 2006). The lack of invertebrate Trk receptors was thought to be due a reduced need for plasticity in the nervous system of insects (Bothwell, 2006). However, evidence has been presented for the existence of Trk-related receptors in the marine mollusk (*Aplysia californica*), the snail (*Lymnaea stagnalis*) and recently in the amphioxus (*Branchiostoma floridae*) (Benito-Gutierrez et al., 2006), suggesting that there was a common ancestor that had some form of a Trk receptor (Sossin, 2006b). One study argues that the common ancestral kinase was a precursor to the Trk, MuSK, Ror and discoidin domain receptor (DDR) families. A subsequent split is then thought to have created the DDR family and a common ancestor of Trk, MuSK, and Ror which eventually split into three separate families by the time of a bilaterian ancestor (Sossin, 2006a).

In mammals, the expression of the neurotrophins and their receptors occurs at early stages of neurogenesis (Barbacid, 1994; Bartkowska et al., 2010). The expression of each Trk family member is complex and depends on the developmental stage and type of cell. Generally, TrkA expression is confined to very specific structures of the central nervous system (CNS) and peripheral nervous system (PNS), whereas TrkB and TrkC have more widespread expression in the CNS and PNS. Interestingly, the expression of TrkA is often distinct from TrkB/TrkC expression in the CNS and PNS (Bartheld and Fritzsch, 2006). Moreover, TrkA expression is essential for the development of normal

sympathetic neurons. In contrast, TrkB is rarely expressed in sympathetic neurons (Brodeur et al., 2009).

Knockout mice null for TrkA, TrkB, or TrkC demonstrated distinct, but some overlapping, abnormalities of the central and peripheral nervous system (Brodeur et al., 2009) – generally correlating with the known expression patterns. For example, TrkA knockout mice have severe cell loss and morphological changes in structures that were known to express TrkA, such as ganglia in the sympathetic nervous system. In contrast, TrkB knockout mice do not demonstrate morphological changes in structures known to express TrkB. This suggests that some of the functions of TrkB can be fulfilled by other mechanisms, perhaps TrkC, since TrkB/TrkC are co-expressed in many structures in the nervous system (Barbacid, 1994).

The initial focus of Trk expression studies was restricted to neuronal cells. However, it is now clear that Trk expression does occur in non-neuronal cells (Shibayama and Koizumi, 1996). The role of Trk family members in non-neuronal cells is not well understood. There are two isoforms of TrkA, differing by only six amino acids in the extracellular domain, which do have specific expression patterns. The TrkA isoform *I* contains 790 amino acids and is expressed in non-neuronal tissue, whereas isoform *II* contains 796 amino acids and is expressed primarily in neuronal tissue (Barbacid, 1994; Barker et al., 1993).

1.3. RTK structure and function

Each RTK consists of an extracellular region (ECR) that binds its regulatory ligand, a single transmembrane domain (TM) and an intracellular domain (ICD) that contains the

juxtamembrane region (JM), a tyrosine kinase domain (TKD), and a C-tail region (**Figure 1.1**).

Activation of RTKs involves ligand binding to the extracellular region, which leads to RTK oligomerization and resulting activation of the intracellular kinase domain. The active kinase *trans*-autophosphorylates tyrosines in its neighboring ICD in the receptor dimer, thereby both enhancing catalytic activity and providing sites for the (SH2 domain-dependent) recruitment of signaling molecules that subsequently activate downstream pathways controlling transcription, metabolism, cell cycle progression, and survival (Lemmon and Schlessinger, 2010; Schlessinger, 2003; Ullrich and Schlessinger, 1990). To prevent aberrant signaling, autoregulatory mechanisms appear to exist in all RTKs, which maintain the kinase domain in an inactive or autoinhibited conformation until it is activated by extracellular ligand-induced oligomerization (Hubbard, 2004; Schlessinger, 2003; Ullrich and Schlessinger, 1990).

Interestingly, there is a subset of RTKs such as the insulin receptor (IRK) and insulin like growth factor 1 receptor (IGF1R) that already exists at the plasma membrane as disulfide linked dimers (De Meyts, 2004; 2008). Furthermore, there are many reports of other RTKs such as EGFR (Chung et al., 2010; Clayton et al., 2005; Gadella and Jovin, 1995), TrkA (Paul S Mischel, 2002; Shen and Maruyama, 2011), and TrkB (Shen and Maruyama, 2012) existing as pre-formed oligomers at the cell surface . The nature of these inactive oligomers is unclear, since it is still recognized that ligand binding is necessary to obtain a fully active RTK oligomer in which the constituent subunits are oriented in the correct conformation for optimal autophosphorylation and subsequent phosphorylation of downstream signaling molecules (Lemmon and Schlessinger, 2010).

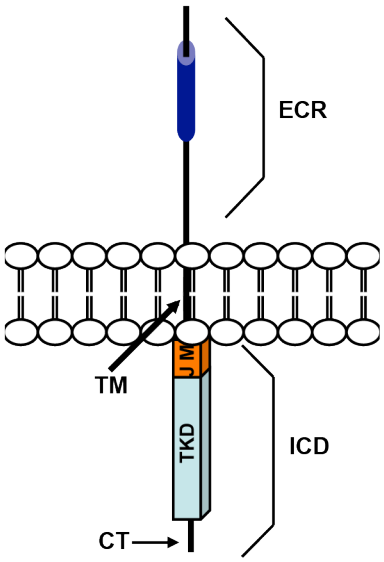

Figure 1.1. **RTK domain structure**. ECR=Extracellular region, TM= Transmembrane domain, ICD = Intracellular domain, JM= Juxtamembrane region, TKD= tyrosine kinase domain, CT=C-tail

1.4. Structure of the tyrosine kinase domain (TKD)

In 1991, the first protein kinase X-ray crystal structure was solved when Taylor and coworkers solved the structure of cAMP dependent protein kinase (PKA) (Knighton et al., 1991a; 1991b). PKA is a serine/threonine kinase, although subsequent structures demonstrate that all protein kinases possess a conserved core composing two lobes, a N-terminal small lobe (N-lobe) and a C-terminal large lobe (C-lobe). The N-lobe usually consists of five β-strands (β1-5) and one α-helix (αC). Also in the 1990s, structures of the insulin receptor kinase (IRK) in the inactive and active states were solved (Hubbard, 1997; Hubbard et al., 1994). The IRK and PKA structures revealed that the inactive

structures are in an 'open' conformation where as the active kinase structures are in a 'closed' conformation (**Figure 1.2**). The N-lobe has been shown to be quite dynamic, and movement of αC and the N-lobe towards the C-lobe is crucial for catalysis. Thus, the orientation of αC (cyan in Figures **1.2 and 1.3**) with respect to the C-lobe can be indicative of an inactive (outward orientation of αC) or active (inward orientation of αC) structure. The predominately helical C-lobe is thought to be more rigid, and contains seven helixes (αD through αI) as well as four short β-strands (β6 through β9). Key features of an inactive and active kinase structure are shown for IRK in **Figures 1.2 and 1.3** and discussed in more detail below.

Between the N-lobe and the C-lobe resides the substrate cleft, where ATP, divalent cations, and peptide substrate bind (**Figure 1.2B and 1.3**). The glycine rich phosphate binding loop (P-loop) between β1-2 in the N-lobe (orange in **Figures 1.2 and 1.3**) accommodates nucleotide binding and is able to make backbone interactions with ATP. The movements of αC mentioned above aid in ATP binding by promoting formation of a salt bridge (**Figure 1.2B and 1.3B**) between a glutamate acid in αC (Glu^{1047} in IRK) and a conserved lysine in β1 (Lys^{1030} in IRK), which is important in positioning the β1 lysine to interact with the α- and β- phosphates of ATP (Huse and Kuriyan, 2002; Jura et al., 2011). Also essential for ATP binding is coordination of magnesium ions in the active site by a conserved aspartate residue (Asp^{1150} in IRK) of the DFG (Asp-Phe-Gly) motif within the activation loop in the C-lobe (Huse and Kuriyan, 2002). Peptide substrate binds in the cleft, with the tyrosine substrate directed towards ATP and another conserved aspartate residue in the C-lobe known as the catalytic base (Asp^{1132} in IRK).

The N-lobe and the C-lobe are connected by the β5-αD loop, also known as the hinge region (**black in Figures 1.2 and 1.3**). Motion and dynamics in the hinge region have

been noted to be important for kinase activation (Hoofnagle et al., 2001; 2004; Lee et al., 2005; Sours et al., 2014; Xiao et al., 2014). Accordingly, one mechanism of autoinhibition proposed for FGFR1 is a network of interactions at the hinge region that act as a "molecular brake" by holding the kinase in an inactive conformation (Chen et al., 2007).

A sequence insert (green in **Figures 1.2 and 1.3**) within the kinase domain also exists in RTKs to varying degrees, with some RTKs having no appreciable kinase insert domain (KID) and others having inserts of up to 100 amino acids (Locascio and Donoghue, 2013; Ullrich and Schlessinger, 1990). Many of the KIDs are thought to be important sites of phosphorylation, since they often contain key tyrosines, serines, or threonines. However, there are several RTKs that have a recognizable short KID loop that do not contained a tyrosine, serine, or threonine and have been termed "non functional" KIDs (Locascio and Donoghue, 2013). The question remains whether the ~10-20 amino acid "non functional" KID loops have additional roles in these RTKs.

Within the C-lobe is the activation loop (magenta in **Figures 1.2 and 1.3**), one of the most important regions of the kinase domain since it is known to influence both substrate binding and kinase activity (Kornev and Taylor, 2010). The activation loop is 20-35 amino acids long, and is defined by the highly conserved DFG motif at the N-terminus and the APE (Ala-Pro-Glu) motif at the C-terminus (Nolen et al., 2004). As shown in **Figure 1.2A**, the activation loop of IRK is situated in the substrate cleft so that a key tyrosine (Tyr^{1162} in IRK) projects towards the catalytic base (Asp^{1132} in IRK) in the inactive structure. However, phosphorylation of the activation loop causes a conformational change making the substrate-binding pockets available for substrate to

bind as shown in the active IRK structure in **Figure 1.2B**. (See below for more information regarding the autoregulation of TKDs.)

Strikingly, crystal structures of all protein kinases solved in their active state share very similar characteristics and remarkably similar structures, whereas inactive (autoinhibited) kinases adopt an array of different configurations that seem to be family-specific (or receptor-specific); suggesting a wide diversity in autoinhibitory mechanisms (Huse and Kuriyan, 2002; Lemmon and Schlessinger, 2010). Indeed, the details of kinase autoinhibition have been shown to differ even within an RTK family where the kinase domains share 90% sequence identity (the FGFR family (Lew et al., 2007)). The mechanism of kinase autoinhibition remains unknown for the Trk receptors, and may differ between TrkA and TrkB, which share ~67% identity in the ICD and 88% in the TKD (Brodeur et al., 2009).

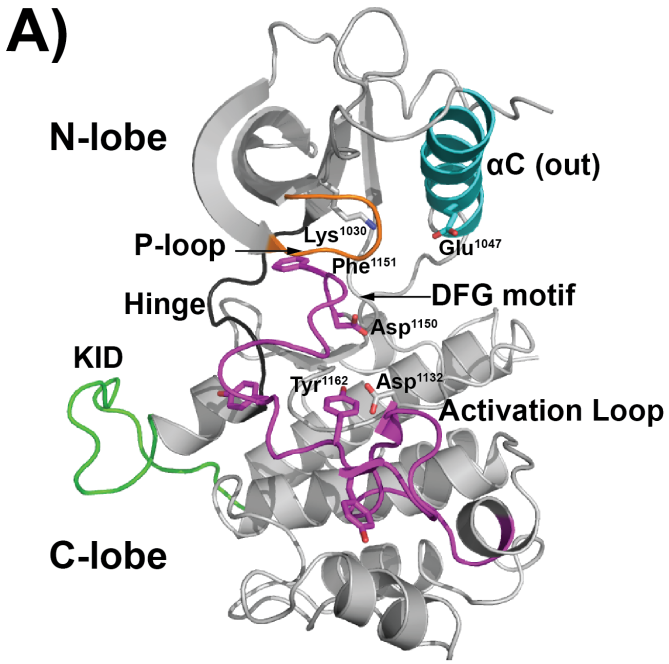

Inactive IRK
(pdb1ir3)

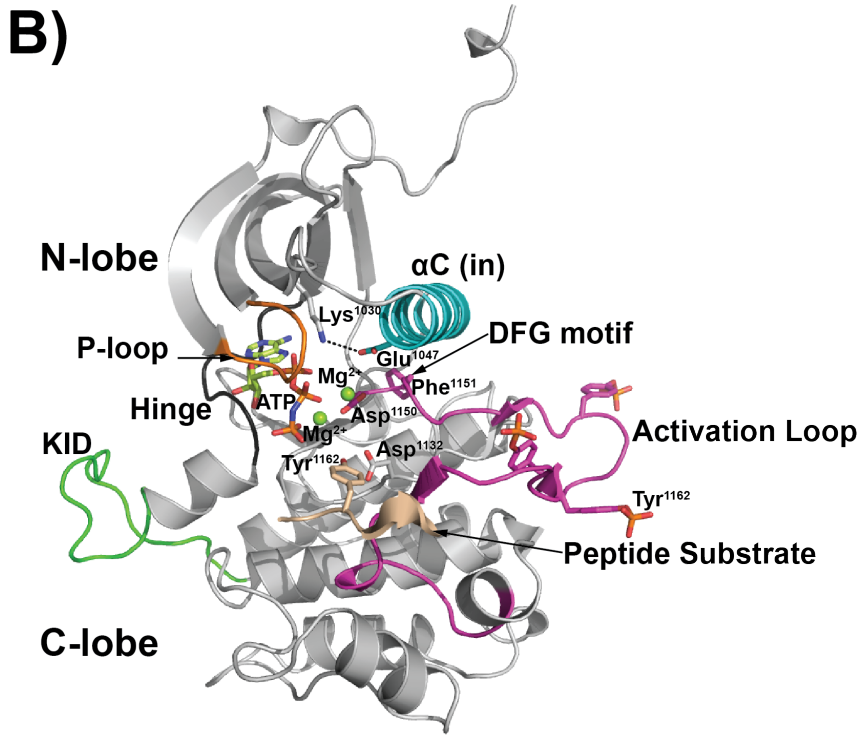

Active IRK
(pdb1irk)

Figure 1.2. Inactive and active structures of the IRK TKD. (A) Inactive structure of the IRK TKD in cartoon representation with side chains of residues discussed in the text in stick representation. Notice that the activation loop (magenta) is located in the cleft between the N-lobe and C-lobe. (B) Active structure of IRK TKD in the same orientation as the inactive structure in (A). Notice that the N-lobe rotates towards the C-lobe in the active structure compared to the inactive structure. The activation loop in the IRK active structure is phosphorylated and no longer obstructs the substrate binding pockets. The following are colored for clarity: P-loop (orange), αC (cyan), hinge (black), KID (green), and activation loop (magenta).

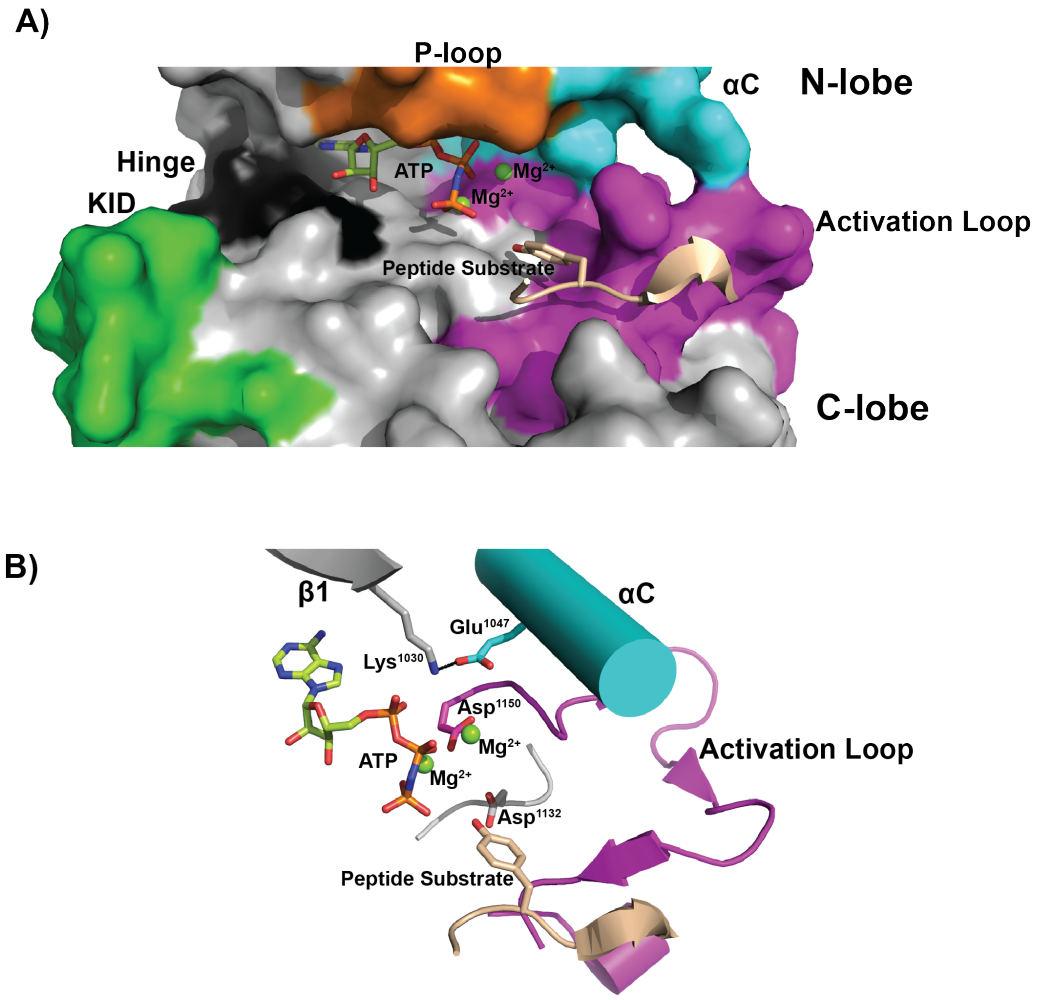

Figure 1.3. Substrate binding pockets. (A) ATP, Mg^{2+} and peptide substrate bind in a cleft between the N-lobe and C-lobe of the IRK TKD (shown in surface representation with specific features colored as in Figure 1.2). (B) Amino acids essential for catalysis include Asp^{1150} (part of the Asp-Phe-Gly motif) which coordinates the magnesium ions in the active site and Asp^{1132}, the catalytic base. Also shown is the Glu^{1047}-Lys^{1030} salt-bridge, which orients Lys^{1030} for coordination of ATP.

1.5. Autoregulatory mechanisms in RTK TKDs.

As mention previously, crystal structures of the insulin receptor TKD in its inactive conformation show how an activation loop tyrosine (Tyr^{1162}) projects into the active site, preventing binding of substrate and restraining the rest of the loop to block ATP binding (**Figure 1.4**, 'Inactive A': activation loop = black line). Upon extracellular ligand binding, tyrosines in the activation loop become autophosphorylated in *trans*, causing a conformational change that allows substrate and ATP to bind the kinase, with the activation loop "relaxing" into a configuration that aids catalysis (**Figure 1.4**, 'Active') (Blume-Jensen and Hunter, 2001; Hubbard, 2004). The Trk receptors also have tyrosines in their activation loop, in a YxxxYY motif similar to that seen in IRK, which have been shown to be autophosphorylated upon TrkA and TrkB activation in cells (Cunningham et al., 1997; Guiton et al., 1995; 1994).

Biochemical, mutational, and crystallographic studies of several RTKs (EphB, Flt3, and MuSK) have demonstrated that the intracellular JM region can alternatively autoinhibit the kinase domain (Griffith et al., 2004; Till et al., 2002; Wybenga-Groot et al., 2001). The precise mode of this autoinhibition is RTK-specific, but generally involves the JM region making contacts with the kinase domain that stabilizes the inactive conformation (**Figure 1.4**, 'Inactive B': JM = red line). In these cases, autophosphorylation of tyrosines in the JM region releases the inhibitory effect. There is one tyrosine in the JM region of both TrkA (Y490 in isoform *I*, or Y496 in isoform *II*) and TrkB (Y516), within an NPxY motif. Several other RTKs (insulin receptor, and FGFR1) employ JM-mediated autoregulatory mechanisms that do not require phosphorylation of the JM region for reversal. Specific residues within the JM region are crucial for correctly stabilizing structural elements within the kinase domain (insulin receptor), or are important for

defining optimal interactions between juxtaposed kinase domains in the activated dimer (FGFR1) (Bae et al., 2010; Hubbard, 2004). In the case of TrkA and TrkC, mutation of the single JM tyrosine to phenylalanine had little effect on autophosphorylation in cell based studies (Obermeier et al., 1994; Stephens et al., 1994). However, mutation of the corresponding JM tyrosine to phenylalanine in TrkB did diminish autophosphorylation in cell based assays (Minichiello et al., 1998; Postigo et al., 2002). Interestingly, recent work in the Lemmon laboratory determined that the JM region of EGFR serves as a kinase-activating (rather than autoinhibitory) element (Hubbard, 2009; Jura et al., 2009; Red Brewer et al., 2009; Thiel and Carpenter, 2007), underscoring the importance of understanding the function of this region in all RTKs.

Additional autoregulatory mechanisms have been shown that involve the C-tail of the RTK blocking its active site, as demonstrated for the Tie2 receptor and suggested for EGFR (**Figure 1.4**, 'Inactive C': C-tail = green line). Both Tie2 and EGFR have relatively long C-tails, whereas the C-tail in the Trk receptors is quite short (just 15 residues).

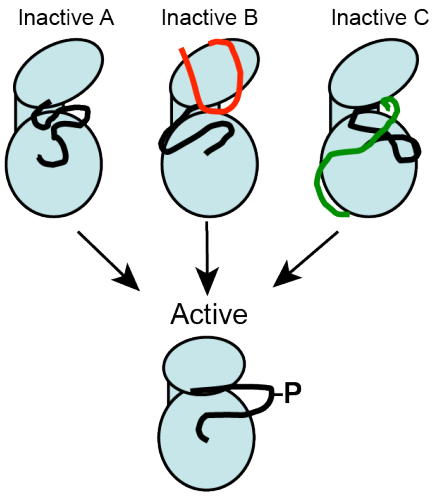

Figure 1.4. Autoregulatory mechanisms of kinase domains. Various kinase inactive configurations are compared to the active form. The mechanisms for autoinhibition can involve the activation loop (A), JM (B) and C-tail (C). Black line = activation loop. Red line = JM. Green line= C-tail.

1.6. The Trk TKDs are part of the IRK TKD superfamily

A classic paper by Hanks et al. in 1988 was the first of its kind to classify all the known protein kinases into families according to primary sequence as well as identify many of the conserved features of a kinase domain. That study identified a subset of RTKs that have similar TKDs and, in particular, a unique motif in their activation loops. This subset of RTKs is known as the IRK TKD family (Hanks et al., 1988). Since the study by Hanks et al. additional kinases have been discovered that contain this motif and have been included in the IRK TKD family (Morris et al., 1994). An alignment of members of the IRK TKD family (**Figure 1.5A**) demonstrates that all members possess a YxxxYY motif in

their activation loop. As a comparison, **Figure 1.5B** shows an alignment of IRK with EGFR and FGFR1, RTKs that do not have the YxxxYY motif. As mentioned above, the activation loop of IRK acts almost like a pseudosubstrate, with the middle tyrosine of the YxxxYY binding as if it were a substrate (Hubbard et al., 1994). Once the tyrosines of the YxxxYY motif become autophosphorylated, the activation loop drastically changes conformation, allowing ATP and peptide substrate access to the substrate binding pockets (Hubbard, 1997). Since all the other members of the IRK TKD family contain the YxxxYY motif, all members were considered likely to utilize the same mechanism of autoinhibition and activation.

Earlier crystal structures of the IGF1R and MuSK TKDs agreed with the hypothesis that RTKs with the YxxxYY motif all have a similar activation loop conformation in the inactive structure – further suggesting these RTKs all have the same autoinhibition mechanism as IRK. However, subsequent structures of the inactive TKDs of Met and Alk surprisingly revealed quite distinct activation loop conformations, challenging the hypothesis that all IRK family members are regulated the same way. High resolution structures of a certain IRK TKD family members, notably from the Trk, Ror, and DDR families, were notably absent from the protein data bank (PDB). A thorough examination of all the inactive TKDs from IRK family members will help elucidate the mechanism of autoregulation within this family as well as aiding interpretation of TKD mutations of IRK TKD family members.

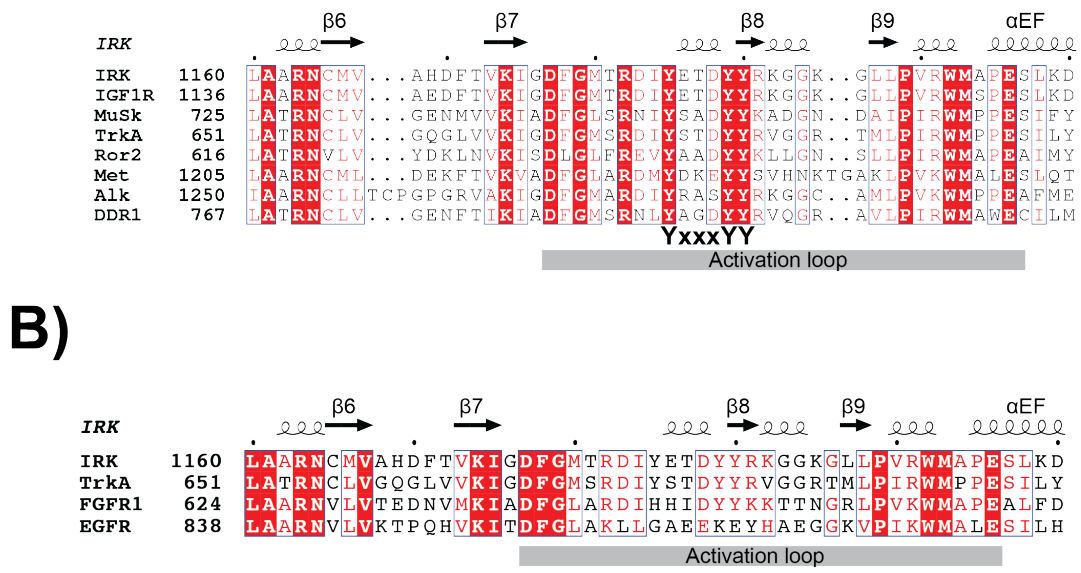

Figure 1.5. Alignment of IRK family TKDs. (A) Activation loop sequences from an alignment of IRK TKD family members. (B) As a comparison, activation loop sequences from an alignment with IRK, TrkA, EGFR, and FGFR.

1.7. RTK signaling specificity

Once activated by extracellular ligand, the TKDs of RTKs *trans*-autophosphorylate tyrosines in the ICD further, both enhancing catalytic activity and creating phosphotyrosine binding sites for SH2 and PTB domains in docking molecules and downstream effectors (**Figure 1.6**). Docking molecules (e.g. Shc and FRS2) interact via additional adapter proteins (such as Grb2 and Crk) with GTPase exchange factors (GEFs) that activate small GTPases such as Ras (via Sos) and Rap1 (via C3G). The

activation of these small GTPases in turn activates B-Raf or C-Raf to promote signaling through the MAPK pathway (Lemmon and Schlessinger, 2010) (**Figure 1.6**). The resulting activation of Erk leads to transcription factor activation, gene expression and cellular responses (Murphy and Blenis, 2006) (**Figure 1.6**). This highly simplified linear description of RTK signaling is shared by many of the RTKs, even though the cellular fates upon receptor activation are quite varied.

In the past 20 years, RTK signaling has been well studied using rat pheochromocytoma (PC12) cells. Important early experiments analyzed signaling differences between activated TrkA and EGFR in these cells. Despite engaging similar complements of downstream signaling molecules, TrkA activation leads to PC12 cell differentiation, whereas EGFR activation leads to cell proliferation (Marshall, 1995). These classic experiments revealed that NGF-induced TrkA activation produces sustained Erk activation in PC12 cells, whereas EGFR activation promotes only transient Erk activation. It is now quite well established that the duration of Erk activation following a signal determines the effect of that signal on cellular fate (i.e. differentiation vs. proliferation) (Murphy and Blenis, 2006). One way in which the different time courses of Erk activation are 'interpreted' to achieve this involves phosphorylation-dependent regulation of immediate early gene product stability (Murphy and Blenis, 2006; Murphy et al., 2004). Both transient and sustained Erk activation leads to induction of immediate early genes (IEG). Several IEG products, such as c-Fos, are quite unstable, but are stabilized by Erk phosphorylation. If Erk activation is transient, the lifetime of the IEG products is very short. However, when (and only when) Erk activation is sustained, Erk phosphorylates and stabilizes IEG products such as c-Fos, allowing them to induce

expression of 'late response' genes involved in differentiation (Murphy and Blenis, 2006; Murphy et al., 2004).

The origin of the differences in time course of Erk activation remains quite unclear, however. Over the years, studies have variously implicated differences in receptor internalization, receptor levels, receptor localization, differential use of small GTPases, and engagement of distinct feedback loops to explain how TrkA and EGFR signaling cause differentiation and proliferation respectively in PC12 cells (Murphy and Blenis, 2006).

Earlier studies comparing signaling by TrkA and EGFR in PC12 cells identified key network properties that may explain the sustained and transient modes of Erk activation respectively. York *et al.* (York et al., 1998) reported that, whereas Erk activation by EGFR signaling occurs largely through the Grb2/Sos/Ras pathway, TrkA signaling also engages the FRS2/Crk/C3G/Rap1 pathway. A key difference between these pathways is that the Grb2/Sos/Ras pathway contains several negative feedback loops, including receptor activation of Ras-GAP and inhibitory Erk phosphorylation of Sos (Lemmon and Schlessinger, 2010). By contrast, Rap1's GAP is not activated by RTKs, and the C3G Rap1 exchanger is not subject to negative feedback. Negative feedback is likely to cause EGFR-induced Erk activation to be transient, and the relative lack of this feedback in TrkA signaling via Rap1 allows a more sustained response. Another study suggested that formation of a long-lived complex between TrkA and the FRS2 docking protein may increase the longevity of its signaling to Erk, and thus more sustained Erk activation (Kao et al., 2001).

Additional modulation of the network is achieved by the underappreciated role of protein phosphatases. Recent studies have revealed that the phospho-turnover of RTKs at the cell surface is very rapid. This suggests that the activity of RTKs has to exceed a threshold controlled in part by surrounding phosphatase activity to increase levels of autophosphorylation (Kleiman et al., 2011).

Interestingly, overexpression of EGFR or IRK converts the cellular proliferation response normally observed for EGFR and IRK activation in PC12 cells into cellular differentiation. These studies reveal that the strength *per se* of the initiating signal can be a determinant of downstream signaling and cellular response (Dikic et al., 1994; Traverse et al., 1994).

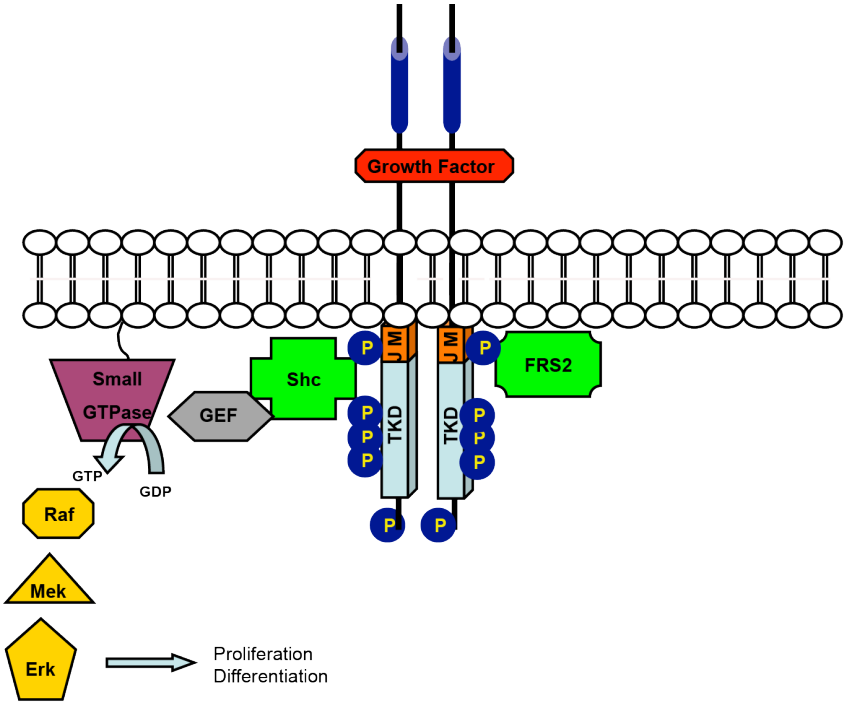

Figure 1.6. Simple schematic of RTK signaling. Growth factor binding to its receptor induces dimerization and activation of the TKD. Autophosphorylation by the TKD creates docking motifs for adapter molecules (green). These molecules interact with GEFs (grey) that activate small GTPases (purple) that in turn activate the MAPK pathway (yellow). The MAPK pathway consists of Raf, Mek and Erk. Activation of Erk leads to activation of transcription factors that elicit cellular responses.

1.8. RTKs in disease

The important role of RTKs in initiating cellular signaling and dictating cellular response is evident by the prevalence of aberrant activity of RTKs in various diseases and in particular cancer. In fact, many RTKs were originally identified as agents promoting tumorigenesis. For example, in the 1980s viral oncogenes from the simian sarcoma virus and avian erythroblastosis virus respectively were determined to transform cells through autocrine activation of PDGFR (by expressing its ligand) and constitutively signaling by an activated EGFR variant (Lemmon and Schlessinger, 2010). Furthermore, several RTKs were initially identified when parts of their coding sequence was found in aberrant soluble fusion proteins that promote tumorigenesis. The Trk (tropomyosin related kinase) receptors were first identified from the trk oncogene in colon cancer, which encodes an oncogenic fusion protein created by chromosomal rearrangement that juxtaposes the coding region for the TrkA TKD with non-muscle tropomyosin, creating a constitutively active tropomyosin/TrkA TKD fusion oncoprotein (Greco et al., 2010). These discoveries highlight some of the mechanisms of RTK dysfunction in cancers. In the case of human cancer, aberrant RTK activation can occur by chromosomal translocation (as with trks), autocrine activation, overexpression, or gain-of-function mutations (Casaletto and McClatchey, 2012; Lemmon and Schlessinger, 2010).

Recent increased sequencing efforts have lead to abundance of data regarding TKD mutations of RTKs in cancer. Interpreting the significance of these mutations remains a challenge, since it is increasingly evident that many mutations revealed by sequencing are “passenger” mutations rather than the “driver” mutations that are actually promoting cell proliferation and tumorigenesis (Dancey et al., 2012). Structural studies have been instrumental in understanding the consequences of mutations.

There are various reports of TKD mutations activating the TKD by disturbing autoinhibitory mechanisms that normally keep the TKD inactive until ligand binds and induces activation. For example, structural studies of the intracellular domain of the stem cell factor receptor (KIT) elucidated the autoinhibitory mechanisms utilized by WT KIT and demonstrated that cancer mutations disturb these autoinhibitory mechanisms (Corless and Heinrich, 2008; Lemmon and Schlessinger, 2010). Mutations in the EGFR TKD identified in non-small-cell lung cancer (NSCLC) have also been shown by structural and biochemical studies to release the EGFR TKD from the autoinhibitory mechanisms that normally hold the WT EGFR TKD in an inactive state (Choi et al., 2006; Zhang et al., 2006). Thus, understanding the mechanism of autoregulation of TKDs is vital for understanding the consequences of TKD mutations.

However, not all RTKs have been as thoroughly studied structurally and biochemically as KIT and EGFR. For example, the mechanism of autoinhibition for the Trk family was not clearly known at the time of starting this thesis, because there were no kinase domain structures available for any member of the Trk family. The mechanism of TKD activation in the case of oncogenic TrkA TKD-containing fusion proteins is thought to involve dimerization mediated by the fusion partner, which frequently contains coiled-coiled domains (Greco et al., 2010). However, if and how mutations activate Trk family members in the intact RTK context is not known. There are reports of mutations of Trk family members in acute myeloid leukemia (Tomasson et al., 2008), colorectal (Bardelli et al., 2003), lung (Davies et al., 2005; Ding et al., 2008; Marchetti et al., 2008), and breast cancers (Stephens et al., 2005) but without structural and biochemical analysis the consequences of these mutations are difficult to predict. Prior to this study, interpretation of some of these mutations was based on homology models of other RTKs

(Tomasson et al., 2008). However, previous reports suggested that at least TrkA has a unique autoinhibitory mechanisms – based on the observation that activating mutations of conserved residues in Met and Kit have a distinct effect in TrkA and in one case abrogates kinase activity of TrkA (Miranda et al., 2002). Thus, interpretation of the mutations of Trk family members in cancer has proven to be challenging since it was not yet known if these mutations were “passengers” or “driver” mutations. Along with mutations of Trk family members in certain cancers, there are other reports that have identified TrkA loss-of-function mutations in congenital insensitivity to pain with anhidrosis (Indo, 2001).

The Trk family has also been implicated in neuroblastoma, a cancer of the sympathetic nervous system and one of most common pediatric neoplasms (Brodeur et al., 2009). The clinical outcomes of neuroblastoma vary greatly, ranging from benign cases that spontaneously regress to malignant cases leading to fatality. Unfortunately, the majority of cases that occur in children older than one year are malignant with long-term survival less than 40% (Brodeur, 2003; Brodeur et al., 2009; Maris et al., 2007). The heterogeneous nature of neuroblastoma is an intriguing biological and clinical dilemma. An interesting correlation is that tumor characteristics are closely related to the expression of TrkA and TrkB. Studies have shown that expression of TrkA occurs in biologically favorable neuroblastomas, whereas expression of TrkB occurs in biologically unfavorable neuroblastomas (Brodeur et al., 1997; 2009). At the start of this study there was no evidence of mutations of TrkA or TrkB in neuroblastoma, but sequencing efforts were just starting to increasingly look at the TKDs of TrkA and TrkB.

Structural and biochemical studies not only provide insight into the consequences of certain mutations, but also provide a framework to therapeutically target the TKDs that

promote turmorigenesis. A thorough understanding of the autoregulatory mechanisms of TKDs is crucial for effective therapies. This requirement was clearly illustrated in recent studies with B-Raf inhibitors, underscoring the consequences of not fully understanding the activation mechanism of a kinase and the organization of the network in which it is embedded. Although certain B-Raf inhibitors have proven very successful in treating some melanomas (driven by mutated B-Raf), the very same inhibitors can actually increase cell proliferation by driving the MAPK pathway in other cellular contexts (Cichowski and Janne, 2010).

Chapter 2:

Assessing the range of kinase autoinhibition mechanisms in the insulin receptor family

NB. The work presented in this chapter was in collaboration with Dr. Jeannine Mendrola from the Lemmon lab and can also be found in Artim et al. (2012) Biochem. J. *448*, 213–220. Work contributed by Dr. Jeannine Mendrola (J.M.) is noted in the appropriate figure and table legends.

2.1. Introduction

Recent clinical success with targeted inhibitors of the EGFR, B-Raf, and ALK kinases underscore both the promise and the challenges of 'personalized' cancer medicine (Dancey et al., 2012; Yauch and Settleman, 2012). Well-defined activating mutations in each of these kinases have been identified as oncogenic "drivers", promoting uncontrolled proliferative or cell survival signaling that can be curbed with specific kinase inhibitors. As genomic analysis of tumors burgeons, however, it is becoming increasingly clear that many mutations found in cancer are "passengers" rather than drivers (Dancey et al., 2012). The ability to determine which mutations in a tumor are oncogenic drivers – and thus which signaling nodes should be targeted therapeutically – will be crucial for advancing personalized medicine in oncology.

For protein kinases – including receptor tyrosine kinases (RTKs), which are frequently found as oncogenic drivers in cancer (Lemmon and Schlessinger, 2010) – a key goal is to understand which mutations increase constitutive kinase activity and signaling. The EGF receptor provides an excellent illustration of how structural understanding of kinase activation mechanisms (Zhang et al., 2006) can explain driver mutations in non-small cell lung cancer (NSCLC) (Sharma et al., 2007). The inactive EGFR TKD is autoinhibited by intramolecular interactions between a short α-helix in its activation loop and another important helix (αC) that is consequently displaced from the position it adopts in the active kinase. This mode of autoinhibition closely resembles that seen in

Src family and cyclin-dependent kinases (CDKs) (Jura et al., 2011). Known driver mutations activate EGFR by destabilizing these intramolecular autoinhibitory interactions. Intriguingly, oncogenic driver mutations that destabilize very similar autoinhibitory interactions are also found in ALK (anaplastic lymphoma kinase) (Bossi et al., 2010; Bresler et al., 2011; Lee et al., 2010), a member of the large insulin receptor kinase (IRK) subfamily of RTKs (Manning et al., 2002; Morris et al., 1994) that is important in neuroblastoma (Carpenter and Mossé, 2012). Despite the fact that the ALK TKD shows closest sequence similarity to IRK family members, the autoinhibitory interactions that define its inactive conformation most closely resemble those in EGFR, Src and CDKs (Hubbard et al., 1994; Jura et al., 2011). As in EGFR, ALK TKD structures reveal hydrophobic interactions between a small α-helix in the activation loop and the crucial αC helix that stabilize the inactive kinase conformation (Bossi et al., 2010; Lee et al., 2010). The side-chains of the ALK residues most frequently mutated in neuroblastoma (Carpenter and Mossé, 2012) (Phe^{1174} and Arg^{1275}) make important contributions to these autoinhibitory interactions, and their mutation causes constitutive ALK activation. Indeed, Phe^{1174} and Arg^{1275} in ALK are structurally equivalent to EGFR residues Val^{769} and Leu^{861} (Bresler et al., 2011), at which activating mutations are also seen in NSCLC (Sharma et al., 2007).

Structural studies have revealed a spectrum of autoinhibitory mechanisms for IRK family RTKs. ALK lies at one extreme, with an EGFR/Src/CDK-like mode of autoinhibition. IRK lies at the other, with a very different autoinhibitory activation loop conformation that simultaneously occludes the ATP-binding site and projects a key tyrosine side-chain (Tyr^{1162}) into the substrate-binding site (Hubbard et al., 1994). The autoinhibitory mechanisms of inactive IGF1R (Munshi et al., 2002) and MuSK (Till et al., 2002) kinases

closely resemble that seen in IRK, with very similar activation loop configurations. However, structures of the inactive TKDs of the IRK family members Met (Wang et al., 2006) and Ron (Wang et al., 2010) have quite distinct activation loop conformations. Since mutations that disrupt autoinhibitory interactions are known to be important oncogenic drivers in ALK (and Met), it seems clear that understanding the mechanism of TKD autoinhibition will be important for predicting which mutations are likely to be significant for IRK family RTKs in cancer or other diseases in which RTK activation is important. Since the cases of Met, ALK, and Ron demonstrate that not all IRK family RTKs are regulated in the same way as IRK, we were motivated to ask how other kinases in this family are regulated. Notably absent from the list of IRK-family TKDs with known structure are members of the Trk, Ror, and DDR subfamilies, which have all been implicated in cancer (Brodeur et al., 2009; Hammerman et al., 2011; Rebagay et al., 2012) and other diseases. Here, we describe crystal structures to 2.4Å resolution of the inactive TKDs from TrkA (a receptor for nerve growth factor (Huang and Reichardt, 2003)) and Ror2 (now known to be a Wnt receptor (Green et al., 2008)). In the context of the other IRK family structures, these new results provide a useful framework for interpreting the consequences of TKD mutations in this family.

2.2. Overview of TrkA and Ror2 Structures

Both the TrkA and Ror2 TKD structures were solved in their unphosphorylated inactive forms (**Figure 2.1**), with no bound nucleotide. Data collection and refinement statistics are shown in **Table 2.1**. The TrkA and Ror2 structures exhibit the common kinase topology consisting of an N-terminal lobe and a larger C-terminal lobe. The N-terminal

lobe consists of a twisted five-stranded β-sheet plus one conserved α-helix, called αC, that plays a key role in the transition from an inactive to an active conformation (Huse and Kuriyan, 2002). The larger C-terminal lobe is predominantly helical, and also contains the activation loop that undergoes key conformational changes upon activation – contributing to the catalytic and substrate binding sites in the active conformation of the TKD, but instead playing an autoinhibitory role in the inactive conformation.

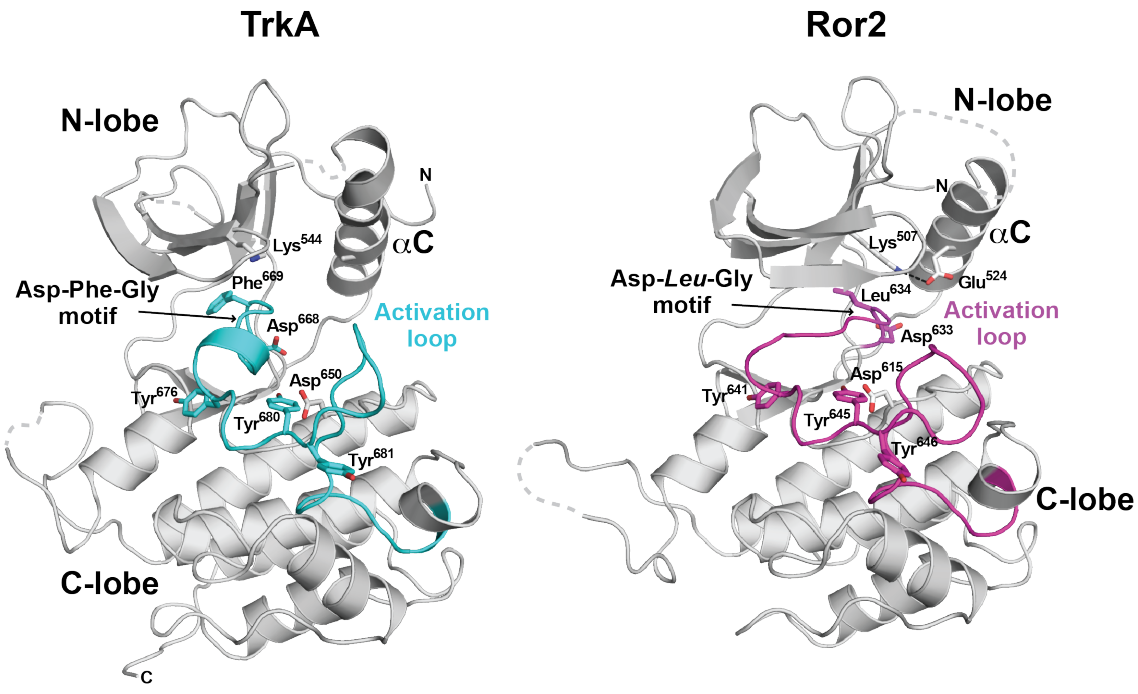

Figure 2.1. Structures of TrkA and Ror2 TKDs

Structures of inactive TKDs from TrkA (*left*) and Ror2 (*right*) in cartoon representation. The amino- and carboxy-terminal lobes (N-lobe and C-lobe) are labeled, as is the catalytically important αC helix. The activation loops are labeled and highlighted in cyan (TrkA) and magenta (Ror2). Side-chains in the DFG motif of TrkA (Asp^{668}, Phe^{669}, Gly^{670}) and the equivalently located D**L**G motif in Ror2 (Asp^{633}, Leu^{634}, Gly^{635}) are shown, and tyrosines from the YxxxYY motif are shown in stick representation. Also shown is the invariant lysine in strand β3 (Lys^{544} in TrkA, Lys^{507} in Ror2), which forms a salt bridge with αC Glu^{524} in Ror2 (but not TrkA). The catalytic base aspartate (Asp^{650} in TrkA, Asp^{615} in Ror2) is also shown and labeled. Molecule A was used for Ror2-TKD. The N- and C-terminal residues of the modeled structure are marked where visible in the orientation shown. (Ror2 TKD was crystallized and the structure solved by J.M.)

Table 2.1. **Data collection and refinement statistics (molecular replacement)**

Each dataset was collected from a single crystal. Values for the highest-resolution shell are shown in parentheses. (Ror2 TKD was crystalized and the structure solved by J.M.)

	TrkA	Ror2
Data collection		
Space group	H32	$C222_1$
Cell dimensions		
a, *b*, *c* (Å)	105.0, 105.0, 203.3	102.8, 112.9, 114.8
α, β, γ (°)	90, 90, 120	90, 90, 90
Resolution (Å)	50.0-2.4	46.9-2.4
R_{sym}	0.065 (0.553)	0.112 (0.565)
I/σ	52.9 (5.3)	21.9 (4.1)
Completeness (%)	99.9 (100)	100 (99.9)
Redundancy	11.1 (11.3)	7.5 (7.3)
Refinement		
Resolution (Å)	2.4	2.4
No. reflections	17195	26251
R_{work} / R_{free}	0.20/0.25	0.17/0.20
No. atoms		
Protein	2261	4274
Ion	0	16 (4 x NO_3^-)
Water	77	228
B-factors		
Protein	76.3	39.1
Ion		49.6
Water	62.6	38.3
R.m.s. deviations		
Bond lengths (Å)	0.004	0.003
Bond angles (°)	0.758	0.643

2.3. Autoinhibition of TrkA and Ror2 TKDs

Both the TrkA and Ror2 TKDs share one of the key autoinhibitory features of IRK (Hubbard et al., 1994), projecting the second tyrosine of the YxxxYY (Tyr-Xaa-Xaa-Xaa-Tyr-Tyr motif found in the activation loop of IRK family kinases into the (tyrosine) substrate binding site. As shown in **Figure 2.2A**, tyrosines Tyr^{680} of TrkA and Tyr^{645} of Ror2 occupy the same position as Tyr^{1162} in IRK (Hubbard et al., 1994) (marked with an asterisk in **Figure 2.2A**), and make similar interactions with both the catalytic base aspartate (Asp^{650} and Asp^{615} in TrkA and Ror2 respectively, Asp^{1132} in IRK) and an arginine conserved in IRK family kinases (Arg^{654} and Arg^{619} in TrkA and Ror2 respectively, Arg^{1136} in IRK). The activation loop conformations of the TrkA and Ror2 TKDs are very similar to those seen in IRK, MuSK, and IGF1R (Hubbard et al., 1994; Munshi et al., 2002; Till et al., 2002) (**Figure 2.2A**), whereas the ALK, Met, and Ron activation loops are quite different (**Figure 2.2B**), as discussed below.

The TrkA and Ror2 TKDs in their inactive conformations also mirror other key aspects of the autoinhibitory mechanisms originally described for IRK (Hubbard et al., 1994) – although Ror2 has several unique features that suggest a slightly different mode of autoinhibition. The activation loop conformation in both the TrkA and Ror2 TKDs is such that it directly occludes the space in which the phosphate moieties of ATP would bind to an active kinase – as previously described for inactive IRK, MuSK, and IGF1R (Hubbard et al., 1994; Munshi et al., 2002; Till et al., 2002). As shown in **Figure 2.3**, backbone and/or side-chain atoms in the region following the DFG (Asp-Phe-Gly) motif occlude the phosphate-binding site, as seen in particular for Met^{671} and Ser^{672} of TrkA and Leu^{636} of Ror2. A switch from this so-called “DFG-out” (inactive) conformation seen in TrkA, Ror2 and inactive IRK to an “DFG-in” (active) configuration reverses this inhibition in the

active IRK structure, as seen at the left of **Figure 2.3**. Like IRK, inactive TrkA also places the side-chain of its DFG motif phenylalanine (Phe^{669}) into the binding site for the adenine ring to further block ATP binding. This feature is common to IRK (Phe^{1151}), MuSK, and IGF1R. However, Ror2 does not mimic this aspect of the autoinhibitory interactions – and has the Phe of its Asp-Phe-Gly motif replaced with a leucine. The unusual DLG (Asp-*Leu*-Gly) motif in Ror2 adopts an "DFG-out"-like conformation (**Figures 2.1 and 2.3**), but it is displaced approximately 4-4.5Å away from the ATP-binding site compared with that in IRK and TrkA, and therefore does not impact the location adopted by the adenine ring in active kinases. Instead, the side-chain of Tyr^{555}, two positions from the gatekeeper residue (Phe^{553}) at the end of strand β5 (and quite distant from the Asp-Phe-Gly motif), occupies an unusual position for inactive kinases, and occludes the predicted binding site for the ATP adenine ring (**Figure 2.3**). The corresponding residue is a tyrosine in numerous other TKDs, although it is replaced by phenylalanine or leucine in others. Regardless of the residue identity, however, the side-chain orientation in all other inactive IR family TKDs, as well as EGFR, FGFRs, and Src family TKDs is orthogonal to that of Tyr^{555} in Ror2, suggesting that the ability of this tyrosine to occlude the ATP binding site may be a feature unique to Ror2. It will be interesting to determine whether Tyr^{555} is a phosphorylation site in Ror2, and whether phosphorylation (or mutation) of this residue enhances kinase activity.

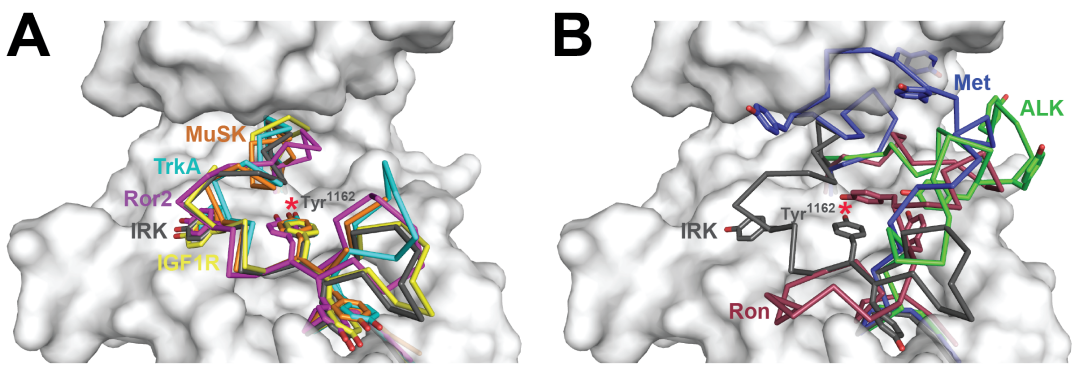

Figure 2.2. Comparison of activation loop configurations in IRK family kinases

Known inactive conformation structures of IRK family kinases (in addition to TrkA and Ror2) were overlaid on that of the insulin receptor (PDB 1IRK (Hubbard et al., 1994): grey – with the TKD shown in surface representation), and their activation loops colored. **(A)** The activation loops of MuSK (PDB 1LUF (Till et al., 2002): orange), TrkA (cyan), Ror2 molecule A (magenta) and IGF1R (PDB 1M7N (Munshi et al., 2002): yellow) align well with that of IRK. **(B)** The activation loops of Ron (PDB 3PLS (Wang et al., 2010): red), Met (PDB 2G15 (Wang et al., 2006): blue), and ALK (PDB 3L9P (Lee et al., 2010): green) are more widely variable and are compared with that of IRK (grey). Tyrosine side-chains in the YxxxYY motif are shown, and the substrate-mimicking tyrosine (Tyr^{1162} in IRK) is marked with a red asterisk.

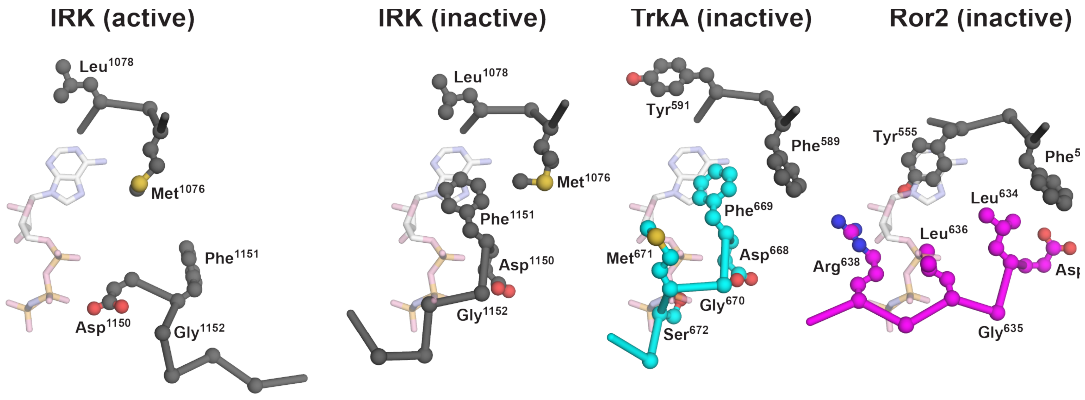

Figure 2.3. ATP binding-site occlusion by the activation loop in inactive IRK, TrkA, and Ror2 TKDs

Structures of the inactive TKDs from IRK (Hubbard et al., 1994), TrkA, and Ror2 were overlaid on the structure of active IRK (PDB 1IR3) determined with bound peptide substrate and a non-hydrolyzable ATP analog, adenylyl imidodiphosphate (AMP-PNP) (Hubbard, 1997). Close-up views of residues surrounding the binding site for AMP-PNP (shown from the 1IR3 structure) are shown for inactive IRK (activation loop colored grey), TrkA (activation loop colored cyan), and Ror2 (activation loop colored magenta). Whereas the 1IR3 (active) structure readily accommodates AMP-PNP, the nucleotide binding site is directly occluded by the activation loop in inactive IRK, TrkA, and Ror2 – with backbone and side-chain clashes with the phosphate groups. In addition, the Asp-Phe-Gly motif phenylalanine (Phe^{1151} in IRK and Phe^{669} in TrkA) blocks the binding site for the adenine ring of AMP-PNP. This inhibitory interaction is not maintained in Ror2, which has a Phe-to-Leu substitution in the DFG motif (yielding DLG), and Tyr^{555} from elsewhere in the TKD takes on a similar role.

2.4. Comparison with ALK, Met, Ron, and IRK autoinhibition

In contrast with the TKDs depicted in **Figure 2.2A**, the activation loops of inactive ALK, Met, and Ron do not interfere directly with ATP binding, and adopt a diverse array of conformations (Figure 2B). Tyrosines in the YxxxYY motif of ALK and Met do not project into the substrate binding site in the manner described above for TrkA, Ror2, and IRK. In Ron, Tyr^{1238} does occupy the substrate tyrosine site, but approaches from quite a different orientation than is seen in IRK and the other TKDs shown in **Figure 2.2**. Autoinhibition of ALK, Met, and Ron instead relies substantially on direct interactions between the activation loop and the αC helix – both displacing the αC helix from the position it adopts in active kinases and distorting the activation loop. This mode of autoinhibition is not employed by IRK (Hubbard et al., 1994) and is also not seen for MuSK or TrkA. Ror2 lies between these two scenarios. In addition to occluding the ATP-binding site like IRK, the Ror2 TKD activation loop also directly contacts the αC helix (**Figure 2.4**). It does so through predicted hydrogen bonds between Asp^{633} from the DLG motif and a αC arginine side-chain (Arg^{528}), made possible because of the 4-4.5Å displaced position of this motif away from the active site in Ror2. It is interesting that the αC helix is displaced further from the position adopted in active kinases in the case of inactive Ror2 than in the TrkA, IRK, MuSK, or IGF1R counterparts, and is closer to the position for the αC helix seen in Met and Ron. Thus, Ror2 appears to employ a "hybrid" mode of autoinhibition that involves both direct occlusion of the ATP-binding site and activation loop/αC interactions. By contrast, TrkA very closely resembles IRK.

The different modes of IRK family kinase autoinhibition are also reflected in their normal (ligand-dependent) activation mechanisms. The TKDs in **Figure 2.2A** resemble IRK,

with the initial activating event likely to be autophosphorylation of the tyrosine side-chain projecting into the substrate-binding site (Tyr^{680} in TrkA, Tyr^{645} in Ror2, Tyr^{1162} in IRK, Tyr^{1135} in IGF1R, and Tyr^{754} in MuSK) – thus reversing autoinhibition (Hubbard et al., 1994; Till et al., 2002). Phosphorylation of other tyrosines in the characteristic activation loop YxxxYY motif in these kinases disrupts additional autoinhibitory interactions (mostly with C-lobe residues) and/or stabilizes the active conformation. The TKDs depicted in **Figure 2.2B** vary. Since Ron places the side-chain of Tyr^{1238} from its activation loop in the substrate-binding site to inhibit the kinase, autophosphorylation of this tyrosine is likely to play a key role in receptor activation (Wang et al., 2010). In both ALK and Met, YxxxYY motif tyrosines instead stabilize autoinhibitory activation loop/αC interactions in the inactive state, without directly impacting the substrate-binding site. In Met, the Tyr^{1234} side-chain (equivalent to IRK Tyr^{1162}) directly contacts αC, and its phosphorylation is required for Met activation (Wang et al., 2006). Similarly, Tyr^{1278} in ALK (the first tyrosine in the YxxxYY motif) contributes directly to autoinhibitory activation loop/αC interactions, and its phosphorylation has been reported to be the initial event in ALK activation (Tartari et al., 2008).

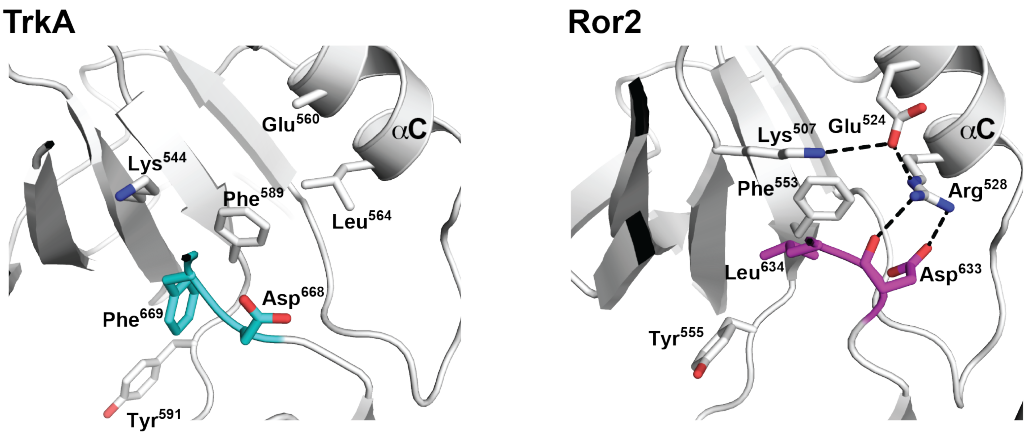

Figure 2.4. DFG motif conformation and activation loop/αC interactions in TrkA and Ror2 TKDs

Left: Close-up of the DFG motif region in TrkA-TKD, with the DFG motif itself colored cyan. Note the absence of salt-bridge between the β3 invariant lysine (Lys^{544}) and αC glutamate (Glu^{560}) – for which complete side-chain density was not seen. Van der Waal's contacts between the Phe^{589} and Leu^{564} side-chains are likely to contribute to stabilization of the αC position.

Right: Close-up of the DFG motif equivalent in Ror2-TKD (colored magenta), which has the sequence DLG – with Leu^{634} replacing the normal phenylalanine at this position in other kinases. Note that the β3 invariant lysine (Lys^{507}) forms a salt-bridge with the αC helix glutamate (Glu^{524}) even in the inactive Ror2 kinase (as also seen in ALK and Met), although the displaced αC helix position prevents Lys^{507} from contributing to an active-like ATP-binding site. The DLG motif of Ror2-TKD in the activation loop also interacts directly with the αC helix, thus stabilizing the inactive state through a mode that more closely resemble autoinhibition in Met, ALK, or EGFR. Arg^{528} in the αC helix interacts

directly with both backbone and side-chain of Asp^{633} in the DLG motif to stabilize this conformation. Mutations at Arg^{528} might be predicted to activate Ror2.

2.5. Possible relevance of TrkA and Ror2 TKD dimers

RTKs are well known to signal as dimers, with extracellular ligand binding inducing either dimerization or the transition from an inactive dimeric form to an active dimer (Lemmon and Schlessinger, 2010). Accordingly, functional significance has been attached to dimers of both active and inactive TKDs. Since the Ror2 TKD crystallized with two molecules in the asymmetric unit, we were therefore interested to ask whether any Ror2 or TrkA TKD dimer – non-crystallographic or crystallographic – might be functionally relevant, perhaps as an 'inactive dimer' of the sort suggested for a symmetric EGFR TKD structure (Jura et al., 2009). During the course of this work, other structures of Trk receptor kinases (Albaugh et al., 2012; Bertrand et al., 2012; Wang et al., 2012) and Ror2 were published or released in the Protein Data Bank (PDB). It was therefore important to determine whether these other structures share any crystal packing modes with the TrkA and Ror2 structures described in the present paper.

The unpublished Ror2 (PDB entry 3ZZW) contains two molecules in the asymmetric unit, in common with our structure. In both cases, the two Ror2 TKD molecules form an antiparallel dimer, burying a total surface area of 1,725$Å^2$ (our structure) and 2,640$Å^2$ (3ZZW) on the two TKDs. However, the surfaces involved in each interface are quite different. Within the Ror2 monomer, all of the structural features described here are maintained in 3ZZW, with the exception that molecule B in 3ZZW has a different DLG motif configuration and position – slightly closer to the "DFG out" conformation seen in

inactive IRK – so that the characteristic Asp^{633}/Arg^{528} hydrogen bond shown in **Figure 2.4** (between activation loop and αC helix) cannot form.

Of the two TrkA TKD structures in the PDB, one (entry 4AOJ) has an inhibitor bound (AZ-23), which forces the Asp-Phe-Gly motif into an "in" (rather than "out") conformation, and much of the activation loop is missing. Otherwise, this structure closely resembles the TrkA structure described here. There are three molecules in the 4AOJ asymmetric unit, but no crystallographic or non-crystallographic packing mode is shared with our TrkA structure. Recently published inhibitor-bound TrkB (Bertrand et al., 2012) and TrkC (Albaugh et al., 2012) structures also closely resemble our TrkA structure, although all but one (PDB code 4ASZ (Bertrand et al., 2012)) has an inhibitor bound, either displacing the DFG motif or flipping it into an "in" configuration. A TrkA structure with no inhibitor bound (Bertrand et al., 2012) was subsequently released (PDB entry 4F01). This closely resembles our structure and, interestingly, does appear to share one crystallographic dimer interface as described below.

We used the PISA (Protein Interfaces, Surfaces and Assemblies) server (Krissinel and Henrick, 2007) to search the PDB for crystal packing modes between TKDs similar to those seen for our Ror2 and TrkA structures. No examples were seen of TKDs that pack like Ror2, but close relatives of one of the TrkA crystallographic dimers were seen both in inhibitor-bound TrkC (PDB entry 3V5Q (Albaugh et al., 2012)) and eight PDB entries describing structures of the inactive TKD from fibroblast growth factor receptor-1 (FGFR1). This crystallographic TrkA dimer is shown in F**igure 2.5A**. A total surface area of 1,314 $Å^2$ is buried in the interface of this dimer, in which the two copies of the αC helix are parallel and directly contact one another. Further contacts are made between the C-terminus of the αC helix in one molecule and the C-terminus of the αE helix in its

neighbor. In addition, the N-terminus of each molecule projects towards the active site of its neighbor, terminating with uninterpretable electron density within the active site – possibly reflecting a mode of intermolecular autoinhibition in an inactive dimer. The N-terminus shows similar behavior in the crystallographic TrkC dimer seen in PDB entry 3V5Q, which buries a surface area of 1,136Å^2. Moreover, Mohammadi *et al*. (Mohammadi et al., 1996) highlighted a remarkably similar dimer when they first reported the structure of the inactive FGFR1 TKD (PDB entry 1FGK) – burying a surface area of 1,657Å^2. The fact that this dimer is seen for three different inactive TKDs, including one (FGFR1) that is only distantly related, suggests that it may be functionally relevant for inactive RTK TKDs. A second non-crystallographic TrkA TKD dimer, shown in Figure 5B, is shared by our TrkA structure and that of Bertrand *et al.* (Bertrand et al., 2012) (PDB entry 4F01) – although was not seen for other TKDs in the PDB. This dimer buries ~1,500 Å^2, primarily contributed by side-chains from the 'hinge' region that links β5 in the N-lobe and αD in the C-lobe, the kinase insert domain (between helices αD and αE), and strand β1 in the N-lobe. These interactions could also contribute directly to TKD autoinhibition in an inactive dimer.

As for many other RTKs, preformed inactive dimers of TrkA (Shen and Maruyama, 2011) and TrkB (Shen and Maruyama, 2012) have been reported based on crosslinking and complementation experiments, formation of which appears to require the intracellular domain. It is possible that one or both of the symmetric dimers of TrkA TKDs shown in Figure 5 plays a role in stabilizing such dimers, along similar lines to a proposed symmetric inactive dimer of EGFR that was observed crystallographically (Jura et al., 2009). Since the tyrosines of the activation loop YxxxYY motif are distant from the dimer interface in both dimers shown in **Figure 2.5**, their *trans*-autophosphorylation following

extracellular nerve growth factor binding would require a substantial rearrangement of such an inactive dimer if it exists in cells.

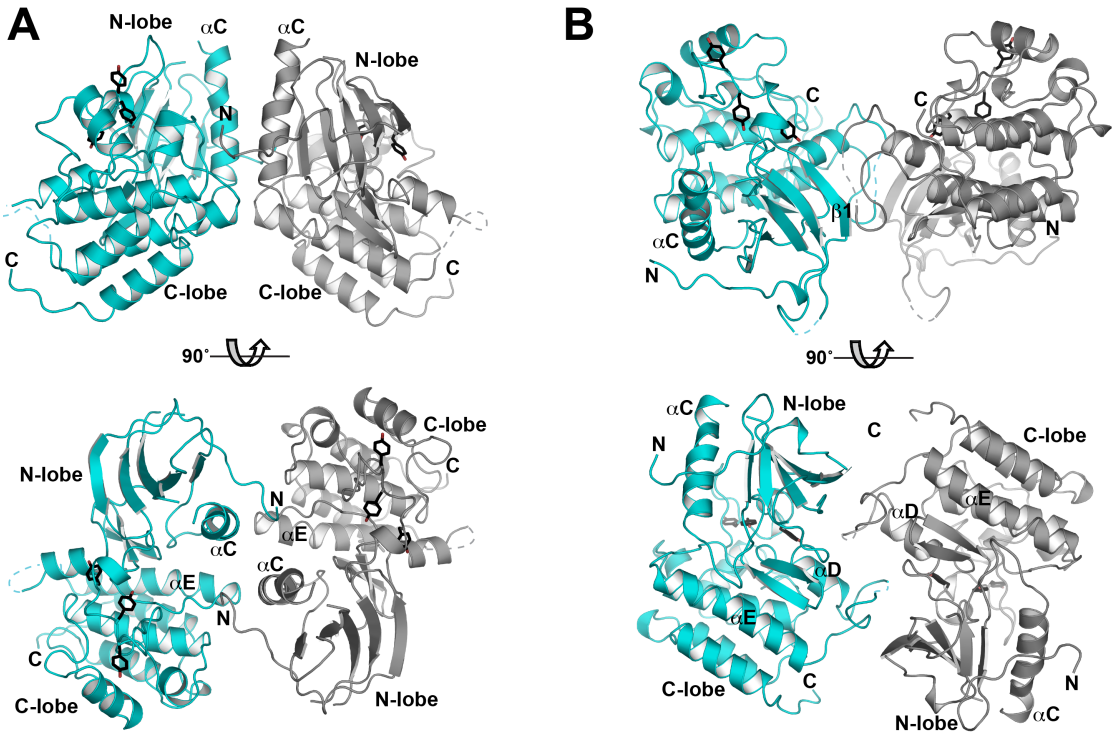

Figure 2.5. Inactive TrkA TKD dimers

Two orthogonal views of crystallographic dimers of TrkA TKDs. One TrkA TKD is colored cyan, and the other grey. **(A)** A dimer that is also found in an inhibitor-bound TrkC TKD crystal structure (PDB entry 3V5Q (Albaugh et al., 2012)) and in inactive FGFR1 TKD structures. The αC helix, which is responsible for the majority of the interactions is labeled, as is αE, the C-terminus of which also makes contributions to the dimer interface. The N- and C-termini of the TKD are marked. Note the projection of the N-terminus towards the TKD active site – a feature that is also seen in the TrkC crystallographic dimer from 3V5Q. **(B)** A dimer that is also found in another TrkA TKD

structure (PDB entry 4F0I (Bertrand et al., 2012)), which involves the 'hinge' region, kinase insert domain and strand β1. This dimer could help maintain the inactive configuration through restraints on the hinge region, for example. No evidence for TrkA TKD dimerization in solution was obtained in analytical ultracentrifugation studies (not shown). Tyrosines in the YxxxYY motif within the activation loop are colored black, to highlight the fact that they are quite distant in this dimer from the active site of the neighboring TKD that may *trans*-phosphorylate them. The tyrosine *trans*-autophosphorylation events that lead to TrkA activation could not occur in the context of this inactive dimer, but would require its reorganization upon extracellular ligand binding – or association with additional receptor molecules.

2.6. Activating mutations in IRK family TKDs

Figure 2.6 summarizes mutations found in the TKDs of IRK family receptor tyrosine kinases in cancer patients, from the COSMIC (Catalog Of Somatic Mutations In Cancer) database (Forbes et al., 2010) and a survey of the literature. Patient mutations are found in all of the TKDs discussed here, except for Ron (not pictured in **Figure 2.6**). Two main points emerge from this inspection. First, ALK and Met – IRK family TKDs with autoinhibitory interactions that do not involve direct occlusion of substrate- or ATP-binding sites – have been found mutated most frequently in cancer patients. With the caveat that this is a limited dataset, this observation may suggest that these TKDs are the most 'vulnerable' to mutational activation in cancer. Second, many of the cancer-associated mutations in ALK and Met are found in the activation loop and αC helix (red

in **Figure 2.6**), presumably reflecting an activating disruption of activation loop/αC helix interactions. Only two such mutations have been reported in these regions of Ror2, whereas only a single example is seen in TrkA and IGF1R and no examples have been reported in MuSK. Since stabilization of the autoinhibitory activation loop/αC interactions seen in ALK and Met (and in EGFR) is distributed over a large number of residues, we suggest that there are many positions at which activating oncogenic driver mutations can occur – which may increase their frequency. By contrast, where autoinhibitory interactions involve projection of an activation loop tyrosine into the substrate binding site, they are more 'focused' on that particular tyrosine – which will reduce the probability of oncogenic mutation. Accordingly, just as activating mutations in the TKD itself are rare in IGFR1R and MuSK, we expect them also to be quite infrequent in TrkA and Ror2 (and close relatives) based on the structures presented here.

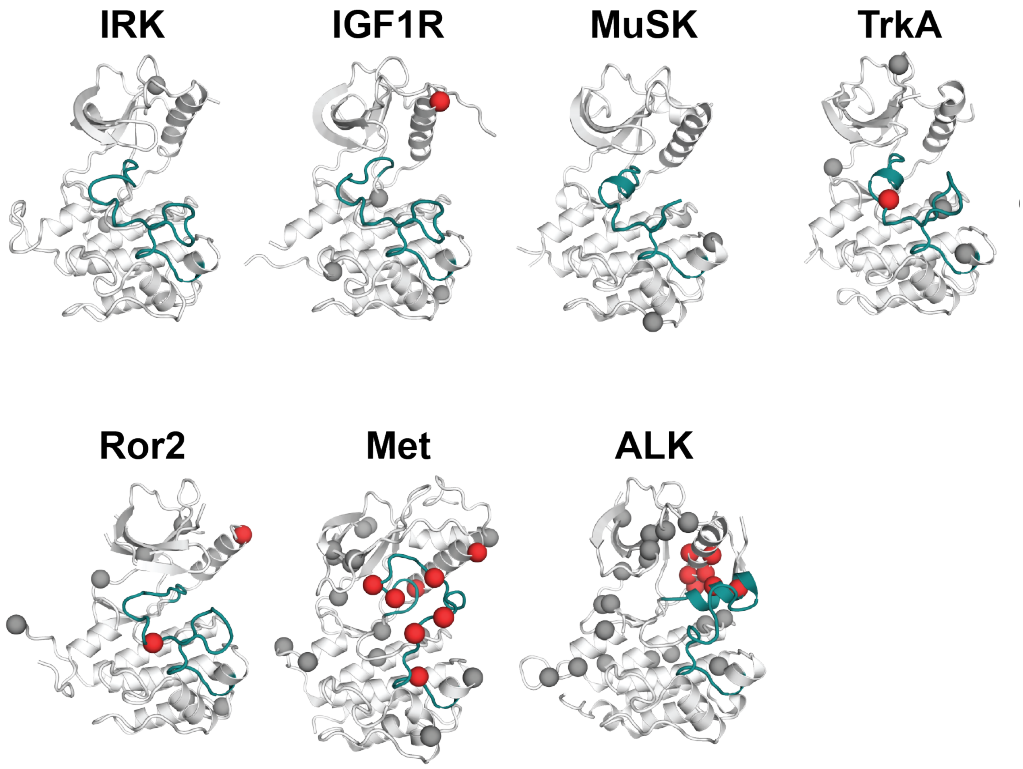

Figure 2.6. Somatic mutations in IRK family kinases in cancer

IRK family TKDs in their inactive conformation (PDB IDs listed in Figure 2) are shown in the same orientation as Figure 1, with the activation loop colored cyan. Sites at which mutations have been reported in cancer patients – in the literature or Catalog Of Somatic Mutations In Cancer (COSMIC: http://www.sanger.ac.uk/genetics/CGP/cosmic/) database (Forbes et al., 2010) – are represented as spheres, colored red if the mutations lie in the activation loop or αC helix. Note that the region of contact between the activation loop and αC helix is the site of many mutations in Met and ALK. TKDs without this autoinhibitory feature have fewer mutations to date, and fewer in the activation loop or αC. These analyses identify a vulnerability in ALK and Met for

oncogenic mutations as described in the text. Ron is not included because no mutations in this TKD have yet been described. IRK is included for comparison.

2.7. Conclusions

In conclusion, we describe crystal structures of the TrkA and Ror2 TKDs in their inactive states. The structures reveal that TrkA closely resembles IRK in its mode of autoinhibition (and presumably activation), relying only on occlusion of the substrate- and ATP-binding sites by the activation loop. On the other hand, Ror2 autoinhibition combines several elements; its activation loop occludes the substrate- and ATP-binding sites as seen in IRK, but with additional unique contributions from a tyrosine side-chain close to the gatekeeper residue. Moreover, interactions between the activation loop and αC contribute to Ror2 autoinhibition, suggesting that additional sites of vulnerability for activating mutations in Ror2 may exist that are not present in IRK, IGF1R and TrkA. We also describe a model for an inactive TrkA TKD dimer that closely resembles inactive dimers seen for the TKDs of TrkC and FGFR1.

Accession codes. Coordinates and structure factors of the TrkA and Ror2 TKDs have been deposited with PDB under the accession codes 4GT5 (TrkA) and 4GT4 (Ror2).

Chapter 3:

Origin of signaling differences between TrkA and TrkB

3.1. Introduction

Receptor tyrosine kinases (RTKs) play a central role in the fate of the cell by transmitting extracellular signals across the cellular membrane to initiate signaling cascades that dictate various cellular behaviors in response to ligand binding to a specific RTK. Ligand binding to the extracellular domain of RTKs promotes oligomerization, in turn activating *trans*-autophosphorylation of the intracellular tyrosine kinase domains (TKD). Autophosphorylation of the TKD activates the kinase further and also produces docking sites for downstream signaling molecules. Engagement of these signaling pathways leads to various cellular outcome such as proliferation, differentiation, or apoptosis (Lemmon and Schlessinger, 2010). As with many kinases, aberrant activity of TKDs either by mutation or altered expression can causes disease. Hence, kinase activity is exquisitely controlled by various factors including autoregulatory mechanisms and substrate specificity (Lemmon and Schlessinger, 2010; Ubersax and Ferrell, 2007).

TrkA and TrkB are members of the tropomyosin-related kinase (Trk) neurotrophin family of RTKs and are the receptors for nerve growth factor (NGF) and brain-derived growth factor (BDNF), respectively. Even though TrkA and TrkB appear to engage similar signaling networks when activated by their respective ligands, several studies have shown that activation of TrkA and TrkB in the same cell type can produce quite different cellular outcomes or responses. One important clinical example is seen in neuroblastoma, where TrkA expression (and activation) promotes cell differentiation and a favorable prognosis, whereas TrkB expression and activation causes cell proliferation and a grave prognosis for neuroblastoma patients (Borrello et al., 1993; Kogner et al., 1993; Matsumoto et al., 1995; Nakagawara et al., 1994a; 1993; 1994b; Suzuki et al.,

1993). How can two homologous RTKs, both thought to engage similar downstream signaling pathways, produces opposite cellular responses?

Classical studies in rat pheochromocytoma (PC12) cells investigating RTK signaling involved in differentiation and proliferation upon activation of endogenous TrkA and EGFR (or IRK), respectively, showed that TrkA activation results in a sustained phospho-Erk response whereas activation of EGFR results in a transient phospho-Erk response (Marshall, 1995; Murphy and Blenis, 2006). The duration of Erk activation has been shown to correlate directly with differentiation (sustained) or proliferation (transient) by phosphorylation-dependent regulation of immediate early gene product stability (Murphy et al., 2004). Other studies have demonstrated that feedback loops are involved in creating a sustained signal (positive feedback) versus a transient signal (negative feedback) (Murphy and Blenis, 2006). Yet, a question still remains as how the input of the signaling cascade affects the dynamics of the network. Overexpression of EGFR (or IRK) results in a sustained phospho-Erk signal and cellular differentiation indicating that the strength of signal from an RTK is an essential determinant of the cellular response (Dikic et al., 1994; Traverse et al., 1994).

Differences in receptor signal strength can be influenced by receptor intrinsic kinase activity, receptor density, receptor endocytosis and trafficking (Murphy and Blenis, 2006). The intrinsic kinase activity of RTKs is central to the function of RTKs and could affect other processes such as receptor trafficking. Thus, examination of the intrinsic kinase activities of the RTK TKDs is a first step for assessing the origin of any signaling differences.

Our hypothesis is that intrinsic properties of the TKDs of the relevant RTKs might define the differences in dynamics and nature of the responses to the individual receptors. For example, differences in the properties of the closely related TrkA and TrkB kinases may play a role in the disparate cellular response upon TrkA and TrkB activation in certain cell types. Varying levels of catalytic activity and autophosphorylation between highly homologous kinases often involved in distinct cellular phenotypes has been reported for the Tec family, Src family, and FGFR family of kinases (Iseki et al., 1999; Joseph et al., 2013; Latour et al., 1996; Lew et al., 2007). In the case of the Tec family, a recent report showed that a difference of six amino acids in the activation loop of Itk and Btk was the source of Btk's increased kinase activity. An Itk kinase harboring Btk's activation loop was more active and produced an elevated and sustained phospho-Erk signal in T cells (Joseph et al., 2013).

In this study, we investigated whether there are differences in kinase activity between TrkA and TrkB TKDs. We show that TrkA autophosphorylates itself faster than does TrkB. However, this difference of autophosphorylation is not due to a difference in kinase activity *per se*, since the kinetic parameters of TrkA and TrkB TKDs were all very similar when phosphorylation of peptide substrates was assessed. We also report data suggesting that the difference in autophosphorylation may be due to self-association of the TrkA TKD that does not occur with its TrkB counterpart. This study sheds light on potential differences between TrkA and TrkB signaling as well as providing a deeper quantitative understanding of Trk TKD activation, which is potentially useful for effective and selective inhibitor design.

3.2. Generation and characterization of TrkA and TrkB kinase domain constructs.

A sequence and structure alignment (**Figure 3.1**) was performed to facilitate the design of analogous TrkA (residues 498-796) and TrkB (residues 542-838) TKD constructs used for protein expression. The TKD constructs used in this study also contain the C-terminal tail (C-tail) since the C-tail in the Trk receptors is only 15 amino acids long. Notice that the TKDs are very similar except for the kinase insert domain (KID). The TrkA and TrkB kinase domain proteins were expressed in baculovirus-infected Sf9 cells and purified as described in Materials and Methods (Chapter 5). Circular dichroism (CD) spectroscopy was first used to assess general secondary structure features of TrkA and TrkB. As seen in **Figure 3.2A**, the general profiles of TrkA and TrkB are very similar and indicative of both proteins being similarly folded and over 65% α-helix (as expected). To assess the thermal stability of these proteins, I also performed temperature melts monitored by CD spectroscopy. TrkA and TrkB TKD proteins were diluted into a compatible buffer for CD analysis (25mM NaH_2PO_4 •K_2HPO_4 pH7.4, 150mM NaCl) at a concentration of 2 μM, and were subjected to increasing temperatures from 1 to 97°C (See Chapter 5, Materials and Methods), and CD was monitored at 222 nm (the α-helix signature minimum). The apparent T_m values for both the TrkA and TrkB TKDs were above 37°C (**Figure 3.2B**), indicating that these proteins are stable during the experimental conditions I used to study these proteins. Specifically, T_m values were 39.5˚C and 47.9˚C for TrkA and TrkB TKDs respectively. Sedimentation equilibrium analytical ultracentrifugation experiments were also performed to ensure that the TrkA and TrkB TKD proteins do not aggregate in solution. As shown in Figure 3.3, both TrkA and TrkB TKDs are primarily monomeric in solution at concentrations of 16.7 μM and 17.6 µM, respectively, with apparent molecular

weights of 35 kDa for TrkA-TKD and 31 kDa for TrkB-TKD. The residuals for a fit of the data to a single monomeric species were small and randomly distributed, indicating no systematic deviation (and therefore a reasonable fit).

Figure 3.1. Alignment of TrkA and TrkB intracellular domains.

A sequence alignment of human TrkA (P04629-1) and TrkB (Q16620-4) intracellular domains showing the secondary structure for the TrkA TKD used to design constructs. Indicated on the alignment are the boundaries of the TrkA and TrkB constructs. The N-

terminal boundary immediately precedes the kinase domain, whereas the C-terminal boundary of the construct coincides with the C-terminus of the full-length protein. Also shown below the sequences are key motifs of each kinase domain including the hinge region (blue box), kinase insert domain (KID, magenta box) and the activation loop (grey box). Clustal Omega was used to generate the alignment and ESPript (http://espript.ibcp.fr) was used to generate the figure (Gouet, 2003; Sievers et al., 2011).

A)

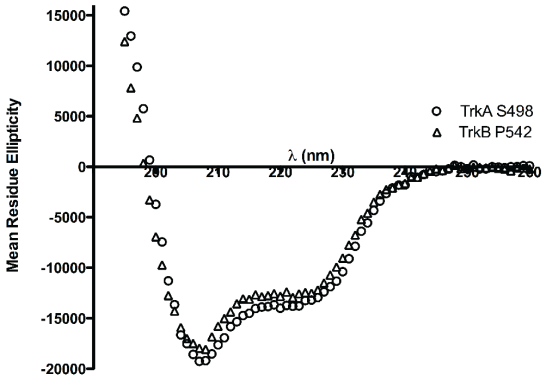

B)

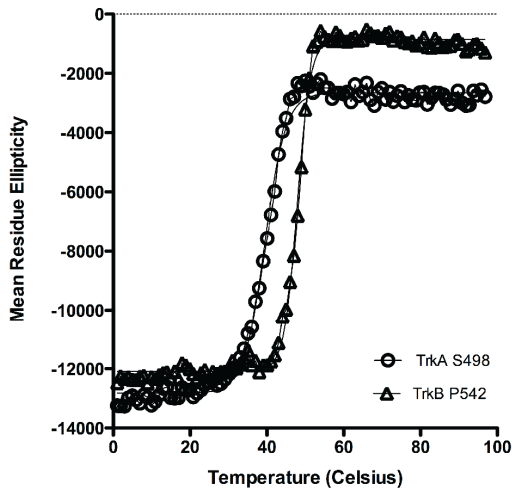

Figure 3.2. TrkA and TrkB TKDs have similar secondary structure composition and are stable at 37°C.

(A) The CD spectra of TrkA and TrkB TKDs show similar features indicating that neither of these constructs are grossly misfolded. The predicted helix and sheet composition determined by the K2D3 server (Louis-Jeune et al., 2011) is 69.7% helix and 1.5% sheet for TrkA-TKD and 66.2% helix and 2.9% sheet for TrkB-TKD. CD measurements in the far UV spectral region (195-260 nm) were performed on an Aviv 62A DS spectropolarimeter. (B) Plotting the CD thermal melts of TrkA and TrkB TKDs demonstrate that both proteins are stable at 37°C. Samples were heated from 1°C to 97°C in 1°C increments with the circular dichroism at 222 nm being measured at each step.

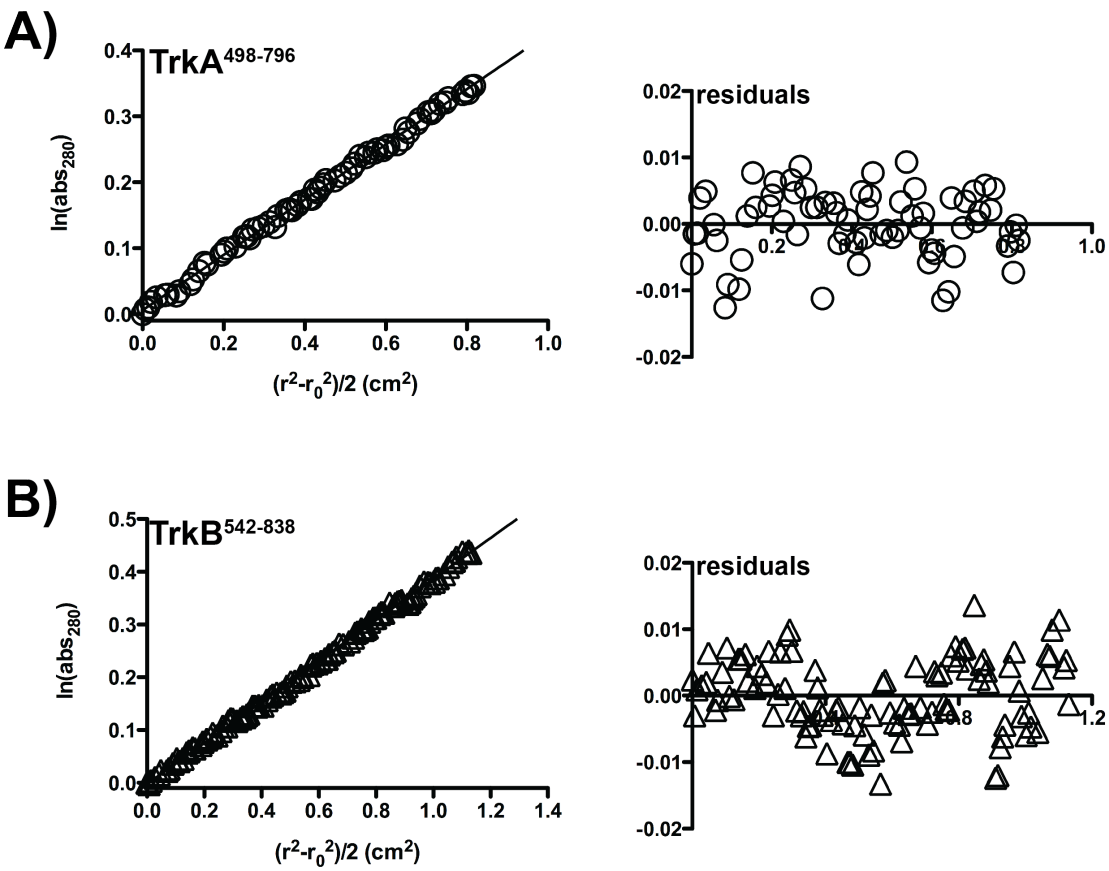

Figure 3.3. TrkA and TrkB TKDs are largely monomeric in solution.

Sedimentation equilibrium (SE) analytical ultracentrifugation (AUC) experiments were performed with 16.7 μM of TrkA-TKD and 17.6 μM of TrkB-TKD to assess protein self-association. To analyze the data, the natural logarithm (ln) of absorbance at 280 nm was plotted against a function of the radius squared (r^2-r_o^2)/2, where r is the radial position in the sample and r_o is the radial position of the meniscus. This analysis provides a straight line (for a single species) with slope proportional to the molecular mass of the species. Data collected at 10,000 rpm with best-fit lines are shown for TrkA-TKD (A) and for TrkB-

TKD (B). The apparent molecular weights calculated for the TrkA and TrkB TKDs are 35 kDa and 31 kDa, respectively. The predicted molecular weights based on sequence for TrkA and TrkB TKDs are 34.8 kDa and 35.1 kDa, respectively. It is important to note that the TrkA-TKD sample for AUC was not treated with phosphatases during purification whereas the TrkB sample was treated with phosphatases during purification. Regardless, the apparent molecular weights suggest that these proteins are mostly monomeric in solution and there are no signs of significant aggregation.

3.3. An autophosphorylation assay reveals differences between TrkA and TrkB TKDs.

Autophosphorylation of the Trk receptors following their activation is well established (Kaplan et al., 1991a; 1991b; Klein et al., 1991a; 1991b; Soppet et al., 1991; Squinto et al., 1991). The full-length Trk receptors contain five known sites of autophosphorylation. Three sites reside in the activation loop as part of the YxxxYY motif, one site lies in the juxtamembrane (JM) region, and another lies in the C-terminal tail (CT) (Guiton et al., 1994; Loeb et al., 1994; Middlemas et al., 1994; Stephens et al., 1994). The TrkA and TrkB TKDs used for this study do not contain the JM region – since its removal was necessary for the production of high levels of homogenous protein – so I only monitored phosphorylation at four tyrosines in my *in vitro* studies.

For an initial qualitative approach to visualizing the progression of TrkA and TrkB TKD autophosphorylation, I used native PAGE. However, the native gels were difficult to interpret due to more than expected species identified on the gels (**Figure 3.4**). We

speculate that these species may arise from heterogeneity of the starting material arising from various types of post translational modification (see below results from mass spectrometry of the starting material), or different combinations of autophosphosphorylation site usage.

For a better, more quantitative, approach to monitoring progression of autophosphorylation, I added trace amounts of γ-^{32}P ATP to the autophosphorylation reaction and visualized its incorporation into the TKD by SDS PAGE-based autoradiography. The image captured by a Phoshorimager was then analyzed using ImageStudio software, and normalized using the near infrared fluorescence signal from protein-bound Coomassie blue stain from the same gel. As shown in **Figure 3.5**, TrkA TKD autophosphorylation occurred faster than TrkB TKD autophosphorylation at both 37° and RT. Interestingly, once both TrkA-TKD and TrkB-TKD autophosphorylation peaked, there was an apparent loss of signal over time. This presumably represents dephosphorylation of the TrkA and TrkB TKD proteins.

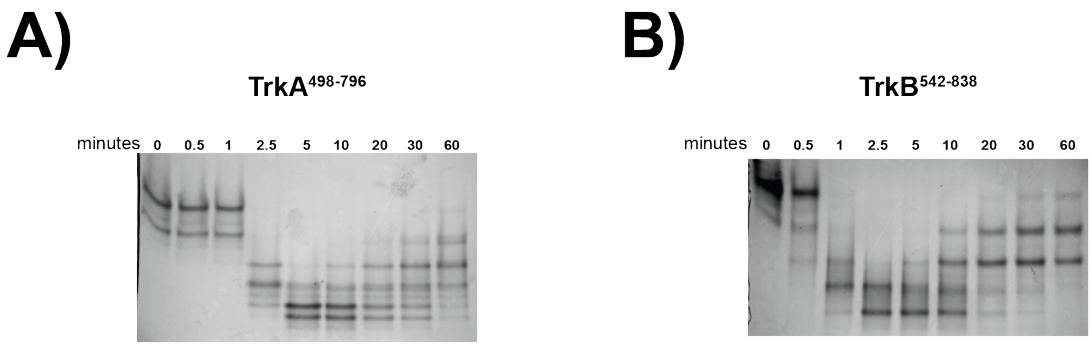

Figure 3.4. Initial native PAGE analysis of TKD autophosphorylation.

Native gels of samples from autophosphorylation reactions with (A) TrkA TKD and (B) TrkB TKD at 10 μM, incubated at 37°C for the indicated times. Both of these constructs have four tyrosines that are known to be autophosphorylated, yet at times there are 5-6 bands on the native gel, presumably reflecting different combinations of autophosphorylation site usage or due to heterogeneous starting material.

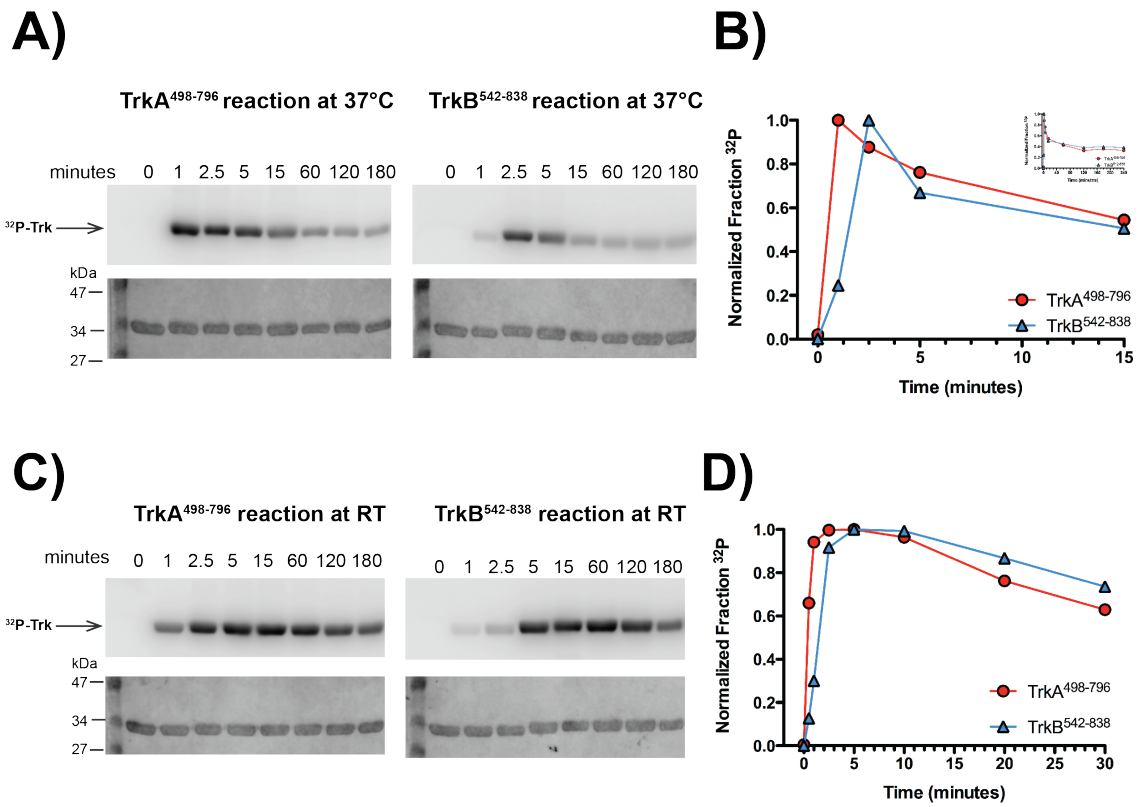

Figure 3.5. TrkA-TKD autophosphorylates faster than TrkB-TKD.

(A) Autoradiographs and Coomassie gel of a time course of TrkA and TrkB TKD autophosphorylation, using 10 μM protein at 37°C. (B) Quantitation of the autoradiography signal normalized by the amount of protein in each lane detected by Coomassie stain for the autophosphorylation reactions at 37°C. (C) Autoradiographs and Coomassie gel of autophosphorylation reactions performed at RT. (D) Quantitation of the RT autophosphorylation experiment as described above.

3.4. TrkA and TrkB TKDs autodephosphorylate in a similar manner

As mentioned above, the initial autophosphorylation reactions demonstrated a loss of ^{32}P signal over time. It was important first to determine whether this reflected a contaminating phosphatase, since phosphatase contamination would impact the interpretation of the autophosphorylation assays. Mass spectrometry analysis of the purified product did show trace amounts of the baculovirus phosphatase (BVP). BVP was initially classified as a protein phosphatase, but subsequent reports have suggested that BVP is only a modest protein phosphatase and is a much more potent RNA 5'-triphosphatase (Takagi et al., 1998). Furthermore, the activity of BVP is greatly reduced by 1 mM $MgCl_2$ or 200 μM sodium vanadate (Gross and Shuman, 1998; Kim and Weaver, 1993; Sheng and Charbonneau, 1993). The TrkA and TrkB autophosphorylation reactions contain 10 mM $MgCl_2$, arguing that BVP should be inhibited under these reaction conditions.

That the observed dephosphorylation was not simply due to a contaminating phosphatase was demonstrated by experiments using several different phosphatase inhibitors including sodium vanadate and the 'Halt' phosphatase inhibitor cocktail. None of these treatments significantly altered the dephosphorylation profile as compared with the control experiment lacking phosphatase inhibitors (**Figure 3.6**). Moreover, preparations generated using a new purification scheme were more homogeneous (**see Chapter 3.5**) and showed no signs of phosphatase contamination by mass spectrometric analysis.

There are numerous scattered reports in the literature demonstrating 'futile' ATPase activity of kinases, reversal of the kinase reaction, or substrate dephosphorylation by

kinases (Al-Hasani et al., 1994; Argetsinger and Shafer, 1992; Bae et al., 2010; Chen et al., 2000; Favelyukis et al., 2001; Fukami and Lipmann, 1983; Gruppuso et al., 1992; Kim et al., 2001; Mendelow et al., 1993; O'Brian and Ward, 1991; Parast et al., 1998; Paudel and Carlson, 1991; Pike et al., 1986; Ward and O'Brian, 1992; Yang et al., 2004). PKA, PKC, phosphorylase kinase, and p38 MAP kinase have all been shown to have intrinsic ATPase activity. For PKA and PKC, at least, this ATPase activity is dependent on solvent accessibility of the substrate binding pocket (Chen et al., 2000; Mendelow et al., 1993; O'Brian and Ward, 1991; Paudel and Carlson, 1991; Ward and O'Brian, 1992; Yang et al., 2004). There are reports that Src, CaM-kinase II, VEGFR2 TKD, and IRK can reverse the kinase reaction with generation of ATP – in an ADP-dependent manner (Argetsinger and Shafer, 1992; Fukami and Lipmann, 1983; Kim et al., 2001; Parast et al., 1998; Pike et al., 1986). On the other hand, there are clear reports of IRK autodephosphorylation generating free inorganic phosphate – which is inconsistent with reversal of the kinase reaction. These IRK studies showed that autodephosphorylation is dependent on the kinase active site, since staurosporine (a promiscuous ATP competitive kinase inhibitor) and EDTA both abolish dephosphorylation (Al-Hasani et al., 1994; Gruppuso et al., 1992). There is additional evidence in the literature of autodephosphorylation of IGF1R and FGFR1 (Bae et al., 2010; Favelyukis et al., 2001). Thus, there is clear precedent for the observation that RTKs autodephosphorylate. It is important to note that many of the above mentioned kinases utilize some variation of pseudosubstrate autoinhibition as a mechanism of autoregulation.

Autodephosphorylation of the TrkA and TrkB TKDs occurred to varying degrees depending on the reaction conditions. One of the factors that seemed to play a role in dephosphorylation was the concentration of Trk TKD protein, as shown for TrkA in

Figure 3.7. Higher concentrations (10 μM TrkA) clearly accelerate autophosphorylation as well as autodephosphorylation compared to reactions with 1 μM TrkA, suggesting that both may be intermolecular reactions.

Taken together, the dephosphorylation of TrkA and TrkB TKDs appears unlikely to be caused by phosphatase contamination. I decided not to pursue the autodephosphorylation of TrkA and TrkB TKDs any further, since this is a phenomenon reported in the literature for other kinases, and appears to be substantially slower than basal RTK dephosphorylation by protein tyrosine phosphatases that is seen in a cellular context (Kleiman et al., 2011). Moreover, autodephosphorylation occurs in a similar manner for both TrkA and TrkB TKDs (**Figure 3.5**), so is unlikely to be an important factor that underlies their signaling differences. These data do argue that the difference in rates of autophosphorylation between TrkA and TrkB TKDs is intrinsic to their TKDs, however, and is not simply due to contaminating phosphatases.

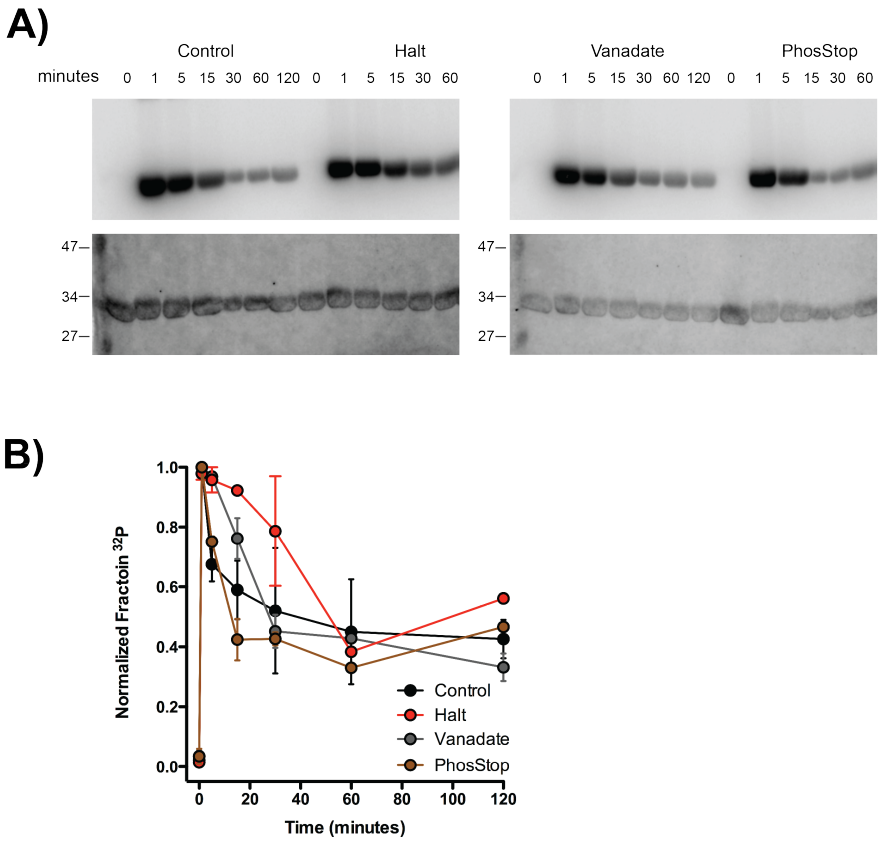

Figure 3.6. Phosphatase inhibitors do not affect dephosphorylation of TrkA-TKD.

Autophosphorylation reactions of TrkA-TKD at 10 μM were performed in the absence of phosphatase inhibitor as in Figure 3.4, but also in the presence of sodium vanadate, 'Halt' cocktail phosphatase inhibitor (including sodium fluoride, sodium orthovanadate, sodium pyrophosphate, and β-glycerophosphate), or 'PhosStop' cocktail phosphatase inhibitor (a proprietary blend of phosphatase inhibitors). (A) Autoradiographs and Coomassie gel of a time course of TrkA-TKD autophosphorylation at 37°C without or with phosphatase inhibitors. (B) Quantitation of the autoradiography signal normalized by the amount of loaded protein detected by Coomassie stain.

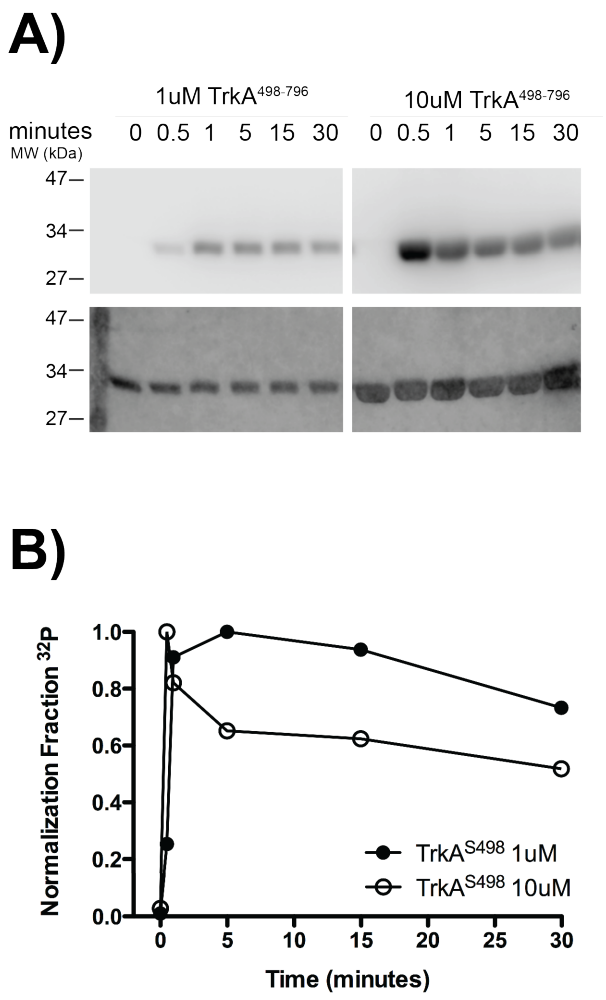

Figure 3.7. Concentration dependence of autodephosphorylation of TrkA-TKD. Autophosphorylation reactions were performed either with 1μM or 10 μM TrkA-TKD. (A) Autoradiographs and Coomassie gel of TrkA-TKD autophosphorylation at 37°C. (B) Quantitation of the autoradiography signal normalized by the amount of protein loaded detected by Coomassie stain.

3.5. Optimizing purification scheme to ensure homogenous TKDs as starting material

Initial attempts to analyze the autophosphorylation of TrkA and TrkB TKDs suggested that the proteins from Sf9 cells are modified. SDS PAGE Western blotting with a general phosphotyrosine antibody (pY20) of TrkA and TrkB TKD autophosphorylation reactions did not yield detectable signal at the zero minute time point. However, there was a weak signal from one of the phosphospecific antibodies (pY676) for both TKDs, demonstrating that the starting material is phosphorylated (shown clearly in **Figure 3.10**). **Figure 3.8** shows that TrkA TKD autophosphorylates faster than TrkB-TKD, but we were concerned about interpreting these results if the two proteins are differently modified during overexpression in Sf9 cells. I therefore used the PhosTag gel approach to further monitor phosphorylation of the starting material and the autophosphorylation reactions. PhosTag gels are polyacrylamide gels with the PhosTag acrylamide reagent coordinated with Zn^{2+} in the resolving gel. Phosphorylated species bind to the acrylamide-associated metal and hence migrate more slowly during gel electrophoresis (Kinoshita and Kinoshita-Kikuta, 2011). It is evident by Coomassie stain and Western blotting of autophosphorylation reactions analyzed on PhosTag gels that the starting material (0 minute time point) is already modified to some degree, particularly for the TrkB TKD (**Figure 3.8C,D**)

We performed LC MS/MS mass spectrometry to investigate post translational modification of the TrkA and TrkB TKD starting material. **Figure 3.9** shows the peptides identified and post translational modification of the TrkA-TKD and TrkB-TKD starting material. These mass spectrometry data confirmed the Western blotting data that both TrkA and TrkB TKDs were tyrosine phosphorylated to some degree. To address

heterogeneity concerns of the starting material, I therefore developed a purification scheme including phosphatase treatments and additional steps of purification (see **Chapter 5, Material and Methods**). As shown in **Figure 3.9** and **Figure 3.10**, this new purification scheme was successful in producing a more homogenous sample as well as ensuring no phosphatase contamination. **Figure 3.9C,D** shows there is much less post translational modification of the TrkA and TrkB TKD samples following the optimized purification scheme. There are still trace amounts of phosphorylation of TrkA and TrkB TKDs, but not in the regions of the TKD that we are most concerned with, namely the activation loop and the C-terminal tail. Phosphospecific Western blotting was also used to examine sample quality of the TrkA-TKD and TrkB-TKD starting materials during all subsequent optimized purifications (**Figure 3.10**).

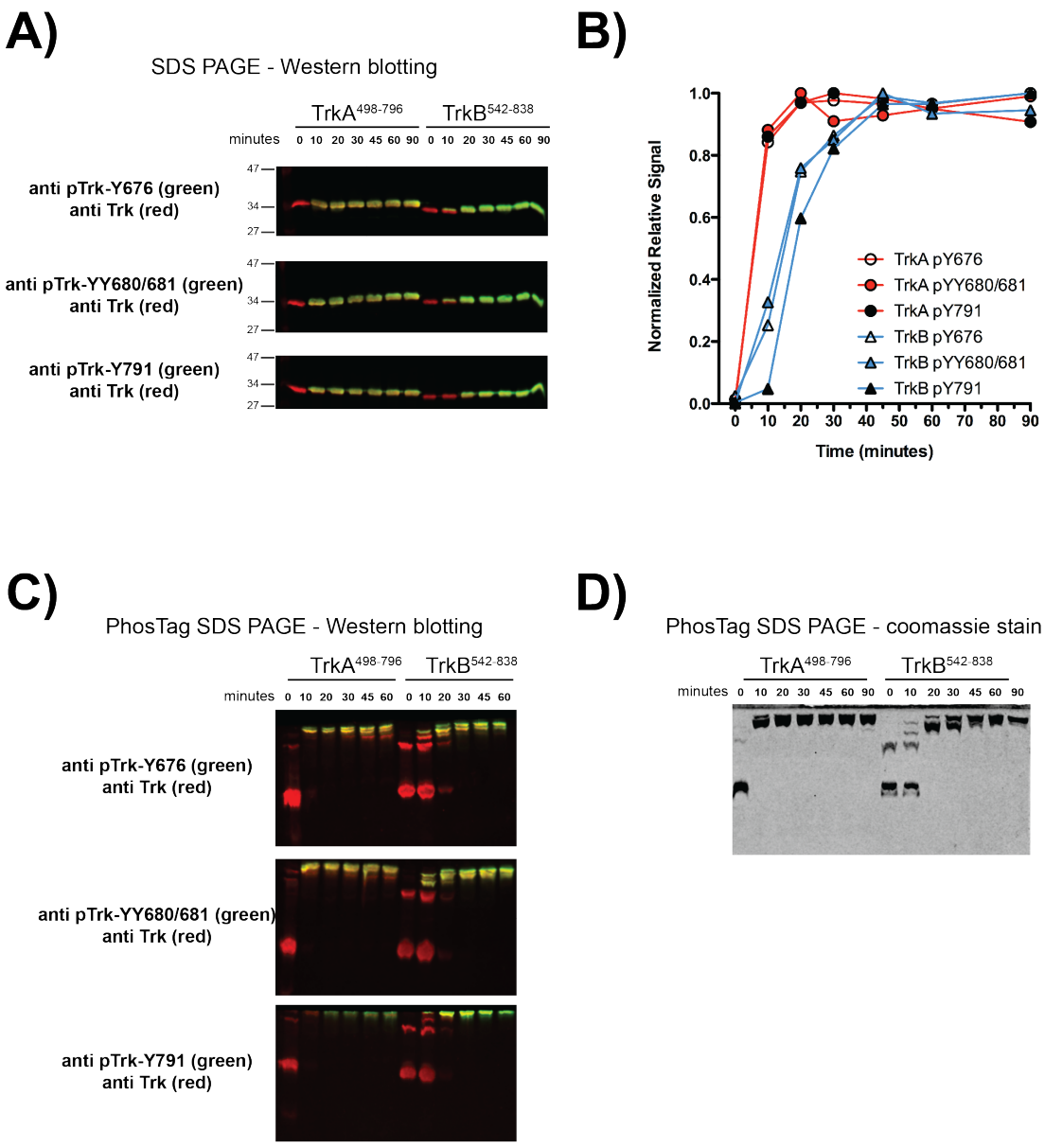

Figure 3.8. Initial assessment of TKD autophosphorylation by phosphospecific antibodies and PhosTag gels.

TrkA-TKD and TrkB-TKD autophosphorylation assays were analyzed using SDS PAGE Western blotting probed with Trk antibodies (red) and phosphospecific antibodies (pY676, pYY680/681, pY791; human TrkA isoform *II* numbering) (green). (A) SDS PAGE

Western blots of TrkA and TrkB TKD autophosphorylation reactions and (B) quantitation of the normalized signals from these plots. (C) PhosTag SDS PAGE Western blots and (D) Coomassie stained PhosTag gel of TrkA and TrkB TKD autophosphorylation reactions.

A)

Untreated TrkA

Legends:
+15.99 : Oxidation +42.01 : Acetylation +79.97 : Phosphorylation

B)

Untreated TrkB

C)

Phosphatase treated TrkA

D)

Phosphatase treated TrkB

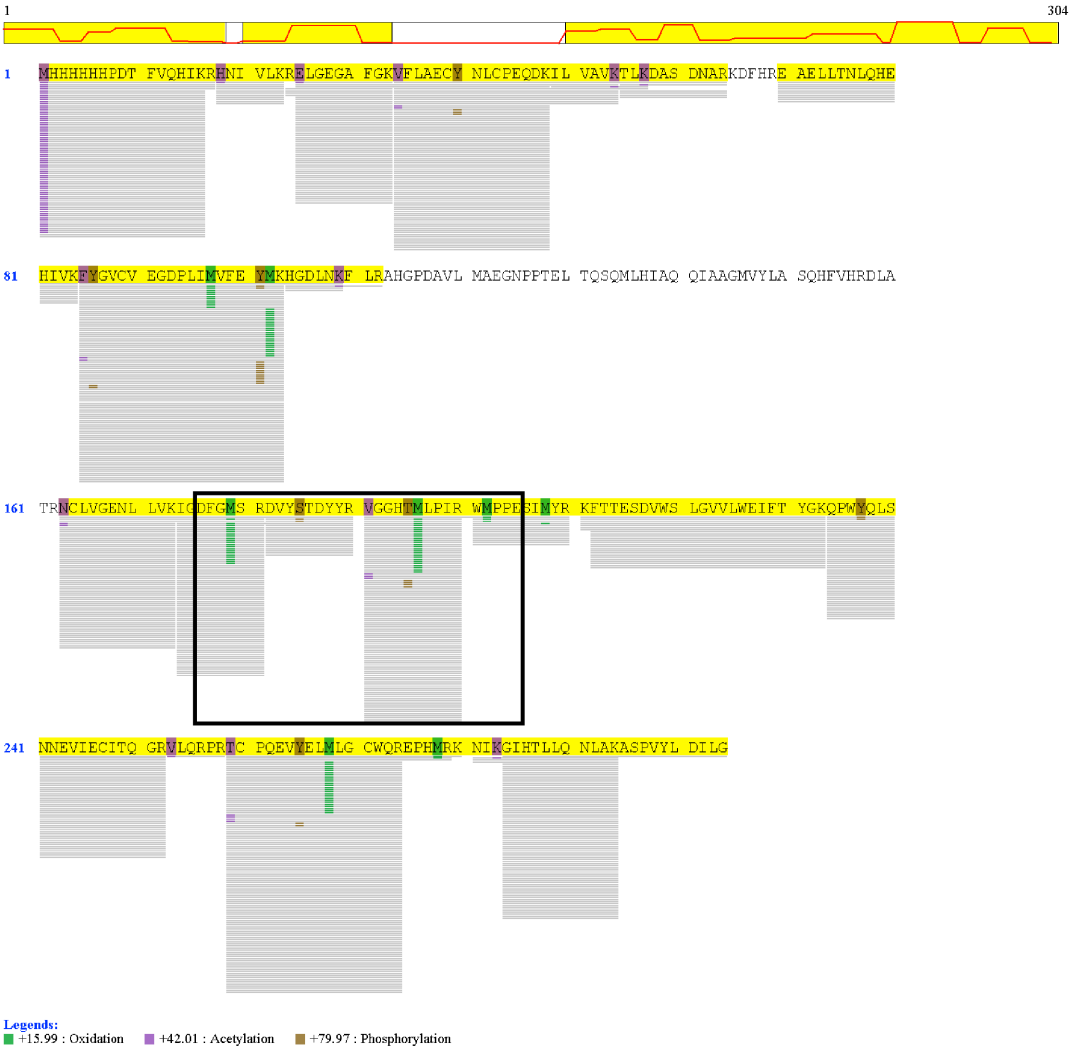

Figure 3.9. Mass Spectrometry analysis of TrkA-TKD and TrkB-TKD plus or minus phosphatase treatment. TrkA-TKD (A) and TrkB-TKD (B) samples not treated with phosphatases. TrkA-TKD (C) and TrkB-TKD (D) samples treated with phosphatase and subject to more purification steps. Samples were submitted to the Wistar Institute proteomic facility for in-solution digestion and LC-MS/MS analysis. The amino acid peptide coverage of the mass spectrometry analysis is showed by grey lines below the Trk sequences. Modified residues are highlighted in green (oxidation), purple (acetylation), and brown (phosphorylation). The activation loop (boxed region in the peptide coverage map) tyrosines are no longer phosphorylated after phosphatase treatment.

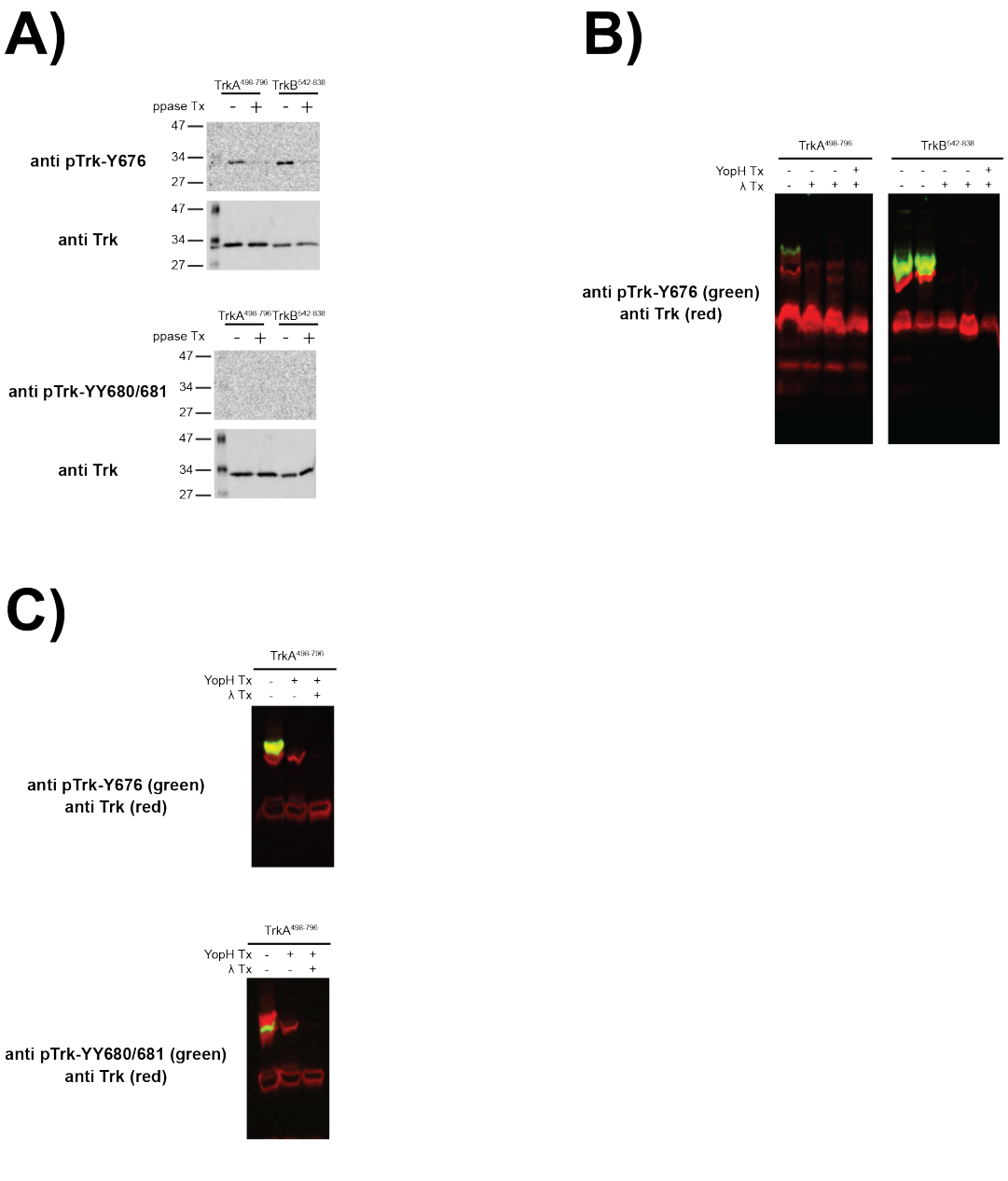

Figure 3.10. Monitoring protein phosphorylation during purification.

(A) Phosphospecific Western blotting of purified protein stock that was also used for the LC-MS/MS mass spectrometry analysis. (B) PhosTag SDS PAGE phosphospecific Western blotting of TrkA and TrkB TKD samples taking during the phosphatase treatment phase of the optimized purification scheme. (C) Another example of PhosTag

SDS PAGE phosphospecific Western blotting of TrkA-TKD during protein purification to ensure the starting material is mostly dephosphorylated.

3.6. TrkA-TKD autophosphorylates faster than TrkB-TKD, and the order of phosphorylation site usage is the same for both TrkA and TrkB TKDs.

The sequential order of phosphorylation has been shown to be vital for stepwise increments of kinase activity for kinases that are dependent on phosphorylation of activation loop residues for full activity (Favelyukis et al., 2001; Furdui et al., 2006). Thus, differences in order can impact both the autophosphorylation profile and ultimate kinase activity. Studies with FGFR, EGFR and Ret RTKs have shown that pathogenic mutations can disturb the autophosphorylation order of the WT receptor, illustrating further that differences in order of autophosphorylation can impact cellular phenotype in important ways (Kim et al., 2012; Lew et al., 2009; Plaza-Menacho et al., 2014).

The autophosphorylation sites of TrkA and TrkB have been identified previously, and autophosphorylation occurs at analogous sites in TrkA and TrkB (Guiton et al., 1994; Loeb et al., 1994; Middlemas et al., 1994; Stephens et al., 1994). The order of phosphorylation of these sites has not been directly studied for either TrkA or TrkB. Comparison of the published order of autophosphorylation for other members of the IRK TKD family (**Table 3.1)** reveals a diversity that does not necessarily correlate with the class of activation loop conformation discussed in Chapter 2. IRK autophosphorylation proceeds in the same order as seen for IGF1R, but autophosphorylation of the MuSK, Met and Alk kinases are all distinct. The Met and Alk activation loop conformations (in

their inactive structures) are distinct from other IRK TKD family members (**Figure 2.2**), so it is not surprising that these kinases employ different orders of autophosphorylation from that seen with IRK and IGF1R. However, the MuSK TKD activation loop superimposes very well with IRK, IGF1R and TrkA in crystal structures (**Figure 2.2**), so it seems surprising that MuSK employs a different order of autophosphorylation site usage than IRK and IGF1R. This observation also opens up the question as to what is the site usage order in the Trk TKDs.

Table 3.1. Previously reported autophosphorylation orders for the IRK TKD family.

RTK	1st Site	2nd Site	3rd Site	Sequence	References
IRK	Yxxx**pY**Y	**pY**xxxpYY	pYxxxpY**pY**	Y1162, Y1158, Y1163	(Wei et al., 1995)
IGF1R	Yxxx**pY**Y	**pY**xxxpYY	pYxxxpY**pY**	Y1135, Y1131, Y1136	(Favelyukis et al., 2001)
MuSk	Yxxx**pY**Y & JM-**pY**	**pY**xxxpY**pY**	-	Y754/Y552, Y750/Y755	(Till et al., 2002)
Met	YxxxY**pY**	Yxxx**pYpY**		Y1235, Y1234	(Chiara, 2003)
Alk	**pY**xxxYY	-	-	Y1278	(Donella-Deana et al., 2005)

I used Western blotting with phosphospecific antibodies to visualize the order of autophosphorylation for the TrkA and TrkB TKDs. The concentrations of Trk TKD used for the autophosphorylation experiments were between 1 μM and 10 μM which is consistent with the estimated concentration of RTKs on the cell surface (Lemmon et al., 1997). The antibodies used recognize phosphorylation at either the first tyrosine of the pYxxxYY motif (anti pY676; TrkA numbers are listed), the second and third tyrosines of the YxxxpYpY motif (anti pYY680/681) or the C-terminal tail tyrosine (anti pY791) of

TrkA and TrkB. The specificity of antibodies targeting Trk autophosphorylation (pYY680/681 and pY791) sites has been previously tested with mutagenesis and peptide competition assays (Choi et al., 2001; Segal et al., 1996).

TrkA and TrkB TKD autophosphorylation assays were conducted at 15°C in order to be able to distinguish differences, and samples taken at the different time points were subjected to either SDS PAGE or PhosTag SDS PAGE for Western blotting and Coomassie staining. Each Western blot was probed with a phosphospecific antibody and a total Trk antibody. For the SDS PAGE Western blots each phosphospecific signal was normalized for total Trk. Normalized signal from a phosphospecific antibody was then expressed as a fraction of the maximum signal seen with that antibody for TrkA or TrkB autophosphorylation respectively. Using these data, the normalized relative signals for each phosphospecific antibody could be compared directly between sites and TKDs (**Figure 3.11**). Quantitation of these Western blots revealed once again that TrkA TKD autophosphorylation at all sites occurs more rapidly than that seen for the TrkB TKD. The order of autophosphorylation, however, appears to be the same for TrkA and TrkB TKDs in the context of the phosphospecific antibodies used here to monitor autophosphorylation. PhosTag SDS PAGE was utilized to further characterize the order and rate of autophosphorylation of TrkA and TrkB TKDs. The PhosTag acrylamide reagent coordinates Zn^{2+}, which is able to bind phosphates of any phosphorylated species. Binding of the phosphorylated proteins to PhosTag-Zn^{2+} lowers their mobility, resulting in band shifts related to the number of phosphates incorporated in a particular phosphorylated species (and thus the degree of PhosTag-Zn^{2+}) binding. Phosphospecific Western blotting was used to identify the various phosphorylated species during a time course of autophosphorylation (**Figure 3.11**). Assignment of the

phosphorylated species is shown on the Coomassie-stained gel in **Figure 3.11D**. The data from various SDS PAGE and PhosTag SDS PAGE phosphospecific Western blots were compiled to determine the order of autophosphorylation for TrkA and TrkB TKDs.

The autophosphorylation experiments were repeated under various conditions, and the rate of TrkA-TKD autophosphorylation was always faster than seen with TrkB-TKD. Furthermore, the order of autophosphorylation for TrkA and TrkB TKDs appeared to be similar for all the conditions we tested. For example, the conclusions made above for the autophosphorylation reactions at 15°C hold true for autophosphorylation reactions performed at 37°C and monitored by phosphospecific Western blotting as described above (**Figure 3.12).**

Monitoring autophosphorylation by Western blotting with phosphospecific antibodies does have some limitations. First, there may be other sites of autophosphorylation that we are missing in this analysis. However, if there were additional sites of autophosphorylation, we would have expected the presence of additional bands or a different band pattern on the PhosTag gels. Another caveat to using phosphospecific antibodies is that resolution can be limited if there is an antibody that recognizes more than one site. One of the antibodies does recognize a dual phosphorylation event in the activation loop (YxxxpYpY), and the specificity of this antibody as been previously tested (Segal et al., 1996). Unfortunately, there are no reliable commercially available antibodies for either of the corresponding singly phosphorylated species. Thus, the first autophosphorylation event of TrkA-TKD and TrkB-TKD that was detected was by the dual specific antibody. There are mass spectrometry based experiments that I could have utilized to examine further the first autophosphorylation event. However, I decided not to pursue any further the order of autophosphorylation since the order of

autophosphorylation appeared to be similar for TrkA and TrkB TKDs and my goal was to investigate differences between these TKDs.

Intriguingly, the order of autophosphorylation site usage for TrkA and TrkB TKDs appears to resemble that seen for Met, rather than IRK/IGFR1 (Table 3.1), with tyrosines 680 and 681 (TrkA) being phosphorylated essentially at the same time (or in no defined order). Both TrkA and TrkB TKDs gave the same results under the conditions we tested. The elevated rate of TrkA-TKD autophosphorylation compared to that seen for TrkB-TKD is clear and reproducible in these experiments, and could possibly underlie some of the observed signaling differences.

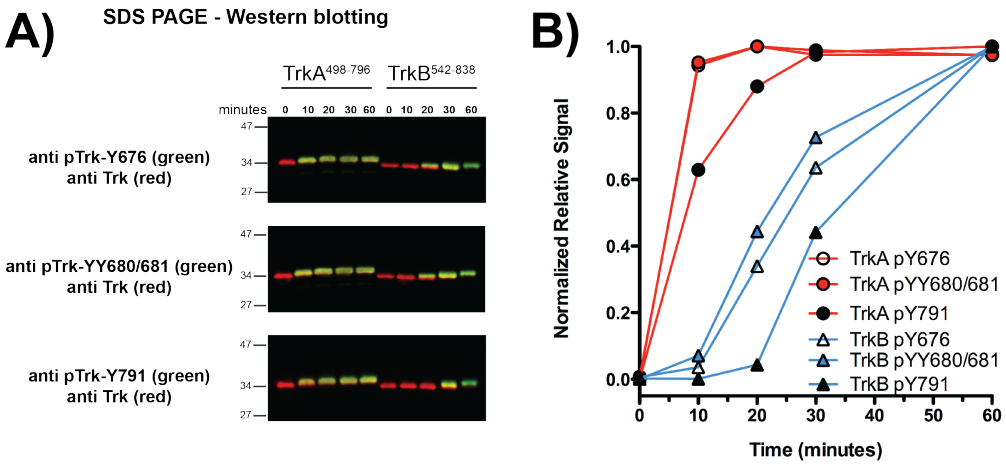
A)
SDS PAGE - Western blotting
TrkA498-796
TrkB542-838
minutes 0 10 20 30 60 0 10 20 30 60
anti pTrk-Y676 (green)
anti Trk (red)
anti pTrk-YY680/681 (green)
anti Trk (red)
anti pTrk-Y791 (green)
anti Trk (red)
47
34
27
B)
Normalized Relative Signal
Time (minutes)
TrkA pY676
TrkA pYY680/681
TrkA pY791
TrkB pY676
TrkB pYY680/681
TrkB pY791

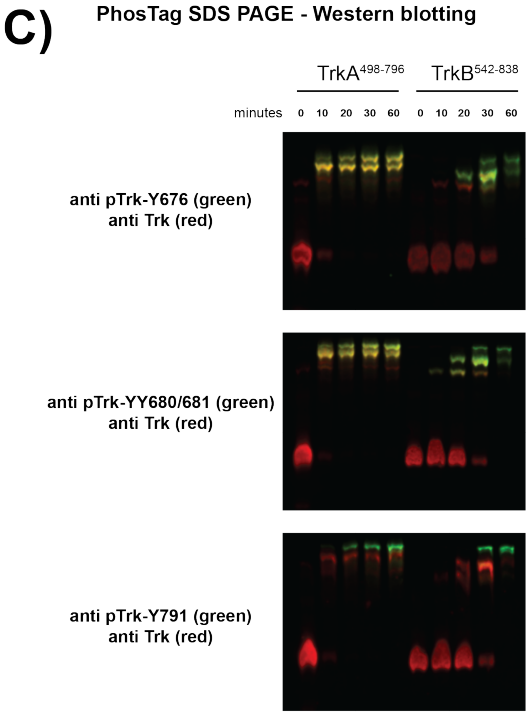
C)
PhosTag SDS PAGE - Western blotting
TrkA498-796
TrkB542-838
minutes 0 10 20 30 60 0 10 20 30 60
anti pTrk-Y676 (green)
anti Trk (red)
anti pTrk-YY680/681 (green)
anti Trk (red)
anti pTrk-Y791 (green)
anti Trk (red)

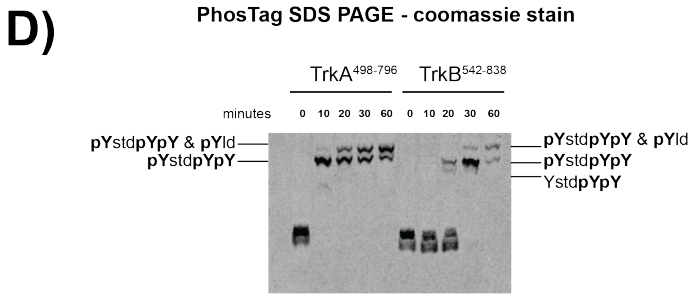
D)
PhosTag SDS PAGE - coomassie stain
TrkA498-796
TrkB542-838
minutes 0 10 20 30 60 0 10 20 30 60
pYstdpYpY & pYld
pYstdpYpY
pYstdpYpY & pYld
pYstdpYpY
YstdpYpY

Figure 3.11. Autophosphorylation is a similarly ordered process for TrkA and TrkB TKDs.

Autophosphorylation assays performed at 15°C with 5 μM TrkA and TrkB TKDs in the presence of 1 mM ATP and 10 mM $MgCl_2$ in a buffer containing 100 mM HEPES pH 7.4, 150 mM NaCl, 2 mM DTT and 'Halt' phosphatase cocktail inhibitor. Samples were taken at the indicated times and analyzed by SDS PAGE and PhosTag SDS PAGE Western blotting and Coomassie stain. (A) SDS PAGE Western blotting with phosphospecific antibodies specified to the left of the images. (B) The normalized relative signals from the Western blots were determined first by normalizing each phosphospecific signal with the total Trk signal. Each normalized signal was then divided and by the maximum signal per phosphospecific antibody per reaction. The resulting plot of normalized relative signal of each phosphospecific antibody clearly shows that TrkB-TKD autophosphorylation is slower than TrkA-TKD autophosphorylation. This analysis also reveals that the order of autophosphorylation appears to be similar for the TrkA and TrkB TKDs. (C) PhosTag SDS PAGE Western blotting with phosphospecific antibodies. (D) Coomassie stained PhosTag gel of autophosphorylation reaction with bands labeled according to phosphospecific Western blotting experiments.

A)

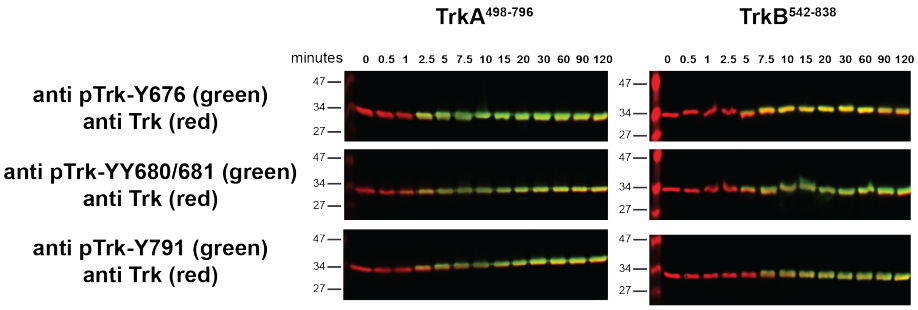

B)

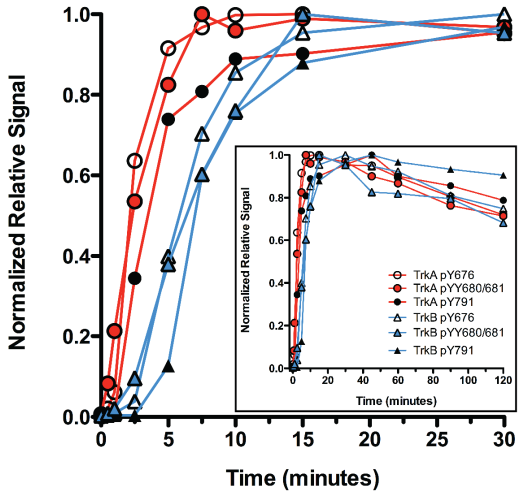

Figure 3.12. Autophosphorylation of TrkA and TrkB TKDs at 37°C.

Autophosphorylation assays performed at 37°C with 1 μM TrkA and TrkB TKDs in the presence of 1 mM ATP and 10 mM $MgCl_2$ in a buffer containing 100 mM HEPES pH 7.4, 150 mM NaCl, 2 mM DTT and 'Halt' phosphatase cocktail inhibitor. Samples were taken at the indicated times and analyzed monitored by SDS Western blotting with phosphospecific antibodies. (A) Two-color Western blots probed with the indicated phosphospecific antibodies (green signal) and pan Trk antibodies (red signal). (B) The normalized relative signals from the Western blots were determined by normalizing each

phosphospecific signal with the total Trk signal, and then dividing each normalized signal by the maximum signal per blot. The normalized relative signal is plotted for each antibody and shows that all the TrkA-TKD autophosphorylation events occur before the TrkB-TKD autophosphorylation events at this TKD concentration.

3.7. Kinetic parameters of TrkA and TrkB TKD peptide phosphorylation do not explain differences in autophosphorylation rates

The difference in autophosphorylation shown for the TrkA and TrkB TKDs could be a result of a difference in the intrinsic kinase activities of the two species. To test this hypothesis, I employed a more quantitative analysis of enzyme activity, monitoring kinase activity by following the incorporation of ^{32}P from ^{32}P-γ-ATP into a peptide mimicking the activation loop of either TrkA (SRDIYSTDYYRVGGRTMLPIR) or TrkB (SRDVYSTDYYRVGGHTMLPIR). **Table 3.2** lists the kinetic parameters measured in these assays, and **Figure 3.13** shows representative data used to obtain the kinetic parameters. As mentioned previously, the TrkA and TrkB TKD proteins are subjected to two treatments of phosphatases to ensure the proteins are fully dephosphorylated (see **subchapter 3.5 and Chapter 5, Materials and Methods**). Experiments were performed both with fully dephosphorylated TKDs, in order to quantitate activity of the maximally autoinhibited form seen in the crystal structure described in Chapter 2, as well as (almost) fully phosphorylated TKDs – as a measure of maximal activity and the activation consequences of autophosphorylation. To obtain phosphorylated TrkA and TrkB TKDs for the latter assays, autophosphorylation was allowed to proceed, and was

quenched at a predetermined time at which autophosphorylation was known to peak (prior to dephosphorylation as monitored by SDS PAGE and PhosTag SDS PAGE phosphospecific Western blotting). It should be noted that the phosphorylated TrkA and TrkB TKD preparations are heterogeneous mixes of phosphorylated species, based on PhosTag gels (**Figure 3.14**). We were unable to phosphorylate TrkA and TrkB TKDs completely, since allowing the autophosphorylation reaction to progress for longer also resulted in increased dephosphorylation – which we can only inhibit with procedures that will also inhibit kinase activity (see above).

Table 3.2 shows that the inactive (unphosphorylated) TrkA and TrkB TKDs have very similar kinetic parameters. Upon autophosphorylation, there is a dramatic change in the kinetic parameters for both TrkA-TKD and TrkB-TKD. Values for k_{cat} increase by ~60-100-fold, with smaller changes in $K_{m,\ ATP}$ (~10-fold reduction) and $K_{m,\ peptide}$ (~5-fold reduction) resulting in overall increases in catalytic efficiency in the range of 400-600 fold. These changes in kinetic parameters between unphosphorylated and phosphorylated TrkA and TrkB TKDs are in the range as those reported for other RTKs that rely on phosphorylation of activation loop tyrosines for full activity (Cobb et al., 1989; Favelyukis et al., 2001; Furdui et al., 2006; Till et al., 2002). The active TrkA and TrkB TKD kinetic parameters are also very similar to one another, indicating that TrkA and TrkB TKDs show very similar catalytic capacity when presented with a peptide substrate while at nanomolar concentrations. However there is a subtle difference in the catalytic efficiency that may contribute but not does explain the observed slower rate of TrkB-TKD autophosphorylation. The catalytic efficiency for ATP is ~1.8-fold decreased for TrkB-TKD in both the inactive and active states.

Table 3.2 Summary of kinetic parameters of TrkA and TrkB TKDs in the inactive (dephosphorylated) or active (phosphorylated) states. Data are shown as mean ± standard deviation of at least 3 experiments.

kinase	$k_{cat,\ ATP}$ (min^{-1})	$K_{m,\ ATP}$ (mM)	$k_{cat}/K_{m,\ ATP}$ ($min^{-1}\ mM^{-1}$)	$k_{cat,\ peptide}$ (min^{-1})	$K_{m,\ peptide}$ (mM)	$k_{cat}/K_{m,\ peptide}$ ($min^{-1}\ mM^{-1}$)
TrkA	19.7 ± 2.2	2.09 ± 0.52	9.8 ± 2.5	20.3 ± 0.6	2.18 ± 0.13	9.3 ± 0.8
TrkB	16.6 ± 6.6	3.20 ± 1.69	5.8 ± 1.9	9.7 ± 3.2	1.17 ± 0.42	9.4 ± 5.2
pTrkA	1144 ± 346	0.18 ± 0.05	6204 ± 673	1456 ± 239	0.364 ± 0.04	3991 ± 309
pTrkB	1033 ± 421	0.29 ± 0.14	3641 ± 423	1482 ± 211	0.390 ± 0.06	3815 ± 266

Despite this similarity in catalytic properties, it is clear that there is a reproducible difference in the autophosphorylation rates seen for the TrkA and TrkB TKDs. One important observation may provide part of the explanation for this autophosphorylation difference despite similar k_{cat} and K_m values in peptide phosphorylation assays. In the process of identifying suitable conditions for the quantitative peptide-based kinase assay described here, I explored many conditions. During these pilot experiments, I found that unphosphorylated TrkA-TKD displayed a greater dependence on concentration for activation than TrkB-TKD, and the effect was quite substantial. Kinase assays in which only TrkA or TrkB concentrations were varied are shown in **Figure 3.15**. Non-linear initial velocity plots were seen for several different TrkA TKD concentrations, evident as low as 60 nM (**Figure 3.15A)**, whereas initial velocities for TrkB-TKD are quite linear, even at 386 nM protein (**Figure 3.15C**). The concentration dependence of TrkA-TKD activation is clearer in plots of initial velocity normalized for concentration. Even higher concentration data overlay quite well when this is done for TrkB-TKD (**Figure 3.15D**), as

they should if there is no concentration dependence. By contrast, none of the TrkA-TKD initial velocities overlay after 2 minutes (**Figure 3.15B)**.

It seems reasonable to propose that the concentration dependence of TrkA-TKD activity is related to its enhanced rate of autophosphorylation in the assays described above. The fact that the TrkA and TrkB TKDs appear to have similar kinase activities is striking, given the reproducible finding that TrkA-TKD autophosphorylation is faster than TrkB-TKD autophosphorylation. The observations that TrkA-TKD lacks a lag phase for autophosphorylation and displays a strong concentration dependence of activation led us to explore the possibility that TrkA-TKD self-associates under the conditions of these experiments.

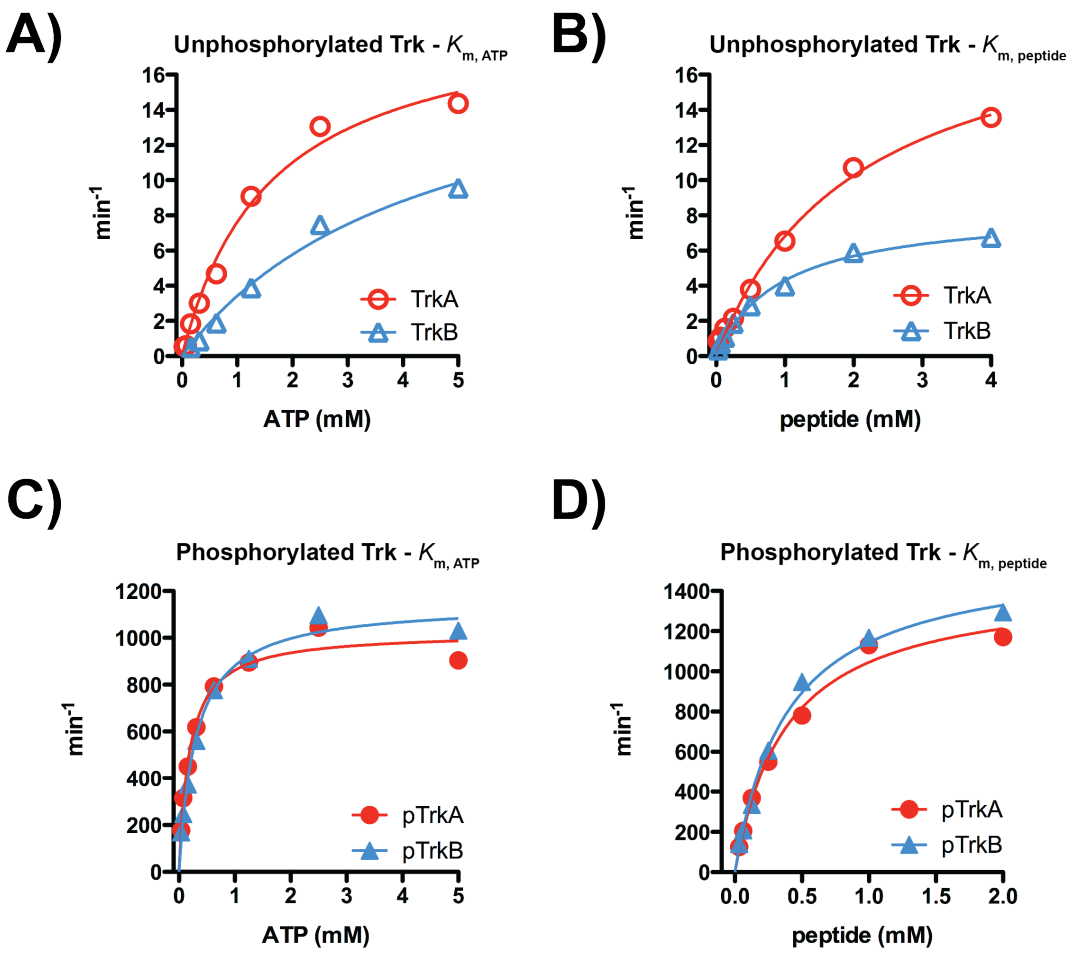

Figure 3.13. Representative data for obtaining enzymatic parameters for TrkA and TrkB TKDs.

Michaelis-Menten plots determining K_m and k_{cat} for ATP (left) or peptide (right) substrates. (A) For $K_{m, ATP}$ determination, dephosphorylated TrkA-TKD at 30 nM and dephosphorylated TrkB-TKD at 400 nM were assayed with variable ATP concentrations (5 mM to 0.039 mM) in the presence of fixed 2 mM peptide substrate and 10 mM $MgCl_2$. (B) For $K_{m, peptide}$ determination, dephosphorylated TrkA-TKD at 30 nM and dephosphorylated TrkB-TKD at 400 nM were assayed with variable peptide concentrations (4 mM to 0.031 mM), fixed 2 mM ATP and 10 mM $MgCl_2$. (C) $K_{m, ATP}$

determined using phosphorylated TrkA-TKD and phosphorylated TrkB-TKD, both at 8 nM. Reaction conditions included a fixed 2 mM concentration of peptide corresponding to their respective activation loops, variable ATP concentrations (5 mM to 0.039 mM) and 10 mM $MgCl_2$. (D) For $K_{m,\ peptide}$ with phosphorylated TrkA and TrkB TKDs, assays were performed as in (C), but peptide concentration was varied (4 mM to 0.031 mM) and ATP concentration fixed at 2 mM ATP.

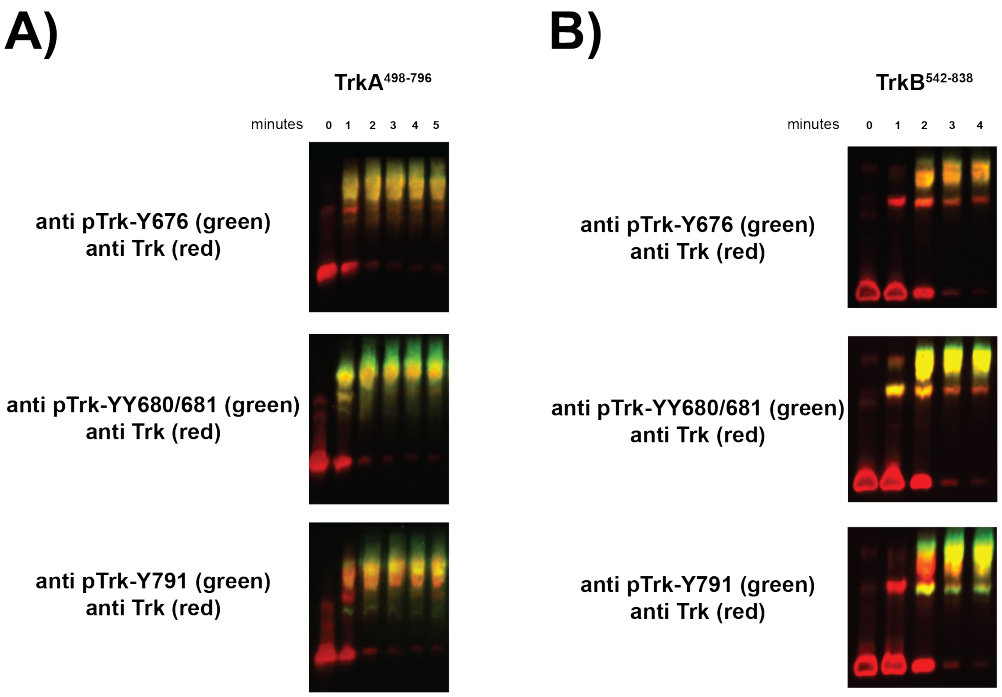

Figure 3.14. Generation of phospho-TKD species.

Autophosphorylation assays were conducted to generate phosphorylated TrkA and TrkB TKDs for enzymatic studies. Western blotting of PhosTag gels with phosphospecific antibodies were used to monitor the reactions. (A) 10 μM TrkA-TKD was incubated at room temperature with 1 mM ATP, 10 mM $MgCl_2$ in a buffer containing 100 mM HEPES

pH 7.4, 150 mM NaCl, 2 mM DTT and Halt phosphatase cocktail inhibitor. At 5 minutes, the reaction was quenched with EDTA to achieve a final concentration of 100mM. (B) 7.5 μM TrkB-TKD was incubated at 30°C with 1 mM ATP, 10 mM $MgCl_2$ in a buffer containing 100 mM HEPES pH 7.4, 150 mM NaCl, 2 mM DTT and Halt phosphatase cocktail inhibitor. At 4 minutes, the reaction was quenched with EDTA to achieve a final concentration of 100mM.

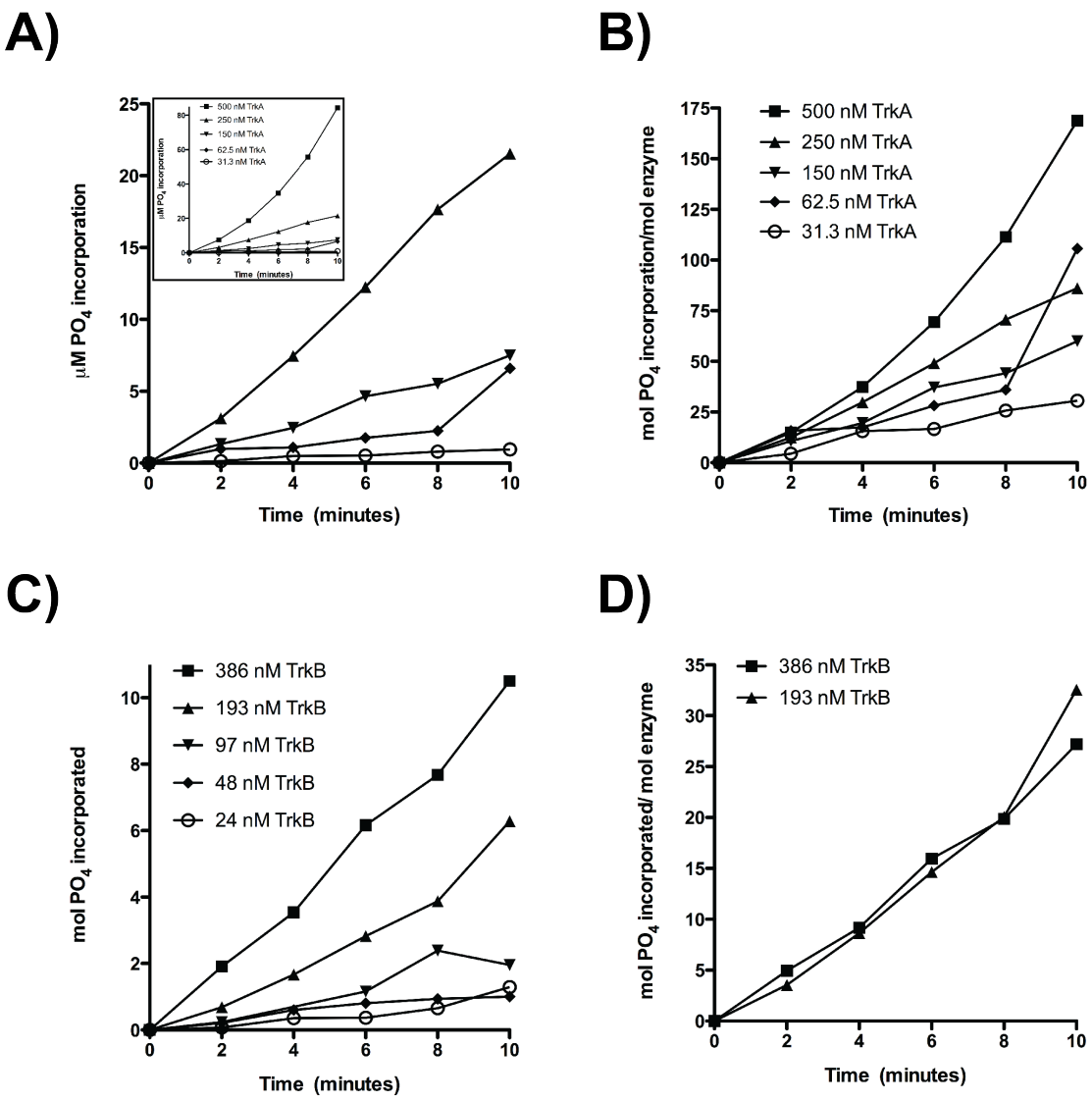

Figure 3.15. Differences in concentration dependence of activation for TrkA and TrkB TKDs.

Peptide-based radioactive kinase assays with 2 mM ATP, 2 mM peptide substrate, 10 mM $MgCl_{2+}$ and various concentrations of TrkA and TrkB TKDs were used to determine the optimal concentration of TrkA-TKD or TrkB-TKD for further kinase assays. (A) Plotting the moles of phosphate incorporated versus time for each concentration of TrkA-

TKD to determine initial rates of reactions shows curvature in most of these reaction profiles. (B) Normalizing initial rates for concentration of TrkA-TKD results in an obvious concentration dependence. (C) Initial rates for TrkB-TKD determined as above appear to be more linear in the higher concentrations than reactions with TrkA-TKD. (D) Normalized initial rates for TrkB-TKD overlay well when normalized for concentration, indicating that TrkB-TKD activity (unlike that of TrkA-TKD) is concentration independent.

3.8. TrkA-TKD crystallographic dimer not observed in TrkB-TKD crystal structures

In a study comparing the inactive structures of the TrkA and TrkB TKDs, Bertrand et al. 2012 reported that the TrkA kinase insert domain (KID) interacts with the hinge region (loop connecting N-lobe and C-lobe), intramolecularly **(Figure 3.16)**. Notably, Glu^{615} and Asp^{616} in the KID of TrkA interact with Arg^{593} and His^{594} in the hinge region, respectively, in the same molecule. However, none of these hinge region – KID interactions are observed in any of the TrkB-TKD structures now available, as a result of displacement of the TrkB KID by the C-terminal tail of TrkB. Hence, the authors postulated that the TrkA hinge region may be more rigid than the TrkB hinge region (Bertrand et al., 2012). Several studies have indicated that hinge region dynamics are important for catalytic activity of kinases such as Erk (Hoofnagle et al., 2001; 2004; Lee et al., 2005; Sours et al., 2014; Xiao et al., 2014). In the case of FGFR2, hinge region interactions are thought to serve as “brakes” that hold the kinase in an inactive conformation (Chen et al., 2007). In FGFR2, interactions are seen between the hinge region (β5-αD loop) and the N-lobe

(Chen et al., 2007). TrkA and TrkB TKDs have similar interactions between the kinase hinge and the N-lobe, but both have far fewer interactions than observed in FGFR2. The hinge region in TrkA predominantly interacts with the KID, which is part of the C-lobe (Bertrand et al., 2012).

Since the TrkA TKD autophosphorylates faster than that of TrkB (and has similar activity in peptide phosphorylation assays), it seems highly unlikely that the intramolecular hinge/KID interactions seen in the TrkA-TKD structure (4F01) reduce TrkA-TKD activity. However, a dimer that 'repurposes' some of these interactions for int*er*molecular interactions, seen in a crystallographic dimer in our studies of TrkA-TKD (PDB 4GT5) may provide an explanation. This dimer shares a similar interface with a crystallographic dimer also seen in the TrkA TKD structure reported by Bertrand et al., 2012 (PDB 4F0I) (**Figure 2.5B)** (Artim et al., 2012; Bertrand et al., 2012)**.** The dimers observed in these TrkA TKD structures are slightly different, but share much of the same dimer interface (**Figure 3.17 and Table 3.3-3.4**). The fact that TrkA-TKD activity is concentration dependent may suggest that it self-associates, and the interactions in this dimer may be important for dimerization (and possibly altered upon self-association with allosteric effects on kinase activity). TrkA TKD dimerization could drive its own activation, and this might cause the observed difference in autophosphorylation rates between TrkA and TrkB.

The two TrkA TKD crystal structures in which similar dimers were seen are from very similar constructs, yet the reported crystallization conditions are different. Furthermore, the two TrkA TKD crystal structures are described by different space groups (4GT5 space group is H32 whereas 4F0I space group is $P4_12_12$) and a different number of molecules are present in the asymmetric unit (4GT5 has one molecule in asymmetric

unit whereas 4F0I has two). These facts suggest that the dimer may therefore have some relevance. Closer inspection of this TrkA TKD dimer interface also identified several key residues in the kinase insert domain (KID) and hinge region of TrkA that form a network of interactions (**Figure 3.17C**). In both structures, Tyr^{591} and Arg^{593} in the hinge region of one monomer interact with Gly^{614} and Glu^{615}, respectively in the KID of a symmetry mate. Another interaction across the interface that was consistent between the TrkA TKD structures was the main chain carbonyl group of Leu^{611} in the KID of one monomer forming a predicted hydrogen bond with the Arg^{599} side-chain from αD of its symmetry mate. Interestingly, many of the residues involved in intramolecular and intermolecular interactions in the TrkA KID-hinge region including Arg^{593}, Arg^{599}, Lys^{609}, Leu^{611}, Glu^{615}, Asp^{616}, and Ala^{618} (human TrkA numbering) are replaced by different amino acids in TrkB (**Tables 3.3, 3.4, 3.5**). The TrkB KID loop is also shorter by two amino acids compared to the TrkA KID loop. These sequences differences in TrkB may contribute to the TrkB KID loop being displaced in the inactive TrkB TKD crystal structure (PDB ASZ) by the TrkB C-terminal tail and thus is in a different conformation than the TrkA KID loop (**Figure 3.18**).

Comparing the TrkB and TrkA TKD structures that are now available in the PDB also reveals slight shifts in the position of key elements – notably for the P-loop and αC helix, which are both relatively shifted towards the C–lobe in the TrkA TKD structures. The movements are subtle, and could just be the result of crystal packing. However, as shown in **Figure 3.18**, the αC helix in TrkA-TKD (cyan) is shifted ~18° towards the C-lobe compared to αC of TrkB-TKD (magenta). As a result the entire N-lobe of TrkA-TKD is shifted ~13° towards its C-lobe (**Figure 3.18**). This shift of the TrkA-TKD N-lobe is noticeable in all of the now-available inactive TrkA-TKD structures (two without inhibitor

and one with inhibitor) and TrkB-TKD structures (one without inhibitor and three with inhibitor), which are shown overlaid in **Figure 3.18**.

The intermolecular KID/hinge interactions seen in TrkA-TKD crystals (**Figure 3.17**) are not seen in any available TrkB-TKD structure. TrkB-TKD does not form this dimer, and in any case, the KID loop of TrkB is in a distinct conformation due to displacement by the C-terminal tail of TrkB. The C-terminal tail of TrkB does not contact the hinge region or the β6-β7 loop as the KID does in the TrkA structures (**Figure 3.18**). Instead, the C-terminal tail makes various contacts with the displaced KID loop and the lip of the activation loop of a symmetry mate.

A)

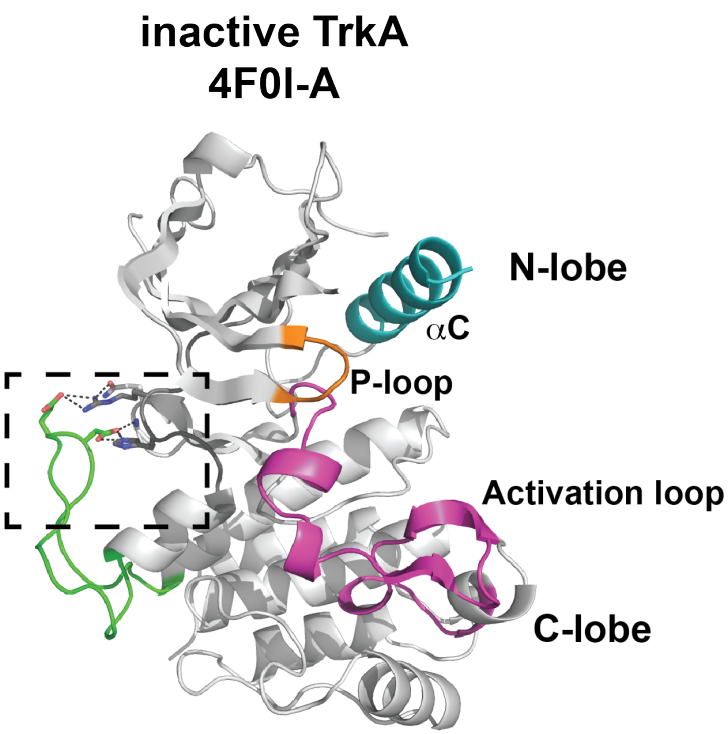
inactive TrkA
4F0I-A
N-lobe
αC
P-loop
Activation loop
C-lobe

B)

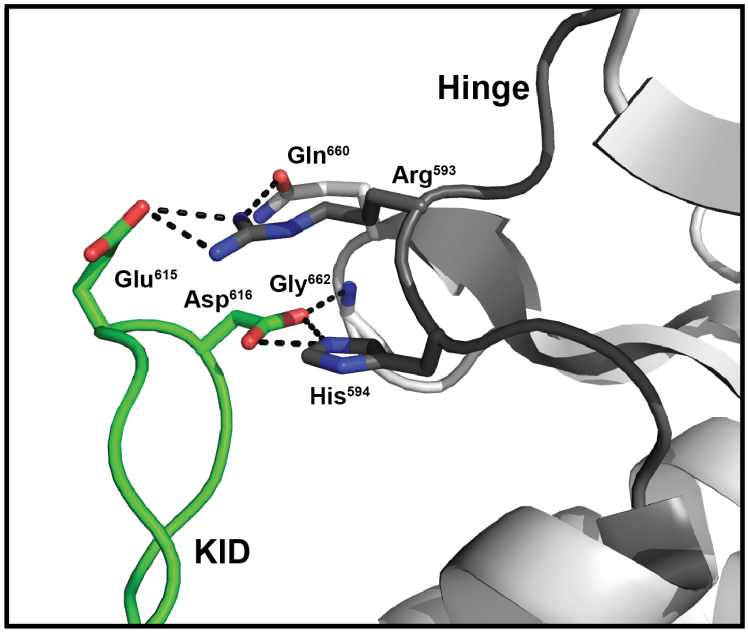
Hinge
Gln660
Arg593
Glu615
Asp616
Gly662
His594
KID

Figure 3.16. TrkA-TKD intramolecular interactions not seen in TrkB-TKD.

(A) The TrkA TKD (PDB 4F0I, chain A) inactive structure reported by Bertrand et al. in cartoon representation. KID/hinge intramolecular interactions they reported are boxed. (B) Close up of KID/hinge intramolecular interactions illustrating that Glu^{615} and Asp^{616} in the KID of TrkA interact with Arg^{593} and His^{594} in the hinge region, respectively. For consistency, all TrkA sequence numbering refers to human isoform *II* and also used in PDB 4GT5.

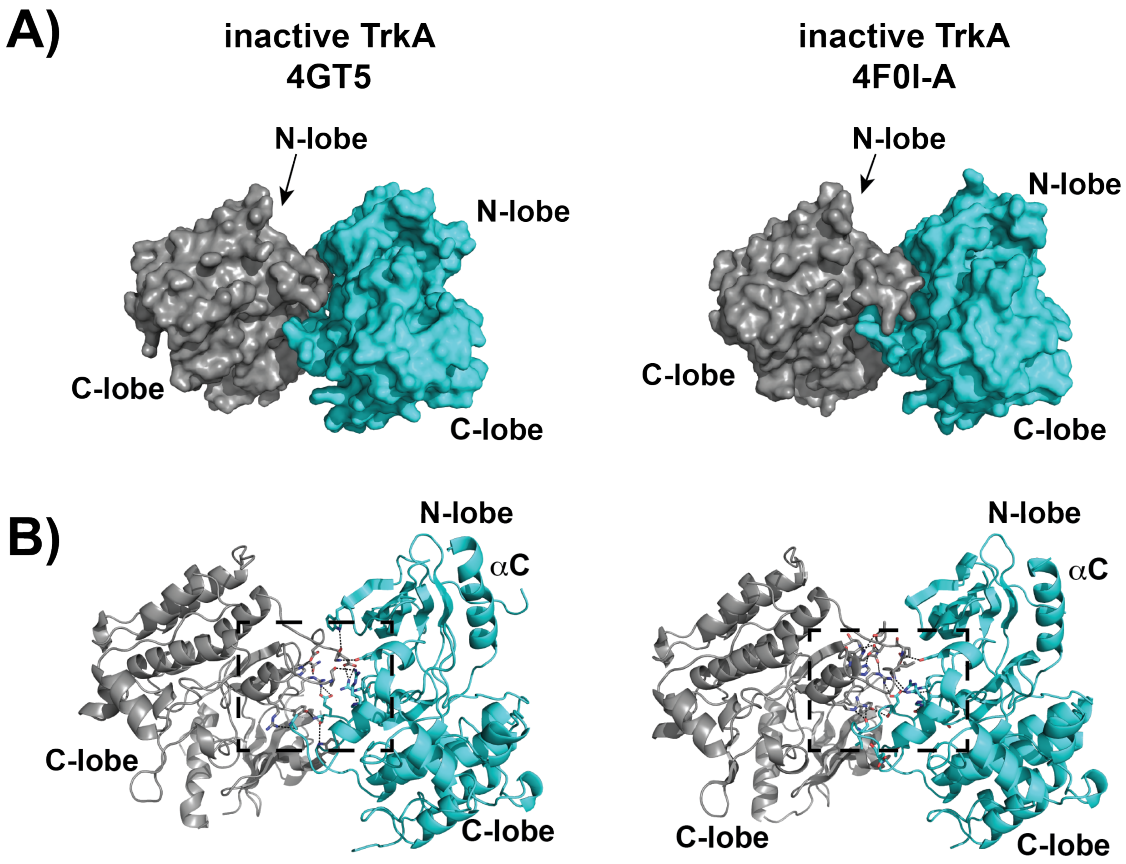
A)
inactive TrkA
4GT5
N-lobe
N-lobe
C-lobe
C-lobe
inactive TrkA
4F0I-A
N-lobe
N-lobe
C-lobe
C-lobe
B)
N-lobe
αC
C-lobe
C-lobe
N-lobe
αC
C-lobe
C-lobe
C)
Gly614
Tyr591
Leu611
Glu615
Arg599
Arg593
Arg593
Tyr591
Glu615
Arg599
Leu611
Gly614
Glu615
Tyr591
Leu611
Arg599
Arg593
Tyr591
Glu615
Arg599
Gly614
Leu611

Figure 3.17. TrkA-TKD dimer interface in two TrkA-TKD structures.

The TrkA-TKD KID/hinge dimer interface shown in surface and cartoon representation. (A) Surface representation of the KID/hinge dimer in 4GT5 and chain A of 4F0I (4F0I-A). Note that the N-lobe of the monomer colored grey is headed into the plane of the page. (B) In the same orientation as the surface representation, cartoon representation is shown of the same dimer for 4GT5 and 4F0IA. (C) A close-up view of the KID/hinge region (boxed area in B) is shown for 4GT5 and 4F0I-A. Intermolecular and intramolecular interactions are shown. The residues involved in common interactions observed in both inactive structures are labeled. Note that the interfaces share many of the same interactions, but there are subtle differences due to the interface in 4GT5 being symmetric and the interface in 4F0I being asymmetric. Chain B of 4F0I is omitted from this figure for clarity, but the interactions of chain B are listed in Tables 3.3 and 3.4 along with a full list of interactions shown in this figure.

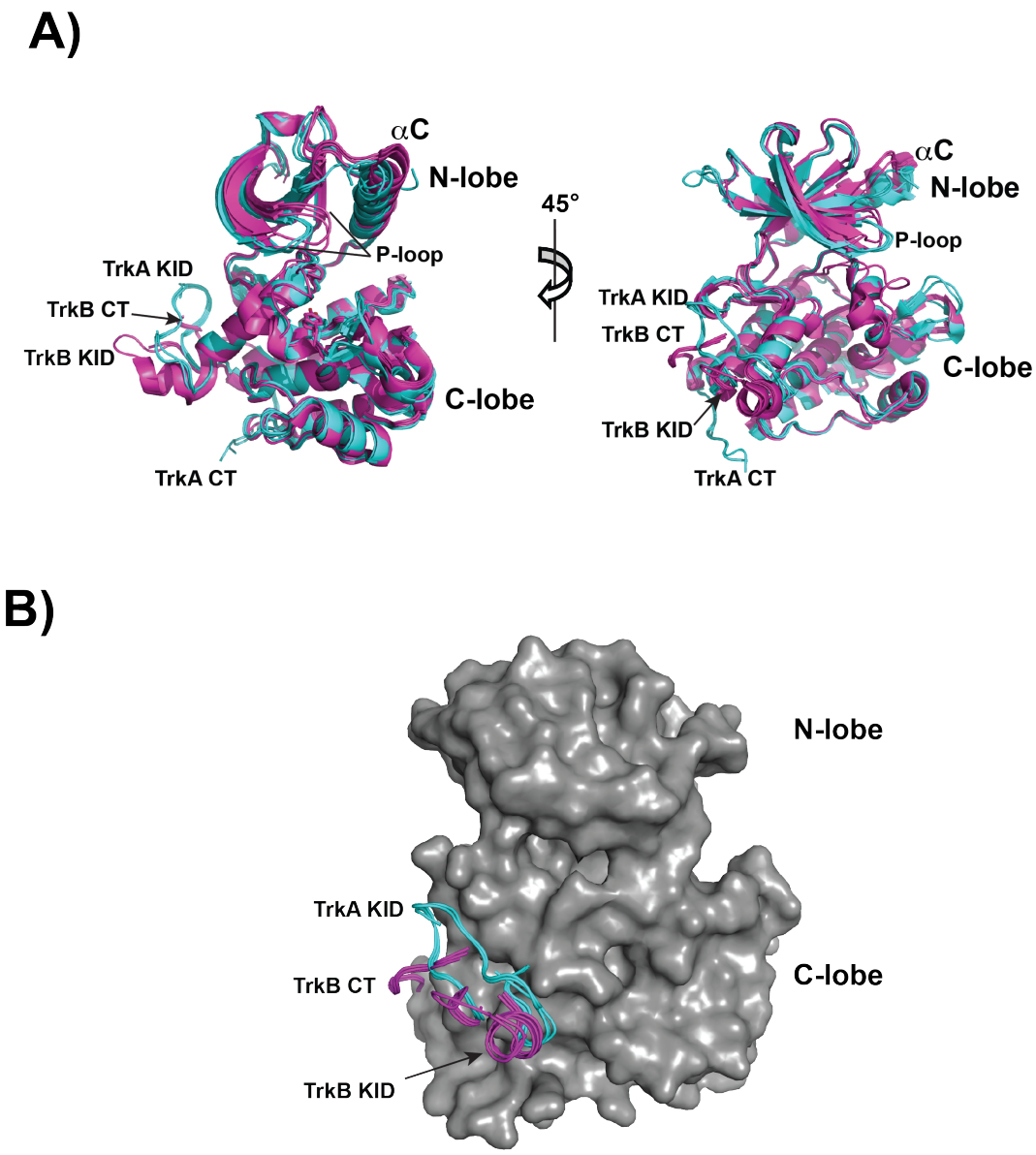

Figure 3.18. Comparison of TrkA and TrkB inactive TKD structures.

(A) Overlay of the two inactive TrkA-TKD (cyan) structures without inhibitor (4GT5 and 4F0I) with the TrkB-TKD (magenta) structures without (4ASZ) or with (4AT4 and 4AT5) inhibitor. Notice the shift of αC and N-lobe towards the C-lobe of the TrkA-TKD structures. This shift corresponds to ~18° and ~13° for αC and N-lobe between the TrkA (4GT5) and TrkB (4ASZ) TKD structures. On the right, the structures are rotated 45° out

of the plane of the page as shown, to illustrate the different conformation of the KID loop in TrkA and TrkB. (B) In the same orientation as the right side of part A, a surface representation of inactive TrkA-TKD (4GT5) is shown in grey, with cartoon representation of the TrkA KID (4GT5 and 4F0I) detailed in cyan. The TrkB KID and C-terminal tail (from 4ASZ, 4AT4, and 4AT5) are shown in magenta in cartoon representation. Even though the N-lobe and αC of the inhibitor bound TrkA-TKD structure (4AOJ) superimposes well with the other TrkA structures, it is omitted from this figure because of a disordered activation loop and KID. Also omitted is one of the TrkB inhibitor bound structures (4AT3) because of unique P-loop and activation loop conformations that are probably due to the presence of inhibitor.

Table 3.3. KID/hinge region intermolecular interactions. Summary of the KID/Hinge dimer interface interactions in the inactive TrkA TKD structures (PDB 4GT5 and PDB 4F0I). The two molecules in the 4F0I structure are designated 4F0I-A (chain A) and 4F0I-B (chain B). Sequence numbering refers to numbering from 4GT5. Residues highlighted are different in the TrkB TKD sequence.

Molecule in A.U.		**Symmetry Mate**				
Residue	Location	Residue	Location	**4GT5**	**4F0I-A**	**4F0I-B**
Trp^{514}	β1	Gly^{614}	KID	X		
Tyr^{591}	Hinge	Gly^{614}	KID	X		X
Tyr^{591}	Hinge	Glu^{615}	KID		X	
Arg^{593}	Hinge	Glu^{615}	KID	X		X
Arg^{599}	αD	Leu^{611}	KID	X	X	X
Asp^{607}	KID	Lys^{609}	KID		X	
Leu^{611}	KID	Arg^{599}	αD	X	X	X
Gly^{614}	KID	Trp^{514}	β1	X	X	
Gly^{614}	KID	Tyr^{591}	Hinge	X	X	
Glu^{615}	KID	Arg^{593}	Hinge	X	X	

Table 3.4. KID/hinge region intramolecular interactions. Summary of interactions of the KID/hinge region within a monomer in the inactive TrkA TKD structure (PDB 4GT5 and PDB 4F0I). The two molecules in the 4F0I structure are designated 4F0I-A (chain A) and 4F0I-B (chain B). Sequence numbering refers to numbering from 4GT5. Residues highlighted are ones that are not present or different in the TrkB sequence.

Residue	Location	Residue	Location	4GT5	4F0I-A	4F0I-B
Arg^{599}	αD	His^{594}	Hinge			X
His^{604}	KID	Ala^{618}	KID		X	X
Glu^{615}	KID	Arg^{593}	Hinge		X	X
Asp^{616}	KID	Arg^{593}	Hinge	X		
Asp^{616}	KID	His^{594}	Hinge	X	X	X
Asp^{616}	KID	Gly^{661}	β6- β7 loop	X	X	X
Asp^{616}	KID	Gln^{660}	β6- β7 loop			
Gln^{660}	β6- β7 loop	Arg^{593}	Hinge		X	

Table 3.5. KID/hinge region amino acid differences between TrkA and TrkB.

TrkA	TrkB	Location
Trp^{514}	Arg^{558}	β1
Arg^{593}	Lys^{637}	Hinge
Arg^{599}	Lys^{643}	αD
Lys^{609}	Val^{653}	KID
Leu^{611}	Met^{655}	KID
Glu^{615}	Asn^{659}	KID
Asp^{616}	-	KID
Ala^{618}	Pro^{660}	KID
Gln^{660}	Glu^{702}	β6- β7 loop
Gly^{661}	Asn^{703}	β6- β7 loop

3.9. TrkA mutant slows down the progression of TrkA-TKD autophosphorylation

The structural observations outlined above prompted us to hypothesize that the dimerization interface seen in crystal structures of TrkA-TKD (but not TrkB-TKD) may play a role in the enhanced TrkA-TKD autophosphorylation rate, and the concentration dependence of its activation. To test this hypothesis, I used site-directed mutagenesis to mutate part of the TrkA KID loop to the corresponding residues seen in the TrkB KID loop. **Figure 3.19** shows an alignment of TrkA, TrkB, and the TrkA KID mutant. Note that this TrkA-TKD KID mutant now has a shorter KID loop (by 2 residues), and lacks Glu^{615} and Asp^{616}, which are central in intermolecular and intramolecular interactions respectively in the TrkA-TKD KID/hinge dimer, as discussed above (**Table 3.3** and **3.4**). To examine the functional consequences of these KID mutations, I employed a radioactive autophosphorylation assay to monitor the autophosphorylation profile for TrkA, TrkA KID, and TrkB TKDs. As shown in **Figure 3.20A**, the TrkA and TrkB TKDs again differed in their rates of autophosphorylation. Furthermore, the TrkA KID mutant does display a slightly slower rate of autophosphorylation than wild-type TrkA-TKD, but is not reduced to the rate seen for TrkB-TKD autophosphorylation. A paired t test was performed for each time point to determine significant differences in the autophosphorylation profiles between TrkA, TrkA KID, and TrkB TKDs. Significant differences occur from 0.75 minutes to 3 minutes (**Figure 3.20B**), with the largest differences between TrkA, TrkA KID, and TrkB occurring in the earlier time points. This time region corresponds to the lag phase of the autophosphorylation profile observed in **Figure 3.11** and **3.12**. The data from these autophosphorylation experiments were also plotted to determine what is the time taken for TrkA, TrkA KID, and TrkB TKDs to reach half maximal autophosphorylation. These plots, along with the statistical significance of

the values obtain for half maximal autophosphorylation, are shown in **Figure 3.22**. As expected, TrkA-TKD reaches half maximal autophosphorylation faster than TrkA KID and TrkB TKDs. Thus, the TrkA KID mutant does appear to reduce TrkA TKD autophosphorylation to some extent, but autophosphorylation of the TrkA KID mutant remains significantly more rapid than that seen for TrkB-TKD.

Taken together, these data are consistent with the crystallographically observed TrkA-TKD dimer interface playing some role in the accelerated autophosphorylation of TrkA-TKD – since mutating part of this interface does significantly disturb TrkA-TKD autophosphorylation. However, the effect is clearly only partial, possibly because we did not fully abolish dimerization with the KID mutations made. Indeed, according to the crystal structures there are other interactions in the crystallographic dimer interface that might also play an important role. There may also be other phenomena causing TrkA-TKD to autophosphorylate faster. Another plausible explanation for a more transient lag phase for TrkA-TKD autophosphorylation is that autophosphorylation of TrkA-TKD itself may promote dimerization, which in turn would further promote autophosphorylation in an effective positive feedback loop. Indeed, we have observed phosphorylation-enhanced dimerization of the EGFR intracellular region, providing a possible precedent for such an effect (Sung Hee Choi, unpublished observations).

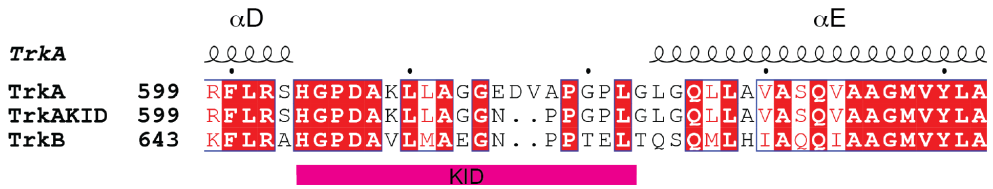

Figure 3.19. **Alignment of TrkA, TrkA KID mutant and TrkB in the KID region.**

This alignment illustrates how part of the KID loop involved in the TrkA-TKD dimer interface was replaced with residues from the TrkB KID loop. The magenta box below the sequences designates the KID loop.

A)

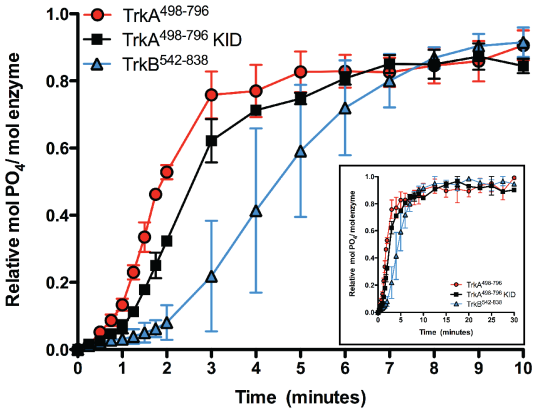

B)

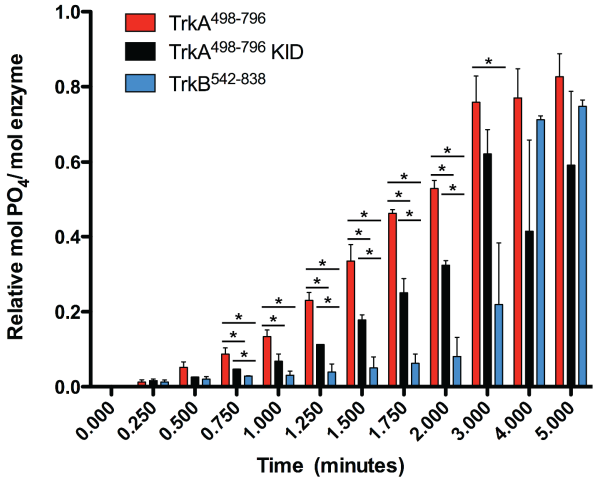

Figure 3.20. Perturbations of the autophosphorylation profile of the TrkA-TKD KID mutant.

(A) Radioactive autophosphorylation assays at RT with 4 μM of TrkA-TKD, TrkA KID-TKD, or TrkB TKD protein (B) Histogram plot of relative moles of phosphate incorporated per mole of enzyme for time points from 0 to 5 minutes. A paired t test was used to compare data obtained with TrkA (n=3), TrkA KID (n=2), and TrkB TKDs (n=2), to determine statistical significance of differences with significance ($P < 0.05$) denoted with an asterisk.

A)

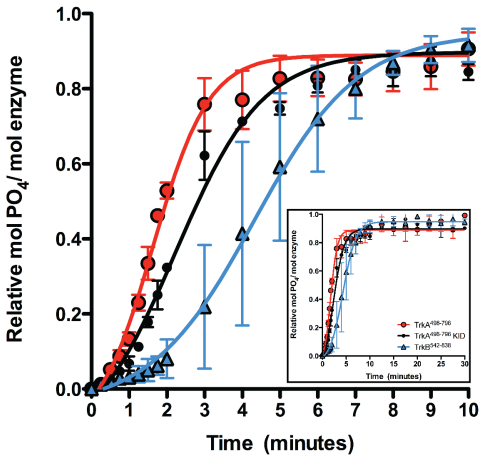

B)

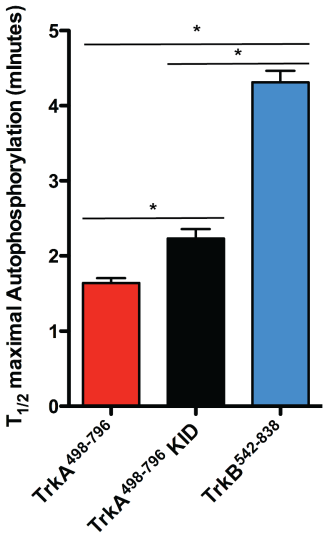

Figure 3.21. Comparison of the time to the half maximal level of TKD autophosphorylation.

(A) Data from **Figure 3.20** were replotted and fit with a four-parameter logistic equation to obtain time to half maximal autophosphorylation. Curves were fit to the 0 to 30 minute data (inset), but only the data from 0 to 10 minute are shown for clarity. (B) Histogram of

the time to half maximal autophosphorylation for TrkA, TrkA KID, and TrkB TKDs. A paired t test was used to determine statistical significance ($P < 0.05$) denoted as an asterisk.

3.10. Phosphorylation of TrkA-TKD may promote its self-association

To investigate further whether phosphorylated TrkA dimerizes, I produced phosphorylated TrkA (pTrkA) and mock treated TrkA (mTrkA) TKDs, the latter having been treated as if to fully phosphorylate the protein, except for the omission of ATP. Both pTrkA and mTrkA TKDs were then purified by size exclusion chromatography (SEC). The chromatogram from SEC revealed that pTrkA TKD elutes earlier than mTrkA TKD, indicating a higher molecular weight or spatial extent for the pTrkA species (**Figure 3.22**). However, preliminary results with pTrkB and mTrkB TKDs also showed a similar elution pattern. Both pTrkA and pTrkB TKDs may have an exposed region (phosphorylated activation loop, perhaps) of the TKD creating an increase in shape leading to both pTrkA and pTrkB TKDs eluting earlier.

I next used sedimentation equilibrium (SE) analytical ultracentrifugation (AUC) in an effort to determine whether pTrkA-TKD dimerizes weakly. The pTrkA and mTrkA TKD samples described above were each loaded at a concentration of 16.7 μM and sedimented at various speeds. A difference in sedimentation was observed between mTrkA and pTrkA TKDs, as shown in **Figure 3.23**. The AUC data were analyzed by plotting the logarithm (ln) of absorbance at 280 nm versus the radius squared $(r^2 - r_o^2)/2$.

The slopes of the linear fits of the data were used to calculate the apparent masses of mTrkA and pTrkA TKDs. A difference of ~6 kDa was observed between the calculated masses of mTrkA and pTrkA TKD species, consistent with a weak self-association of pTrkA-TKD.

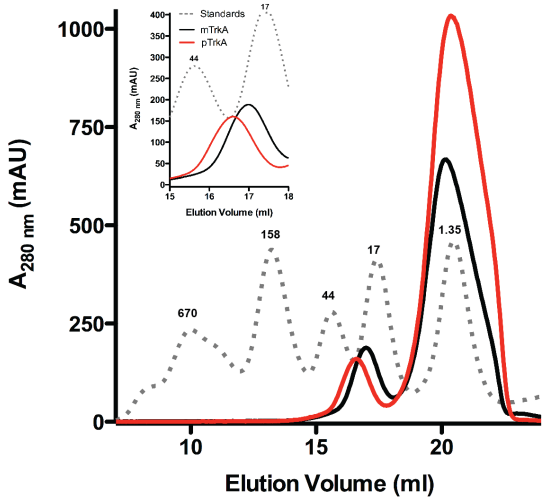

Figure 3.22. Difference in size exclusion chromatography profiles between mTrkA and pTrkA TKDs.

Size exclusion chromatography (SEC) profiles of mTrkA-TKD (black line), pTrkA-TKD (red line) and standards (grey dashed line). The molecular weight of the standards (BioRad) in kDa is listed above each standard peak. Preliminary results indicate a similar elution pattern for pTrkB and mTrkB TKDs.

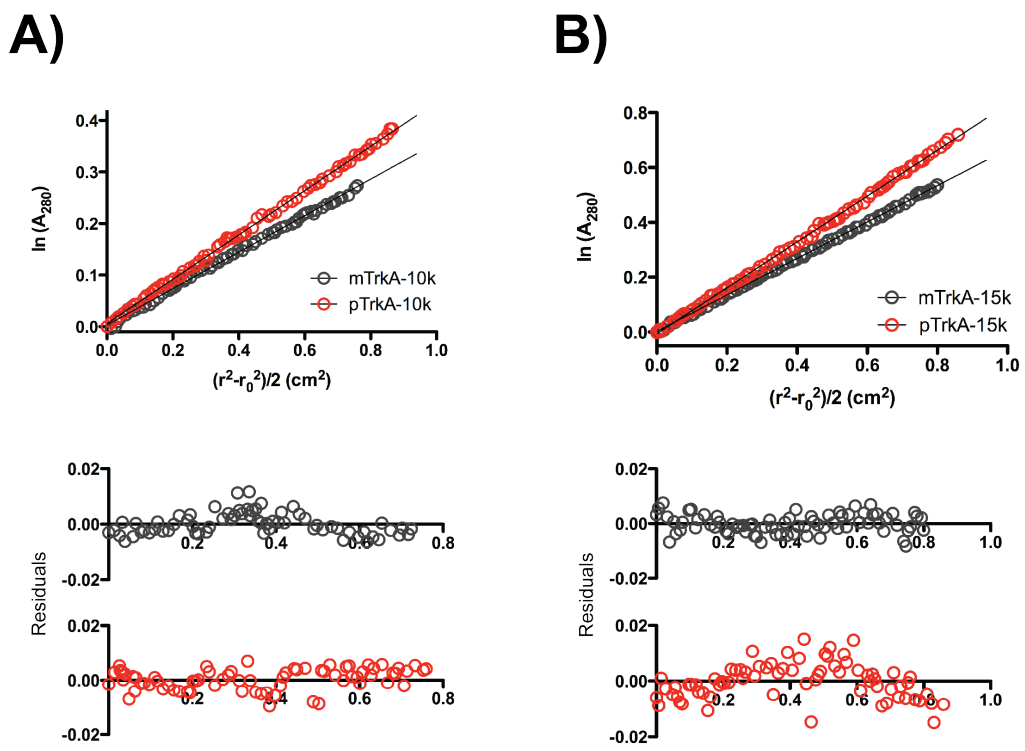

Figure 3.23. Sedimentation equilibrium analytical ultracentrifugation experiments with mTrkA and pTrkA TKDs.

Sedimentation equilibrium analytical ultracentrifugation experiments were performed with 16.7 μM of pTrkA-TKD and 16.7 μM of mTrkA-TKD to assess whether there is any difference in behavior of these two species in solution. To analyze the data, we generated a plot of the natural logarithm (ln) of absorbance at 280 nm versus the radius squared (r^2-r_o^2)/2, where r is the radial position in the sample and r_o is the radial position of the meniscus. For a single species, this analysis provides a straight line with slope proportional to the molecular mass of that single species (or weight average molecular

weight of multiple species). Data collected at 10,000 rpm (A) and 15,000 rpm (B) both show a difference of ~6 kDa between the calculated masses of mTrkA and pTrkA TKDs.

3.11. Conclusions

TrkA and TrkB are homologous RTKs that are thought to initiate similar signaling pathways upon ligand-induced activation of their TKDs. However, various reports have demonstrated that TrkA and TrkB expression and activation result in quite distinct cellular outcomes when TrkA and TrkB are expressed in the same cell type. The different outcomes appear to be correlated with sustained activation of the Erk pathway when TrkA is engaged by its ligand (leading to differentiation) and by more transient activation of the Erk pathway when receptors such as TrkB, EGFR, and IR are activated by their ligands (leading to proliferation, at least in the case of PC12 cells). Thus, it appears that the difference in signaling specificity may arise not from activation of different signaling components *per se*, but from different kinetics of activation – likely with the engagement of different positive and/or negative feedback elements in the pathway. Recent reports demonstrated that homologous kinases in the same family may have different intrinsic kinase activities and activation kinetics (Joseph et al., 2013; Latour et al., 1996; Lew et al., 2007). Furthermore, previous studies have demonstrated that the strength of an initiating signal from an RTK can dictate the cellular response (Dikic et al., 1994; Traverse et al., 1994). Therefore, we sought to determine whether there is an intrinsic difference between the TKDs of TrkA and TrkB that may underlie the distinct cellular responses downstream of TrkA and TrkB activation.

We show that the isolated TrkA TKD autophosphorylates faster than TrkB TKD. This faster autophosphorylation rate cannot be explained by differences in the order of autophosphorylation site usage. The TrkA and TrkB TKDs appear to have similar intrinsic kinase activities, raising the question of what is the source of the difference in autophosphorylation rates. Notably, TrkB-TKD autophosphorylation has a non-linear lag phase that was not present in TrkA-TKD. Previous reports have characterized a non-linear phase of TrkB autophosphorylation (Iwasaki et al., 1997). The authors concluded that the non-linear phase is the result of slow *cis* phosphorylation that occurs prior to *trans* phosphorylation. However, the dominant result observed in those experiments was *trans* phosphorylation. The *cis* phosphorylation described by the authors only occurred during conditions with very low concentrations of ATP. Furthermore, the reaction conditions are very different from the conditions used in this study. Most importantly, Iwasaki et al. were using ng/μl concentrations of full length TrkB intracellular domain with 20 μM to 100 μM of ATP in the presence of $MnCl_2$ instead of $MgCl_2$ (Iwasaki et al., 1997).

To address the difference of autophosphorylation between TrkA and TrkB TKDs, we describe a unique TrkA-TKD crystallographic dimer that is not observed in the TrkB-TKD structures. We used site directed mutagenesis to disrupt this dimer and show that these mutations do have a minor effect on slowing autophosphorylation when compared to WT TrkA-TKD. The fact that the effect is modest may reflect incomplete disruption of the dimer, or may suggest (as we suspect is likely) that additional mechanism also contribute to the faster rate of TrkA-TKD autophosphorylation. Indeed, our data further suggest that phosphorylation of TrkA-TKD may also promote dimerization, suggesting that the elevated rate of TrkA-TKD autophosphorylation compared to TrkB-TKD may be

caused in part by TrkA self-association. Such a self-association, phosphorylation-induced mechanism could promote a stronger and more sustained TrkA-mediated signal in the cell when TrkA is activated. Indeed, an autophosphorylation-induced activation of an RTK would constitute a positive feedback loop, which is exactly what would be required for the switch-like sustained response seen with TrkA differentiative signaling. A similar phenomenon, although not yet defined in molecular terms, has also been observed *in vitro* for the EGFR intracellular domain (unpublished). Further cellular studies are needed to test whether this TrkA-TKD self-association may play a role in dictating the nature and kinetics of the cellular response seen upon TrkA activation by its ligands.

Chapter 4:

Conclusions and future directions

4.1. Conclusions

The similar activation loop conformation of many of the IRK TKD family members suggests that these kinases utilize the same autoregulatory mechanisms. As discussed in Chapter 2, there is a subset of IRK TKD family members that have a different activation loop conformation and these kinases possess a different autoregulatory mechanism. Analysis of the reported cancer related mutations of the IRK TKD family members clearly demonstrates that mutations occur more frequently or over a wider range of residues in IRK TKD family members that do not utilize pseudosubstrate inhibition, whereas the IRK TKDs that employ pseudosubstrate inhibition have very few reported cancer mutations. Instead, some of the RTKs in the IRK TKD family (IR, IGF1R, Trk) that use pseudosubstrate inhibition show altered expression in cancer more often (or rather) than mutations (Belfiore and Malaguarnera, 2011; Davidson et al., 2003; Lagadec et al., 2009; Larsson et al., 2006; Tanaka et al., 2009). Indeed, many of the initially reported TrkB cancer mutations present in the activation loop have now been shown not to be gain of function mutations (Harada et al., 2011).

Altered or increased expression of an RTK can impact the signaling network in which it is embedded in a multitude of ways. Overexpression can overload receptor trafficking pathways, thus ultimately producing more receptors at the cell surface. However, in the case of PC12 cells, over expression of RTKs (EGFR and IR) and activation causes cells to differentiate. Altered and/or overexpression of an RTK could cause “novel” protein interactions that modulate and drive the network into a proliferative response. Proteomic approaches should be able to determine the existence of novel RTK-protein interactions that would dictate the signaling specificity. Along with proteomic approaches, I would

argue that a thorough and quantitative analysis of the kinetics of RTK activation is needed to understand and interpret the effect of RTK expression in a particular cell type.

In Chapter 3, I address signaling specificity differences between activation of TrkA and TrkB. TrkA and TrkB are very homologous proteins, yet activation and expression of each in neuroblastoma cells produces quite distinct cellular outcomes. It is noteworthy that neuroblastoma cells are of sympathetic origin and TrkA is known to play important roles in the development and maintenance of the sympathetic nervous system. On the contrary, TrkB is rarely expressed in the sympathetic nervous system. Thus, quantitatively understanding the kinetics of TrkA and TrkB activation is essential to fathom the resulting differences upon their expression and activation in neuroblastoma cells. Furthermore investigating the activation of TrkA and TrkB will provide insight into what are also other factors that shapes the signaling response in a particular cell type, for example the threshold of activation set by surrounding phosphatases.

I show that indeed the activation of TrkA and TrkB could be distinct since TrkA TKD autophosphorylates itself faster than TrkB TKD and that this, in part, may be due to an increased self-association of the TrkA TKD. Upon TrkA activation by ligand binding, a self-association mechanism could promote a stronger and more sustained TrkA-mediated signal in the cell. Indeed, a stronger ability to autophosphorylate and induced activation of an RTK could contribute to a sustained response seen with TrkA differentiative signaling. Further cellular studies are needed to test whether this TrkA-TKD self-association and faster rate of autophosphorylation aids in shaping the downstream signaling network causing sustained Erk activation and cellular differentiation upon TrkA activation by its ligand.

There are reports that show that homologous protein-tyrosine kinases with distinct catalytic activities have specific roles in the cellular context in which they are normally expressed. For example, the members of the Tec family, Itk and Btk are soluble kinases exclusively expressed in T cells and B cells, and downstream of T cell and B cell receptor activation, respectively (Joseph et al., 2013). Joseph et al. demonstrated that Btk's increase kinase activity (increase in k_{cat}) is due to dynamics of its activation loop and an Itk chimera harboring Btk's activation loop displays an increase in kinase activity (Joseph et al., 2013). Importantly, this Itk chimera changed the shape of the signaling network in T cells to a sustained cellular signal. Differences in intrinsic kinase activity have also been shown between ZAP-70 and Syk, members of the Syk family of nonreceptor protein-tyrosine kinases that are expressed in distinct hemopoietic cells (Latour et al., 1996).

These examples along with the data presented in this dissertation suggest that kinase activity is an imporatant component of the signaling network in which that particular kinase is embedded. The type of difference of kinase activity (increase k_{cat}) within the Tec and Syk families could undoubtedly be distinct from any differences within an RTK family since each is uniquely embedded (receptor compared to soluble tyrosine kinase) in the signaling network.

Quantitatively understanding the kinase activity at various levels of the network will be fruitful in understanding the spatial threshold set by phosphatase. In particular, studies need to be performed in various cell lines to determine if cell specific responses of expressing and activating a RTK is determined by a quantitative relationship between kinase activity compared to the surrounding phosphatase.

4.2. Future Directions

The work described in this dissertation provides a foundation for future biochemical and structural studies of the Trk family. The autoinhibitory mechanism utilized by the Trk TKDs is similar to IRK and involves pseudosubstrate autoinhibition by the activation loop. Further structural and biochemical studies of Trk intracellular domain (ICD) constructs that include the juxtamembrane region would be insightful in fully understanding the regulatory mechanisms of the Trk family. In the case of TrkA, mutation of the single JM tyrosine in TrkA to phenylalanine had little effect on autophosphorylation (Obermeier et al., 1994; Stephens et al., 1994), whereas mutation of the corresponding JM tyrosine to phenylalanine in TrkB did diminish autophosphorylation in cell-based assays (Minichiello et al., 1998; Postigo et al., 2002). The full-length ICD constructs tend to have poor expression, but now that the experimental framework is established it should be feasible to obtain enough protein to determine the influence (if any) of the juxtamembrane region of TrkA and TrkB on the kinase activity and autophosphorylation *in vitro*.

I have shown that the isolated TrkA TKD autophosphorylates itself faster than its TrkB counterpart and this may be due in part to TrkA-TKD self-association that is not observed for TrkB. Further analytical ultracentrifugation studies are needed to thoroughly investigate the characteristics of TrkA-TKD self-association. It will be interesting to perform these studies under various conditions to determine if binding of ATP or inhibitor influences TrkA self-association. Performing analytical ultracentrifugation studies with the TrkA KID mutant will also be informative to determine whether the mutations studied hinder TrkA-TKD self-association. Further mutations to disturb the crystallographic dimer interface would also aid in characterizing the residues

important for TrkA-TKD self-association. Analytical ultracentrifugation experiments with phosphorylated TrkB-TKD and mock treated TrkB-TKD need to be conducted to truly determine if phosphorylation promoting dimerization is exclusively occurring in TrkA or if it is a more general phenomenon. If it is a more general phenomenon, further characterizing the TrkA KID/hinge region interactions role on autophosphorylation will be key in understanding the intrinsic differences between the TrkA and TrkB TKDs.

The studies in this dissertation were performed with soluble TrkA and TrkB TKDs. To mimic ligand-induced RTK dimerization, the histidine-tagged TrkA and TrkB TKD should be clustered (via its histidine tag) on the surface of small unilamellar vesicles containing lipid molecules with a nickel-nitrilotriacetate head group (Ni-NTA DOGS). This approach has been shown to mimic ligand-induced activation for the EGFR TKD (Zhang et al., 2006) and ALK (Bresler et al., 2011). TKD clustering on the surface of the Ni-NTA-containing vesicles promotes trans-autophosphorylation (and thus activation), and has also been shown for EGFR (Zhang et al., 2006) to drive allosteric components of dimerization-induced activation. Autophosphorylation assays of TrkA and TrkB TKDs that are clustered on lipid vesicles will begin to determine the physiological significance of differences in autophosphorylation.

A vital next step in this project is to determine the significance of the faster TrkA-TKD autophosphorylation and ligand-independent TrkA self-association in cells. The best approach for the cell experiments would be to generate chimeric receptors containing the extracellular region of PDGFR and either the TrkA or TrkB intracellular domain to truly investigate the role of the intracellular domain including the TKD in defining the difference between TrkA and TrkB signaling. This approach would allow for expression matching which will be vital for interpreting any result (see below). Thus, once the proper

cells system is established, it will be essential to first validate the rate difference in autophosphorylation of TrkA and TrkB in cells. Introducing TrkA KID/hinge region mutations in the cellular context will be very informative to measure the autophosphorylation and downstream signaling response.

These cell culture experiments may prove to be difficult because the cell type chosen will greatly affect the results. These experiments should be conducted in several cell types, starting with neuroblastoma cell lines as well as PC12 cells since there is a wealth of knowledge regarding the signaling network in these contexts. Furthermore, PC12 cells can behave like sympathetic neurons when subjected to NGF and this may due to the fact that chromaffin cells (the cell type PC12 originate from) are derived from the same neural crest progenitor as sympathetic neurons (Greene 1976). However, TrkB is not normally expressed in PC12 cells and expressing TrkB and activating it in PC12 does lead to differentiation. This result could simply be due to overexpressing TrkB and not obtaining the level of TrkB needed for a proliferative response. Previous reports have shown that overexpressing EGFR and IRK converts the normal proliferative response upon activation of EGF and insulin into a differentiative response. Thus, expression levels of TrkA and TrkB need to be carefully matched in all future cell experiments.

The above-mentioned biochemical and structural experiments along with the cellular experiments will be instrumental to truly understand the origin of signaling differences between TrkA and TrkB expression and activation. Furthermore, a deeper quantitative understanding and how it relates to the TrkA and TrKB signaling differences in the cellular context will be required for safe and specific therapies targeting TrkA or TrkB.

Chapter 5:

Materials and Methods.

5.1. Plasmid Construction

DNA encoding the intracellular domain residues 498-796 of human TrkA (NCBI reference sequence NM_002529.3) and residues 542-838 of human TrkB (NCBI reference sequence XP_005252001.1) were amplified by PCR to include a coding sequence for an N-terminal hexahistidine tag and unique *EcoRI* and *XhoI* restriction sites for TrkA and TrkB. Residues 452-753 of human Ror2 (NCBI reference sequence NM_004560.3) was also amplified by PCR to include a coding sequence for an N-terminal hexahistidine tag and unique *SpeI* and *XhoI* restriction sites for Ror2. Appropriately digested fragments were subcloned into the pFastBac1 vector (Invitrogen) using the indicated restriction sites. The Bac-to-Bac expression system (Invitrogen) was then used for generation of recombinant baculoviruses and for protein expression in *Spodoptera frugiperda* Sf9 cells.

5.2. Protein Production and Purification

Sf9 cells at 1.5-2 x 10^6/ml were infected with recombinant baculovirus, and harvested by centrifugation after 3 days. Sf9 cells expressing histidine-tagged TrkA$^{498-796}$ (~7 liters of medium) were lysed by sonication in 100 ml of 50 mM $NaKPO_4$, pH 8.0, containing 300 mM NaCl, 5% glycerol, 10 mM imidazole, 10 mM 2-mercaptoethanol, 0.5 mM PMSF and protease inhibitor cocktail (Roche). The lysate was then mixed with Ni-NTA beads (Qiagen) for 1 hour at 4°C. Beads were washed in 50 column-volumes of lysis buffer (described above), and bound TrkA-TKD was eluted with increasing concentrations of imidazole in 25 mM MES, pH 6, containing 300 mM NaCl, 5% (w/v) glycerol, 10 mM 2-mercaptoethanol, 0.5 mM PMSF and protease inhibitor cocktail (Roche). Eluted protein

was then further purified using a Fractogel SO_3^- cation exchange column (EMD) equilibrated with 25 mM MES, pH 6, containing 5% glycerol, 2 mM DTT and eluting with a gradient from 10 mM to 1 M NaCl. TrkA was then applied to a HiTrap Butyl Sepharose HP column (GE Healthcare) in 25 mM MES, pH 6, containing 150 mM NaCl and 2 mM DTT, eluting with a gradient from 0.8 M to 0 M $(NH_4)_2SO_4$, and subjected to a final step of size exclusion chromatography using a Superdex 200 column (GE Healthcare) equilibrated in 25 mM MES, pH 6, containing 250 mM NaCl and 2 mM DTT.

Sf9 cells expressing histidine-tagged Ror2 TKD (~8 liters of medium) were lysed by sonication in 150 ml of lysis buffer, composed of 20 mM $NaKPO_4$, pH 8.0, containing 200 mM NaCl, 10 mM 2-mercaptoethanol, 1 mM PMSF, 10 μM benzamidine, 2.3 μM leupeptin, 2 μM aprotinin, and 3 μM pepstatin (Sigma). Cell lysates containing Ror2 TKD protein were mixed with Ni-NTA beads (Qiagen) for 30 minutes at 4°C, which were then washed with lysis buffer prior to elution of protein in lysis buffer containing 200 mM imidazole. Eluted protein was passed through a Fractogel TMAE column (EMD) equilibrated with 25 mM Tris-HCl, pH 8, containing 100 mM NaCl and 2 mM DTT to remove anionic contaminants, and was then passed through a CHT2.1 hydroxyapatite column (Bio-Rad) equilibrated in 20 mM HEPES, pH 8, containing 2.5 mM $NaKPO_4$, 200 mM NaCl, 2 mM DTT, and 1 mM PMSF, prior to loading on to a HiTrap Butyl Sepharose HP column (GE Healthcare) in 25 mM Tris-HCl, pH 8, containing 125 mM NaCl and 2 mM DTT. Ror2-TKD was eluted from butyl sepharose with a gradient from 0.5 M to 0 M $(NH_4)_2SO_4$ in this same buffer, and then subjected to size exclusion chromatography using a Superdex 200 column (GE Healthcare) equilibrated in 20 mM Tris-HCl, pH 7.5, containing 120 mM NaCl and 1 μM TCEP.

The purification scheme described above for TrkA-TKD was used for the crystallization studies and initial autophosphorylation assays. However, the purification scheme was optimized for further studies of TrkA and TrkB TKDs due to heterogeneity of post translation modification and to ensure no phosphatase contamination. The cells were lysed and bound to Ni-NTA beads as described above for TrkA-TKD. However, the bound TrkA or TrkB TKD was eluted with increasing concentrations of imidazole in 50 mM $NaKPO_4$, pH8, containing 300 mM NaCl, 5% (w/v) glycerol, 10 mM 2-mercaptoethanol, 0.5 mM PMSF and protease inhibitor cocktail (Roche). Eluted protein was then further purified using a Fractogel SO_3^- cation exchange column (EMD) equilibrated with 25 mM MES, pH 6, containing 5% glycerol, 2 mM DTT and eluting with a gradient from 10 mM to 1 M NaCl. TrkA and TrkB TKD proteins were concentrated to ~ 5-6 mls and treated with YopH phosphatase at 2 μM for 1 hour at 30° in the presence of 1mM EDTA. Pilot experiments with YopH had lower activity at a higher pH an observation previously reported. Furthermore, EDTA was added during the phosphatase treatment since protein tyrosine phosphatase activity is not dependent on metals and in some cases metal ions can inhibit their activity. (Lu and Zhu, 2011; Zhang et al., 1992; Zhang, 2003). YopH was purified away using a Fractogel SO_3^- cation exchange column (EMD) equilibrated with 25 mM HEPES, pH 8, containing 5% glycerol, 2 mM DTT. YopH is highly basic and binds very effectively to the cation exchange column at pH 8 where as both TrkA and TrkB TKDs do not bind. TrkA and TrkB TKD proteins were then concentrated to a volume of ~5-6 ml and treated with 2 μM λ phosphatase in the presence of 5 mM $MnCl_2$ for 1 hour at 30°. Pilot experiments and previous reports showed greater activity of λ phosphatase at pH 8 and with $MnCl_2$ (Barik, 1993; Zhuo et al., 1993). λ phosphatase was purified away by using a Fractogel SO_3^- cation exchange

column (EMD) equilibrated with 25 mM MES, pH 6, containing 5% glycerol, 2 mM DTT and eluting with a gradient from 10 mM to 1 M NaCl. TrkA or TrkB TKD was then applied to a HiTrap Butyl Sepharose HP column (GE Healthcare) in 25 mM MES, pH 6, containing 150 mM NaCl and 2 mM DTT, eluting with a gradient from 0.8 M to 0 M $(NH_4)_2SO_4$, and subjected to a final step of size exclusion chromatography using a Superdex 200 column (GE Healthcare) equilibrated in 25 mM Hepes, pH 8, containing 150 mM NaCl and 2 mM DTT.

YopH BL21 cells were grown in 1 liter of LB with 50 µg/ml streptomyocin at 37°C until a density of ~0.6 $OD_{600\ nm}$. At that point, the cells were cooled down to 18°C and induced with 1mM isopropyl β-D-1-thiogalactopyranoside (IPTG) and grown overnight. Cells were harvested by centrifugation at 2,000 x g for 15 minutes at 4°C. Cells were lysed by sonication in 50 mM Hepes, pH 7.4, 300 mM NaCl, 10% glycerol, 10 mM imidazole, 10 mM 2-mercaptoethanol, 0.5 mM PMSF and protease inhibitor cocktail (Roche). Protein lysate was incubated with Ni-NTA beads (Qiagen) for 1 hour at 4°C and then washed with 20 mM imidazole prior to eluting with 300 mM imidazole. YopH was then loaded on to a Fractogel SO_3^- cation exchange column (EMD) equilibrated with 25 mM MES, pH 6, containing 5% glycerol, 2 mM DTT and eluting with a gradient from 10 mM to 1 M NaCl. Fractions corresponding to the peak were pooled, concentrated and loaded on to a size exclusion Superdex 200 column (GE Healthcare) equilibrated in 25 mM MES, pH 6, containing 250 mM NaCl and 2 mM DTT.

λ phosphatase was expressed and purified essentially as described (Zhuo et al., 1993). However, the first purification step was phenyl-sepharose chromatography and not Bio-Gel A chromatography. Instead, after the phenyl-sepharose column, the λ phosphatase fractions were pooled, concentrated and loaded on to a size exclusion (Superdex 200)

column (GE Healthcare) equilibrated in 25 mM Tris, pH 7.5, containing 150 mM NaCl. Purified λ phosphatase was stored at -80°C at 20 mg/ml in the buffer used for size exclusion chromatography plus a final concentration of 10% glycerol.

5.3. Crystallization and Structure Determination

Crystals were obtained using the hanging drop vapor diffusion method, by mixing equal volumes of protein and reservoir solutions and equilibrating over the reservoir solution at 21˚C. For TrkA$^{498-796}$ TKD, protein was concentrated to ~6 mg/ml in 25 mM MES, pH 6, containing 250 mM NaCl and 2 mM DTT and then diluted with water to 3.25 mg/ml. Crystals were obtained with a reservoir solution of 1.5 M NaCl, 0.1 M MES pH 6.5, and 0.2 M Na/K phosphate. For Ror2$^{452-753}$, protein was concentrated to 7.2 mg/ml in 20 mM Tris-HCl, pH7.5, containing 125 mM NaCl, and 1 μM TCEP, and crystals were obtained over a reservoir containing 20% PEG3350 and 0.2 M $Mg(NO_3)_2$ (Hampton Research PEG Ion Screen 16). Prior to flash freezing in liquid nitrogen, TrkA$^{498-796}$ crystals were cryo-protected in reservoir solution containing 40 % (w/v) dextrose, and Ror2$^{452-753}$ crystals were cryo-protected in reservoir solution containing 20% (w/v) glycerol. Diffraction data were collected at beamline 23ID-B of GM/CA@APS (Advanced Photon Source) and were processed using HKL2000 (Otwinowski and Minor, 1997) (Table 1). TrkA$^{498-796}$ crystallized in space group H32 with one molecule in the asymmetric unit, and Ror2$^{452-753}$ crystallized in space group $C222_1$ with 2 molecules in the asymmetric unit.

Structures were solved by molecular replacement with Phaser (Collaborative Computational Project, 1994), using coordinates for the MuSK tyrosine kinase domain (PDB 1LUF) (Till et al., 2002) as search model. Cycles of manual building/rebuilding using Coot (Emsley and Cowtan, 2004) were alternated with rounds of refinement

employing REFMAC (Collaborative Computational Project, 1994), plus composite omit maps calculated with CNS (Brunger et al., 1998). Later stages employed PHENIX (Adams et al., 2010), with TLS refinement (Winn et al., 2001). PROCHECK (Laskowski et al., 1993) identified no residues in the disallowed region of the Ramachandran plot. Structure figures were generated using PyMOL (The PyMOL Molecular Graphics System, Version 1.5.0.4, Schrödinger, LLC). Data collection and refinement statistics are shown in Table 1. The final refined TrkA model includes amino acids 498-534, 537-548, 550-610, and 614-793. There is additional density close to the N-terminus of TrkA structure that we could not model confidently, projecting towards the active site. The final Ror2 structure is missing density for residues 452-463 at the N-terminus. In addition, residues 512, 516, 576-580, and 752-753 in chain A could not be confidently modeled, and nor could residues 515, 573-580, and 753 in chain B. Cys^{694} in both chain A and chain B of the Ror2 TKD appears to form a disulfide bond with an equivalent residue in a symmetry mate.

5.4. Circular dichroism

TrkA and TrkB TKD proteins were diluted to 2 μM into a buffer containing 25 mM NaH_2PO_4 •K_2HPO_4 pH7.4, 150 mM NaCl. CD spectra and thermal melting curves were obtained on an Aviv 62A DS spectropolarimeter (Aviv Associates, NJ) with a 1 mm pathlength sample holder. The wavelength scan was performed at 1°C. The thermal melting curves were obtained by heating samples from 1°C to 97°C in 1°C increments with the circular dichroism at 222 nm being measured at each step. Mean residue ellipticity was determined using the formula $MRE = \theta_d*0.1*MRW/(d*c)$, where θ_d =

observed ellipticity (mdeg), *MRW* = mean residue weight (MW of protein/number of residues), *d* = pathlength in cm, *c* = concentration of protein in mg/ml. The K2D3 server was used to predict the helical and sheet composition of TrkA and TrkB TKDs (Louis-Jeune et al., 2011).

5.5. Sedimentation equilibrium analytical ultracentrifugation experiments

All sedimentation equilibrium (SE) analytical ultracentrifugation (AUC) experiments were performed at 4°C using a Beckman Coulter™ Optima XL-A instrument. Initial SE AUC experiments to assess protein aggregation were performed with 16.7 μM of TrkA-TKD and 17.6 μM of TrkB-TKD. The TrkA-TKD sample for AUC was not treated with phosphatases during purification where as the TrkB-TKD sample was treated with phosphatases during purification. Data shown were collected at 10,000 rpm. To assess the behavior of pTrkA-TKD and mTrkA-TKD in solution, SE AUC experiments were performed with 16.7 μM of pTrkA-TKD and 16.7 μM of mTrkA-TKD. Data were collected at 10,000 rpm and 15,000 rpm.

To analyze the data, we generated a plot of the natural logarithm (ln) of absorbance at 280 nm versus a function of the radius squared $(r^2 - r_o^2)/2$, where r is the radial position in the sample and r_o is the radial position of the meniscus. This analysis provides a straight line with slope proportional to the molecular mass for a single species.

5.6. Autophosphorylation Assays

All autophosphorylation reactions were conducted in the presence of 1 mM ATP (Sigma-Aldrich) and 10 mM $MgCl_2$ in a buffer containing 100 mM HEPES pH 7.4, 150 mM NaCl, 2 mM DTT and 1x 'Halt' phosphatase inhibitor cocktail (Thermo Scientific #1862495), which contains sodium fluoride, sodium orthovanadate, sodium pyrophosphate, and β-glycerophosphate. Figure legends indicate the concentration of TrkA and TrkB TKD proteins, which ranged from 1 to 10 μM and indicate the temperature the reactions were incubated which ranged from 15°C -37°C. The autophosphorylation reactions were analyzed by various gel-based methods including native PAGE, SDS-PAGE autoradiography, SDS-PAGE Western blotting, and PhosTag SDS-PAGE. The autophosphorylation reactions analyzed by native PAGE and SDS-PAGE autoradiography did not contain 1x Halt phosphatase inhibitor cocktail unless indicated in the figure legend. For the phosphatase inhibitor comparison experiment, 'PhosStop' inhibitor cocktail inhibitor (a proprietary blend of phosphatase inhibitors) was purchased from Roche.

5.7. Gel based Assays

Native PAGE was conducted following the Laemmli protocol (Laemmli, 1970), except that SDS was not included in the gel or electrophoresis buffers. Thus, samples were separated on a 7.5 % native gel with a pH 6.8 Tris-HCl stacking gel and a pH 8.8 Tris-HCl resolving gel. The electrophoresis running buffer used was a Tris-glycine pH 8.8 buffer. Gels were stained at room temperature with Coomassie brilliant blue R-250. Coomassie stained native gels were imaged on a Kodak Image Station 440 CF.

Autoradiographs and Coomassie gels were used to monitor a time course of TrkA and TrkB autophosphorylation. Samples were separated on a 12.5% Laemmli gel by SDS-PAGE, gels were stained at room temperature with Coomassie brilliant blue R-250, destained and then dried using a gel dryer (Thermo electron corporation). Dried gels were applied to a storage phosphor screen for overnight exposure. Phosphor screens were then imaged using a Storm 820 phosphorimager (Molecular Dynamics®). The autoradiography signal was normalized by the amount of protein in each lane detected by Coomassie stain.

For SDS PAGE Western blotting, samples were separated on a 12.5% Laemmli gel, transferred to nitrocellulose and then blocked with blocking buffer (LI-COR Biosciences blocking buffer diluted 1:2 with PBS). Membranes incubated with primary antibody diluted in blocking buffer overnight at 4°C, washed with PBS with 1% Tween, and then incubated with secondary antibody diluted in blocking buffer. Membranes were washed with PBS with 1% Tween and then subjected to a final wash with just PBS. Membranes were imaged using the Odyssey® FC (LI-COR Biosciences) imaging station.

PhosTag gels were made using the PhosTag™ acrylamide reagent (Wako Pure Chemical Industries, Ltd., catalog # AAL-107) along with $ZnCl_2$ as previously described (Kinoshita and Kinoshita-Kikuta, 2011)). The composition of reagents for optimal separation of phosphorylated Trk TKD species was 25 μM PhosTag™ acrylamide reagent and a 10% acrylamide gel using acrylamide:bis solution (29:1). Gels were run at a constant 70V for 3 hours. PhosTag gels were stained at room temperature for ~15-20 minutes with Coomassie brilliant blue R-250. For Western blotting, prior to transferring to nitrocellulose, PhosTag gels were soaked in transfer buffer containing 1mM EDTA for 15

minutes and then washed for 15 minutes in transfer buffer without EDTA. The rest of the Western blot protocol was performed as described above.

For Western blotting, the goat anti-pan-Trk antibody (catalog number: sc-11-g) and rabbit anti-phospho-Trk pY676 (catalog number: sc-130222) antibodies were used at a 1:500 dilution and are from Santa Cruz. The rabbit anti-phospho Trk pYY680/681 (catalog number: 4621)) and rabbit anti-pY791 (catalog number: 4168) were used at 1:1000 dilution. Note that the Cell Signaling phospho antibodies are sold using the TrkA isoform *I* numbering, thus pYY674/675 and pY785 corresponds to pYY680/681 and pY791 in isoform *II,* respectively. The secondary antibodies used were IRDye® 800CW donkey anti-rabbit IgG (# 926-32213) and IRDye® 680RD donkey anti-goat IgG (# 926-68074) from LI-COR Biosciences.

The normalized relative signals from the Western blots were determined first by normalizing each phosphospecific signal with the total Trk signal. Each normalized signal was then divided and by the maximum signal per phosphospecific antibody per reaction.

5.8 Generation and purification of phospho-Trk TKD

Autophosphorylation reactions were conducted to generate phospho-Trk for enzymatic studies. Western blotting of PhosTag gels with phosphospecific antibodies (see Western blotting methods) were used to monitor the reactions. TrkA-TKD at 10 μM was incubated at room temperature with 1 mM ATP, 10 mM $MgCl_2$ in a buffer containing 100 mM HEPES pH 7.4, 150 mM NaCl, 2 mM DTT. At 5 minutes, the reaction was quenched with

EDTA to achieve a final concentration of 100mM. TrkB-TKD at 7.5 μM was incubated at 30°C with 1 mM ATP, 10 mM $MgCl_2$ in a buffer containing 100 mM HEPES pH 7.4, 150 mM NaCl, 2 mM DTT and 1x Halt phosphatase inhibitor cocktail. At 4 minutes, the reaction was quenched with EDTA to achieve a final concentration of 100mM. Samples were spin filtered with SpinX columns and loaded on to a Superdex 200 column (GE Healthcare) equilibrated in 25 mM Hepes, pH 8, containing 150 mM NaCl and 2 mM DTT and 1x Halt phosphatase inhibitor cocktail. BioRad gel filtration standards (# 151-1901) were used to assess pTrk and mTrk TKD elution peaks.

5.9. Quantitative kinase assays

The quantitative kinase assays employed a peptide mimic of the TrkA and TrkB activation loop. The TrkA activation loop peptide (SRDIYSTDYYRVGGRTMLPIR) and TrkB peptide (SRDVYSTDYYRVGGHTMLPIR) were purchased from CanPeptide.

Reactions were performed at room temperature in a buffer containing 100 mM HEPES pH 7.4, 150 mM NaCl, 0.5 mg/ml BSA, 2 mM DTT, 10 mM $MgCl_2$,1x Halt phosphatase inhibitor cocktail and trace amounts of γ-^{32}P ATP (20-40 μCi). For $K_{m,\ ATP}$ determination, TrkA and TrkB TKDs were assayed with variable ATP concentrations (5 mM to 0.039 mM) in the presence of fixed 2 mM peptide substrate and 10 mM $MgCl_2$. For $K_{m,\ peptide}$ determination, TrkA and TrkB TKDs were assayed with variable peptide concentrations (4 mM to 0.031 mM), fixed 2 mM ATP and 10 mM $MgCl_2$. The protein concentration used for these experiments were 30 nM dephosphorylated TrkA-TKD, 400 nM dephosphorylated TrkB-TKD and 8 nM of both phosphorylated TrkA and phosphorylated TrkB TKDs.

Samples were taken at each time point, spotted onto pieces of P81 phosphocellulose squares (Millipore # 20-134), and immediately quenched with 0.5% phosphoric acid. The phosphocellulose squares were then washed extensively with 0.5% phosphoric acid and dried with acetone. A Tri-Carb 2900TR liquid scintillation analyzer (PerkinElmer) was used to measure the incorporated radioactivity of each phosphocellulose square. Initial rates were determined under conditions of <10% product formation – ensuring linearity – converted to specific activity, normalized for enzyme concentration and data fit to the Michaelis-Menten equation ($v_o = v_{max}[S]/(K_m+[S])$) using GraphPad Prism version 5.0.

5.10. Radioactive autophosphorylation assays

Radioactive autophosphorylation assays were performed at RT with 4 μM of TrkA-TKD, TrkA KID, or TrkB TKD protein in the presence of 2mM ATP, 10 mM $MgCl_2$ 100 mM HEPES pH 7.4, 150 mM NaCl, 2 mM DTT, 1x Halt phosphatase inhibitor cocktail and trace amounts of γ-^{32}P ATP (40 μCi). Samples taken at each time point were processed as above for the quantitative kinase assay samples. Counts from the scintillation analyzer were converted to moles of phosphate incorporated using measured γ-^{32}P-ATP specific activity and then normalized to enzyme concentration. Each reaction data set was converted to percent maximum moles of phosphate incorporated normalized to enzyme concentration.

Data were plotted and analyzed by several methods. Histogram plots were generated to compare relative moles of phosphate incorporated per mole of enzyme for time points from 0 to 5 minutes. A paired *t* test was used to compare data obtained with TrkA-TKD (n=3), TrkA KID-TKD (n=2), and TrkB-TKD (n=2), to determine statistical significance of

differences, with significance ($P < 0.05$) denoted with an asterisk. Data were also plotted and fitted with a four-parameter logistic equation to obtain time to half maximal autophosphorylation. Curves were fit to the 0 to 30 minute data. Histogram plots were used to compare the time to half maximal autophosphorylation for TrkA, TrkA KID, and TrkB TKDs. A paired *t* test was used to determine statistical significance ($P < 0.05$) denoted as an asterisk. GraphPad Prism version 5.0 was used to plot the data and perform the paired t tests.

References

Adams, P.D., Afonine, P.V., Bunkoczi, G., Chen, V.B., Davis, I.W., Echols, N., Headd, J.J., Hung, L.W., Kapral, G.J., Grosse-Kunstleve, R.W., et al. (2010). PHENIX: a comprehensive Python-based system for macromolecular structure solution. Acta Cryst (2010). D66, 213-221 [Doi:10.1107/S0907444909052925] 1–9.

Al-Hasani, H., Paßlack, W., and Klein, H.W. (1994). Phosphoryl exchange is involved in the mechanism of the insulin receptor kinase. Febs Letters *349*, 17–22.

Albaugh, P., Fan, Y., Mi, Y., Sun, F., Adrian, F., Li, N., Jia, Y., Sarkisova, Y., Kreusch, A., Hood, T., et al. (2012). Discovery of GNF-5837, a Selective TRK Inhibitor with Efficacy in Rodent Cancer Tumor Models. ACS Med. Chem. Lett. *3*, 140–145.

Anderson, D., Koch, C.A., Grey, L., Ellis, C., Moran, M.F., and Pawson, T. (1990). Binding of SH2 domains of phospholipase C gamma 1, GAP, and Src to activated growth factor receptors. Science *250*, 979–982.

Argetsinger, L.S., and Shafer, J.A. (1992). The reversible and irreversible autophosphorylations of insulin receptor kinase. The Journal of Biological Chemistry *267*, 22095–22101.

Artim, S.C., Mendrola, J.M., and Lemmon, M.A. (2012). Assessing the range of kinase autoinhibition mechanisms in the insulin receptor family. Biochem. J. *448*, 213–220.

Bae, J.H., Boggon, T.J., Tome, F., Mandiyan, V., Lax, I., and Schlessinger, J. (2010). Asymmetric receptor contact is required for tyrosine autophosphorylation of fibroblast growth factor receptor in living cells. Proceedings of the National Academy of Sciences *107*, 2866–2871.

Barbacid, M. (1994). The Trk family of neurotrophin receptors. Journal of Neurobiology *25*, 1386–1403.

Bardelli, A., Parsons, D.W., Silliman, N., Ptak, J., Szabo, S., Saha, S., Markowitz, S., Willson, J.K., Parmigiani, G., Kinzler, K.W., et al. (2003). Mutational analysis of the tyrosine kinome in colorectal cancers. Science *300*, 949.

Barik, S. (1993). Expression and biochemical properties of a protein serine/threonine phosphatase encoded by bacteriophage lambda. Proceedings of the National Academy of Sciences of the United States of America *90*, 10633–10637.

Barker, P.A., Lomen-Hoerth, C., Gensch, E.M., Meakin, S.O., Glass, D.J., and Shooter, E.M. (1993). Tissue-specific alternative splicing generates two isoforms of the trkA receptor. The Journal of Biological Chemistry *268*, 15150–15157.

Bartheld, von, C.S., and Fritzsch, B. (2006). Comparative analysis of neurotrophin receptors and ligands in vertebrate neurons: tools for evolutionary stability or changes in neural circuits? Brain Behav Evol *68*, 157–172.

Bartkowska, K., Turlejski, K., and Djavadian, R.L. (2010). Neurotrophins and their receptors in early development of the mammalian nervous system. Acta Neurobiol Exp (Wars) *70*, 454–467.

Belfiore, A., and Malaguarnera, R. (2011). Insulin receptor and cancer. Endocrine-Related Cancer *18*, R125–R147.

Benito-Gutierrez, E., Garcia-Fernandez, J., and Comella, J.X. (2006). Origin and evolution of the Trk family of neurotrophic receptors. Molecular and Cellular Neurosciences *31*, 179–192.

Bertrand, T., Kothe, M., Liu, J., Dupuy, A., Rak, A., Berne, P.F., Davis, S., Gladysheva, T., Valtre, C., Crenne, J.Y., et al. (2012). The crystal structures of TrkA and TrkB suggest key regions for achieving selective inhibition. Journal of Molecular Biology *423*, 439–453.

Blume-Jensen, P., and Hunter, T. (2001). Oncogenic kinase signalling. Nature *411*, 355–365.

Borrello, M.G., Bongarzone, I., Pierotti, M.A., Luksch, R., Gasparini, M., Collini, P., Pilotti, S., Rizzetti, M.G., Mondellini, P., and De Bernardi, B. (1993). trk and ret proto-oncogene expression in human neuroblastoma specimens: high frequency of trk expression in non-advanced stages. Int. J. Cancer *54*, 540–545.

Bossi, R.T., Saccardo, M.B., Ardini, E., Menichincheri, M., Rusconi, L., Magnaghi, P., Orsini, P., Avanzi, N., Borgia, A.L., Nesi, M., et al. (2010). Crystal structures of anaplastic lymphoma kinase in complex with ATP competitive inhibitors. Biochemistry *49*, 6813–6825.

Bothwell, M. (2006). Evolution of the neurotrophin signaling system in invertebrates. Brain Behav Evol *68*, 124–132.

Bresler, S.C., Wood, A.C., Haglund, E.A., Courtright, J., Belcastro, L.T., Plegaria, J.S., Cole, K., Toporovskaya, Y., Zhao, H., Carpenter, E.L., et al. (2011). Differential inhibitor sensitivity of anaplastic lymphoma kinase variants found in neuroblastoma. Sci Transl Med *3*, 108ra114.

Brodeur, G.M. (2003). Neuroblastoma: biological insights into a clinical enigma. Nat Rev Cancer *3*, 203–216.

Brodeur, G.M., Nakagawara, A., Yamashiro, D.J., Ikegaki, N., Liu, X.G., Azar, C.G., Lee, C.P., and Evans, A.E. (1997). Expression of TrkA, TrkB and TrkC in human neuroblastomas. Journal of Neuro-Oncology *31*, 49–55.

Brodeur, G.M., Minturn, J.E., Ho, R., Simpson, A.M., Iyer, R., Varela, C.R., Light, J.E., Kolla, V., and Evans, A.E. (2009). Trk receptor expression and inhibition in neuroblastomas. Clin. Cancer Res. *15*, 3244–3250.

Brunger, A.T., Adams, P.D., Clore, G.M., DeLano, W.L., Gros, P., Grosse-Kunstleve, R.W., Jiang, J.S., Kuszewski, J., Nilges, M., Pannu, N.S., et al. (1998). Crystallography & NMR system: A new software suite for macromolecular structure determination. Acta Crystallogr D Biol Crystallogr *54*, 905–921.

Burnett, G., and Kennedy, E.P. (1954). The enzymatic phosphorylation of proteins. The Journal of Biological Chemistry *211*, 969–980.

Carpenter, E.L., and Mossé, Y.P. (2012). Targeting ALK in neuroblastoma—preclinical and clinical advancements. Nature Reviews Clinical Oncology *9*, 391–399.

Carpenter, G., King, L., and Cohen, S. (1978). Epidermal growth factor stimulates phosphorylation in membrane preparations in vitro. Nature *276*, 409–410.

Casaletto, J.B., and McClatchey, A.I. (2012). Spatial regulation of receptor tyrosine kinases in development and cancer. Nat Rev Cancer *12*, 387–400.

Chen, G., Porter, M.D., Bristol, J.R., Fitzgibbon, M.J., and Pazhanisamy, S. (2000). Kinetic Mechanism of the p38-α MAP Kinase: Phosphoryl Transfer to Synthetic Peptides. Biochemistry *39*, 2079–2087.

Chen, H., Ma, J., Li, W., Eliseenkova, A.V., Xu, C., Neubert, T.A., Miller, W.T., and Mohammadi, M. (2007). A molecular brake in the kinase hinge region regulates the activity of receptor tyrosine kinases. Molecular Cell *27*, 717–730.

Chiara, F. (2003). Mutations in the met Oncogene Unveil a "Dual Switch" Mechanism Controlling Tyrosine Kinase Activity. The Journal of Biological Chemistry *278*, 29352–29358.

Choi, D.Y., Toledo-Aral, J.J., Segal, R., and Halegoua, S. (2001). Sustained signaling by phospholipase C-gamma mediates nerve growth factor-triggered gene expression. Molecular and Cellular Biology *21*, 2695–2705.

Choi, S.H., Mendrola, J.M., and Lemmon, M.A. (2006). EGF-independent activation of cell-surface EGF receptors harboring mutations found in gefitinib-sensitive lung cancer. Oncogene *26*, 1567–1576.

Chung, I., Akita, R., Vandlen, R., Toomre, D., Schlessinger, J., and Mellman, I. (2010). Spatial control of EGF receptor activation by reversible dimerization on living cells. Nature *464*, 783–787.

Cichowski, K., and Janne, P.A. (2010). Drug discovery: Inhibitors that activate. Nature *464*, 358–359.

Clayton, A.H.A., Walker, F., Orchard, S.G., Henderson, C., Fuchs, D., Rothacker, J., Nice, E.C., and Burgess, A.W. (2005). Ligand-induced dimer-tetramer transition during the activation of the cell surface epidermal growth factor receptor-A multidimensional microscopy analysis. The Journal of Biological Chemistry *280*, 30392–30399.

Cobb, M., Sang, B., Gonzalez, R., GOLDSMITH, E., and Ellis, L. (1989). Autophosphorylation activates the soluble cytoplasmic domain of the insulin receptor in an intermolecular reaction. The Journal of Biological Chemistry *264*, 18701–18706.

Cohen, P. (2002). The origins of protein phosphorylation. Nat. Cell Biol. *4*, E127–E130.

Cohen, S. (1962). Isolation of a mouse submaxillary gland protein accelerating incisor eruption and eyelid opening in the new-born animal. The Journal of Biological Chemistry *237*, 1555–1562.

Cohen, S., and Levi-Montalcini, R. (1957). Purification and properties of a nerve growth-promoting factor isolated from mouse sarcoma 180. Cancer Research *17*, 15–20.

Cohen, S. (1965). The stimulation of epidermal proliferation by a specific protein (EGF). Dev. Biol. *12*, 394–407.

Collaborative Computational Project, N.4. (1994). The CCP4 suite: programs for protein crystallography. Acta Cryst (1994). D50, 760-763 [Doi:10.1107/S0907444994003112] 1–4.

Collett, M.S., and Erikson, R.L. (1978). Protein kinase activity associated with the avian sarcoma virus src gene product. Proceedings of the National Academy of Sciences of the United States of America *75*, 2021–2024.

Corless, C.L., and Heinrich, M.C. (2008). Molecular pathobiology of gastrointestinal stromal

sarcomas. Annu Rev Pathol *3*, 557–586.

Cunningham, M.E., Stephens, R.M., Kaplan, D.R., and Greene, L.A. (1997). Autophosphorylation of activation loop tyrosines regulates signaling by the TRK nerve growth factor receptor. The Journal of Biological Chemistry *272*, 10957–10967.

Dancey, J.E., Bedard, P.L., Onetto, N., and Hudson, T.J. (2012). The genetic basis for cancer treatment decisions. Cell *148*, 409–420.

Davidson, B., Reich, R., Lazarovici, P., Nesland, J.M., Skrede, M., Risberg, B., Trop, C.G., and Fl renes, V.A. (2003). Expression and Activation of the Nerve Growth Factor Receptor TrkA in Serous Ovarian Carcinoma. Clinical Cancer Research *9*, 2248–2259.

Davies, H., Hunter, C., Smith, R., Stephens, P., Greenman, C., Bignell, G., Teague, J., Butler, A., Edkins, S., Stevens, C., et al. (2005). Somatic mutations of the protein kinase gene family in human lung cancer. Cancer Research *65*, 7591–7595.

De Meyts, P. (2004). Insulin and its receptor: structure, function and evolution. Bioessays *26*, 1351–1362.

De Meyts, P. (2008). The insulin receptor: a prototype for dimeric, allosteric membrane receptors? Trends in Biochemical Sciences *33*, 376–384.

Dikic, I., Schlessinger, J., and Lax, I. (1994). PC12 cells overexpressing the insulin receptor undergo insulin-dependent neuronal differentiation. Curr. Biol. *4*, 702–708.

Ding, L., Getz, G., Wheeler, D.A., Mardis, E.R., McLellan, M.D., Cibulskis, K., Sougnez, C., Greulich, H., Muzny, D.M., Morgan, M.B., et al. (2008). Somatic mutations affect key pathways in lung adenocarcinoma. Nature *455*, 1069–1075.

Donella-Deana, A., Marin, O., Cesaro, L., Gunby, R.H., Ferrarese, A., Coluccia, A.M.L., Tartari, C.J., Mologni, L., Scapozza, L., Gambacorti-Passerini, C., et al. (2005). Unique Substrate Specificity of Anaplastic Lymphoma Kinase (ALK): Development of Phosphoacceptor Peptides for the Assay of ALK Activity †. Biochemistry *44*, 8533–8542.

Ek, B., Westermark, B., Wasteson, A., and Heldin, C.H. (1982). Stimulation of tyrosine-specific phosphorylation by platelet-derived growth factor. Nature *295*, 419–420.

Emsley, P., and Cowtan, K. (2004). Coot: model-building tools for molecular graphics. Acta Crystallogr D Biol Crystallogr *60*, 2126–2132.

Favelyukis, S., Till, J.H., Hubbard, S.R., and Miller, W.T. (2001). Structure and autoregulation of the insulin-like growth factor 1 receptor kinase. Nat. Struct Biol. *8*, 1058–1063.

Fischer, E.H., and Krebs, E.G. (1955). Conversion of phosphorylase b to phosphorylase a in muscle extracts. The Journal of Biological Chemistry *216*, 121–132.

Fischer, E.H., Graves, D.J., Crittenden, E.R.S., and Krebs, E.G. (1959). Structure of the site phosphorylated in the phosphorylase b to a reaction. The Journal of Biological Chemistry *234*, 1698–1704.

Forbes, S.A., Tang, G., Bindal, N., Bamford, S., Dawson, E., Cole, C., Kok, C.Y., Jia, M., Ewing, R., and Menzies, A. (2010). COSMIC (the Catalogue of Somatic Mutations in Cancer): a resource

to investigate acquired mutations in human cancer. Nucleic Acids Research *38*, D652–D657.

Fukami, Y., and Lipmann, F. (1983). Reversal of Rous sarcoma-specific immunoglobulin phosphorylation on tyrosine (ADP as phosphate acceptor) catalyzed by the src gene kinase. Proceedings of the National Academy of Sciences of the United States of America *80*, 1872–1876.

Furdui, C.M., Lew, E.D., Schlessinger, J., and Anderson, K.S. (2006). Autophosphorylation of FGFR1 kinase is mediated by a sequential and precisely ordered reaction. Molecular Cell *21*, 711–717.

Gadella, T.W., and Jovin, T.M. (1995). Oligomerization of epidermal growth factor receptors on A431 cells studied by time-resolved fluorescence imaging microscopy. A stereochemical model for tyrosine kinase receptor activation. The Journal of Cell Biology *129*, 1543–1558.

Gouet, P. (2003). ESPript/ENDscript: extracting and rendering sequence and 3D information from atomic structures of proteins. Nucleic Acids Res. *31*, 3320–3323.

Greco, A., Miranda, C., and Pierotti, M.A. (2010). Rearrangements of NTRK1 gene in papillary thyroid carcinoma. Molecular and Cellular Endocrinology *321*, 44–49.

Green, J.L., Kuntz, S.G., and Sternberg, P.W. (2008). Ror receptor tyrosine kinases: orphans no more. Trends in Cell Biology *18*, 536–544.

Griffith, J., Black, J., Faerman, C., Swenson, L., Wynn, M., Lu, F., Lippke, J., and Saxena, K. (2004). The structural basis for autoinhibition of FLT3 by the juxtamembrane domain. Molecular Cell *13*, 169–178.

Gross, C.H., and Shuman, S. (1998). Characterization of a baculovirus-encoded RNA 5'-triphosphatase. J. Virol. *72*, 7057–7063.

Gruppuso, P.A., Boylan, J.M., Levine, B.A., and Ellis, L. (1992). Insulin receptor tyrosine kinase domain auto-dephosphorylation. Biochemical and Biophysical Research Communications *189*, 1457–1463.

Gschwind, A., Fischer, O.M., and Ullrich, A. (2004). The discovery of receptor tyrosine kinases: targets for cancer therapy. Nat Rev Cancer *4*, 361–370.

Guiton, M., Gunn-Moore, F.J., and Tavare, J.M. (1995). Critical role for the phosphorylation of tyrosines 674 and 675 in signalling by the Trk tyrosine kinase. Biochem. Soc. Trans *23*, 176S.

Guiton, M., Gunn-Moore, F.J., Stitt, T.N., Yancopoulos, G.D., and Tavare, J.M. (1994). Identification of in vivo brain-derived neurotrophic factor-stimulated autophosphorylation sites on the TrkB receptor tyrosine kinase by site-directed mutagenesis. The Journal of Biological Chemistry *269*, 30370–30377.

Hammerman, P.S., Sos, M.L., Ramos, A.H., Xu, C., Dutt, A., Zhou, W., Brace, L.E., Woods, B.A., Lin, W., Zhang, J., et al. (2011). Mutations in the DDR2 kinase gene identify a novel therapeutic target in squamous cell lung cancer. Cancer Discov *1*, 78–89.

Hanks, S.K., Quinn, A.M., and Hunter, T. (1988). The protein kinase family: conserved features and deduced phylogeny of the catalytic domains. Science *241*, 42–52.

Harada, T., Yatabe, Y., Takeshita, M., Koga, T., Yano, T., Wang, Y., and Giaccone, G. (2011). Role and relevance of TrkB mutations and expression in non-small cell lung cancer. Clin. Cancer Res. *17*, 2638–2645.

Hoofnagle, A.N., Resing, K.A., Goldsmith, E.J., and Ahn, N.G. (2001). Changes in protein conformational mobility upon activation of extracellular regulated protein kinase-2 as detected by hydrogen exchange. Proceedings of the National Academy of Sciences of the United States of America *98*, 956–961.

Hoofnagle, A.N., Stoner, J.W., Lee, T., Eaton, S.S., and Ahn, N.G. (2004). Phosphorylation-dependent changes in structure and dynamics in ERK2 detected by SDSL and EPR. Biophysical Journal *86*, 395–403.

Huang, E.J., and Reichardt, L.F. (2003). Trk receptors: roles in neuronal signal transduction*. Annual Review of Biochemistry *72*, 609–642.

Hubbard, S.R. (1997). Crystal structure of the activated insulin receptor tyrosine kinase in complex with peptide substrate and ATP analog. The EMBO Journal *16*, 5572–5581.

Hubbard, S.R. (2004). Juxtamembrane autoinhibition in receptor tyrosine kinases. Nature Reviews *5*, 464–471.

Hubbard, S.R., Wei, L., Ellis, L., and Hendrickson, W.A. (1994). Crystal structure of the tyrosine kinase domain of the human insulin receptor. Nature *372*, 746–754.

Hubbard, S.R. (2009). The juxtamembrane region of EGFR takes center stage. Cell *137*, 1181–1183.

Hunter, T., and Eckhart, W. (2004). The discovery of tyrosine phosphorylation: It's all in the buffer! Cell *116*, S35–S39.

Hunter, T., and Sefton, B.M. (1980). Transforming gene product of Rous sarcoma virus phosphorylates tyrosine. Proceedings of the National Academy of Sciences of the United States of America *77*, 1311–1315.

Huse, M., and Kuriyan, J. (2002). The conformational plasticity of protein kinases. Cell *109*, 275–282.

Indo, Y. (2001). Molecular basis of congenital insensitivity to pain with anhidrosis (CIPA): Mutations and polymorphisms inTRKA (NTRK1) gene encoding the receptor tyrosine kinase for nerve growth factor. Hum. Mutat. *18*, 462–471.

Iseki, S., Wilkie, A.O., and Morriss-Kay, G.M. (1999). Fgfr1 and Fgfr2 have distinct differentiation- and proliferation-related roles in the developing mouse skull vault. Development *126*, 5611–5620.

Iwasaki, Y., Nishiyama, H., Suzuki, K., and Koizumi, S. (1997). Sequential Cis/Trans Autophosphorylation in TrkB Tyrosine Kinase. Biochemistry *36*, 2694–2700.

Joseph, R.E., Kleino, I., Wales, T.E., Xie, Q., Fulton, D.B., Engen, J.R., Berg, L.J., and Andreotti, A.H. (2013). Activation loop dynamics determine the different catalytic efficiencies of B cell- and T cell-specific tec kinases. Science Signaling *6*, ra76.

Jura, N., Endres, N.F., Engel, K., Deindl, S., Das, R., Lamers, M.H., Wemmer, D.E., Zhang, X.,

and Kuriyan, J. (2009). Mechanism for Activation of the EGF Receptor Catalytic Domain by the Juxtamembrane Segment. Cell *137*, 1293–1307.

Jura, N., Zhang, X., Endres, N.F., Seeliger, M.A., Schindler, T., and Kuriyan, J. (2011). Catalytic Control in the EGF Receptor and Its Connection to General Kinase Regulatory Mechanisms. Molecular Cell *42*, 9–22.

Kao, S., Jaiswal, R.K., KOLCH, W., and Landreth, G.E. (2001). Identification of the mechanisms regulating the differential activation of the mapk cascade by epidermal growth factor and nerve growth factor in PC12 cells. The Journal of Biological Chemistry *276*, 18169–18177.

Kaplan, D.R., Hempstead, B.L., Martin-Zanca, D., Chao, M.V., and Parada, L.F. (1991a). The trk proto-oncogene product: a signal transducing receptor for nerve growth factor. Science *252*, 554–558.

Kaplan, D.R., Martin-Zanca, D., and Parada, L.F. (1991b). Tyrosine phosphorylation and tyrosine kinase activity of the trk proto-oncogene product induced by NGF. Nature *350*, 158–160.

Kasuga, M., Karlsson, F.A., and Kahn, C.R. (1982). Insulin stimulates the phosphorylation of the 95,000-dalton subunit of its own receptor. Science *215*, 185–187.

Kim, D., and Weaver, R.F. (1993). Transcription Mapping and Functional Analysis of the Protein Tyrosine/Serine Phosphatase (PTPase) Gene of the Autographa californica Nuclear Polyhedrosis Virus. Virology *195*, 587–595.

Kim, S.A., Hudmon, A., Volmer, A., and Waxham, M.N. (2001). CaM-Kinase II Dephosphorylates Thr286 by a Reversal of the Autophosphorylation Reaction. Biochemical and Biophysical Research Communications *282*, 773–780.

Kim, Y., Li, Z., Apetri, M., Luo, B., Settleman, J.E., and Anderson, K.S. (2012). Temporal Resolution of Autophosphorylation for Normal and Oncogenic Forms of EGFR and Differential Effects of Gefitinib. Biochemistry *51*, 5212–5222.

King, N. (2004). The unicellular ancestry of animal development. Dev. Cell *7*, 313–325.

Kinoshita, E., and Kinoshita-Kikuta, E. (2011). Improved Phos-tag SDS-PAGE under neutral pH conditions for advanced protein phosphorylation profiling. Proteomics *11*, 319–323.

Kleiman, L.B., Maiwald, T., Conzelmann, H., Lauffenburger, D.A., and Sorger, P.K. (2011). Rapid phospho-turnover by receptor tyrosine kinases impacts downstream signaling and drug binding. Molecular Cell *43*, 723–737.

Klein, R., Jing, S.Q., Nanduri, V., O'Rourke, E., and Barbacid, M. (1991a). The trk proto-oncogene encodes a receptor for nerve growth factor. Cell *65*, 189–197.

Klein, R., Nanduri, V., Jing, S., Lamballe, F., Tapley, P., Bryant, S., Cordon-Cardo, C., Jones, K.R., Reichardt, L.F., and Barbacid, M. (1991b). The trkB tyrosine protein kinase is a receptor for brain-derived neurotrophic factor and neurotrophin-3. Cell *66*, 395–403.

Knighton, D.R., Zheng, J.H., Eyck, Ten, L.F., Ashford, V.A., Xuong, N.H., Taylor, S.S., and Sowadski, J.M. (1991a). Crystal structure of the catalytic subunit of cyclic adenosine monophosphate-dependent protein kinase. Science *253*, 407–414.

Knighton, D.R., Zheng, J.H., Eyck, Ten, L.F., Xuong, N.H., Taylor, S.S., and Sowadski, J.M. (1991b). Structure of a peptide inhibitor bound to the catalytic subunit of cyclic adenosine monophosphate-dependent protein kinase. Science *253*, 414–420.

Kogner, P., Barbany, G., Dominici, C., Castello, M.A., Raschellá, G., and Persson, H. (1993). Coexpression of messenger RNA for TRK protooncogene and low affinity nerve growth factor receptor in neuroblastoma with favorable prognosis. Cancer Research *53*, 2044–2050.

Kornev, A.P., and Taylor, S.S. (2010). Defining the conserved internal architecture of a protein kinase. Biochimica Et Biophysica Acta (BBA) - Proteins & Proteomics *1804*, 440–444.

Krebs, E.G., and Fischer, E.H. (1956). The phosphorylase b to a converting enzyme of rabbit skeletal muscle. Biochimica Et Biophysica Acta *20*, 150–157.

Krissinel, E., and Henrick, K. (2007). Inference of macromolecular assemblies from crystalline state. Journal of Molecular Biology *372*, 774–797.

Laemmli, U.K. (1970). Cleavage of structural proteins during the assembly of the head of bacteriophage T4. Nature *227*, 680–685.

Lagadec, C., Meignan, S., Adriaenssens, E., Foveau, B., Vanhecke, E., Romon, R., Toillon, R.A., Oxombre, B., Hondermarck, H., and Le Bourhis, X. (2009). TrkA overexpression enhances growth and metastasis of breast cancer cells. Oncogene *28*, 1960–1970.

Larsson, O., Girnita, A., and Girnita, L. (2006). Role of insulin-like growth factor 1 receptor signalling in cancer. British Journal of Cancer *96*, R2–R6.

Laskowski, R.A., MacArthur, M.W., Moss, D.S., and Thornton, J.M. (1993). PROCHECK: a program to check the stereochemical quality of protein structures. Journal of Applied Crystallography *26*, 283–291.

Latour, S., Chow, L.M., and Veillette, A. (1996). Differential intrinsic enzymatic activity of Syk and Zap-70 protein-tyrosine kinases. The Journal of Biological Chemistry *271*, 22782–22790.

Lee, C.C., Jia, Y., Li, N., Sun, X., Ng, K., Ambing, E., Gao, M.-Y., Hua, S., Chen, C., Kim, S., et al. (2010). Crystal structure of the ALK (anaplastic lymphoma kinase) catalytic domain. Biochem. J. *430*, 425–437.

Lee, T., Hoofnagle, A.N., Resing, K.A., and Ahn, N.G. (2005). Hydrogen exchange solvent protection by an ATP analogue reveals conformational changes in ERK2 upon activation. Journal of Molecular Biology *353*, 600–612.

Lemmon, M.A., Bu, Z., Ladbury, J.E., Zhou, M., Pinchasi, D., Lax, I., Engelman, D.M., and Schlessinger, J. (1997). Two EGF molecules contribute additively to stabilization of the EGFR dimer. The EMBO Journal *16*, 281–294.

Lemmon, M.A., and Schlessinger, J. (2010). Cell signaling by receptor tyrosine kinases. Cell *141*, 1117–1134.

Levi-Montalcini, R. (1952). Effects of mouse tumor transplantation on the nervous system. Ann. N. Y. Acad. Sci. *55*, 330–344.

Levi-Montalcini, R., and Cohen, S. (1960). Effects of the extract of the mouse submaxillary

salivary glands on the sympathetic system of mammals. Ann. N. Y. Acad. Sci. *85*, 324–341.

Lew, E.D., Bae, J.H., Rohmann, E., Wollnik, B., and Schlessinger, J. (2007). Structural basis for reduced FGFR2 activity in LADD syndrome: Implications for FGFR autoinhibition and activation. Proceedings of the National Academy of Sciences *104*, 19802–19807.

Lew, E.D., Furdui, C.M., Anderson, K.S., and Schlessinger, J. (2009). The Precise Sequence of FGF Receptor Autophosphorylation Is Kinetically Driven and Is Disrupted by Oncogenic Mutations. Sci. Signal. *2*, ra6–.

Locascio, L.E., and Donoghue, D.J. (2013). KIDs rule: regulatory phosphorylation of RTKs. Trends in Biochemical Sciences *38*, 75–84.

Loeb, D.M., Stephens, R.M., Copeland, T., Kaplan, D.R., and Greene, L.A. (1994). A Trk nerve growth factor (NGF) receptor point mutation affecting interaction with phospholipase C-gamma 1 abolishes NGF-promoted peripherin induction but not neurite outgrowth. Journal of Biological Chemistry *269*, 8901–8910.

Louis-Jeune, C., Andrade-Navarro, M.A., and Perez-Iratxeta, C. (2011). Prediction of protein secondary structure from circular dichroism using theoretically derived spectra. Proteins.

Lu, L., and Zhu, M. (2011). Metal-based inhibitors of protein tyrosine phosphatases. Anticancer Agents Med Chem *11*, 164–171.

Manning, G., Whyte, D.B., Martinez, R., Hunter, T., and Sudarsanam, S. (2002). The protein kinase complement of the human genome. Science *298*, 1912–1934.

Marchetti, A., Felicioni, L., Pelosi, G., Del Grammastro, M., Fumagalli, C., Sciarrotta, M., Malatesta, S., Chella, A., Barassi, F., Mucilli, F., et al. (2008). Frequent mutations in the neurotrophic tyrosine receptor kinase gene family in large cell neuroendocrine carcinoma of the lung. Hum. Mutat. *29*, 609–616.

Maris, J.M., Hogarty, M.D., Bagatell, R., and Cohn, S.L. (2007). Neuroblastoma. The Lancet *369*, 2106–2120.

Marshall, C.J. (1995). Specificity of receptor tyrosine kinase signaling: Transient versus sustained extracellular signal-regulated kinase activation. Cell *80*, 179–185.

Matsumoto, K., Wada, R.K., Yamashiro, J.M., Kaplan, D.R., and Thiele, C.J. (1995). Expression of Brain-derived Neurotrophic Factor and p145TrkB Affects Survival, Differentiation, and Invasiveness of Human Neuroblastoma Cells. Cancer Research *55*, 1798.

Mendelow, M., Prorok, M., Salerno, A., and Lawrence, D.S. (1993). ATPase-promoting dead end inhibitors of the cAMP-dependent protein kinase. The Journal of Biological Chemistry *268*, 12289–12296.

Middlemas, D.S., Meisenhelder, J., and Hunter, T. (1994). Identification of TrkB autophosphorylation sites and evidence that phospholipase C-gamma 1 is a substrate of the TrkB receptor. The Journal of Biological Chemistry *269*, 5458–5466.

Minichiello, L., Casagranda, F., Tatche, R.S., Stucky, C.L., Postigo, A., Lewin, G.R., Davies, A.M., and Klein, R. (1998). Point mutation in trkB causes loss of NT4-dependent neurons without major effects on diverse BDNF responses. Neuron *21*, 335–345.

Miranda, C., Zanotti, G., Pagliardini, S., Ponzetto, C., Pierotti, M.A., and Greco, A. (2002). Gain of function mutations of RTK conserved residues display differential effects on NTRK1 kinase activity. Oncogene *21*, 8334–8339.

Mohammadi, M., Schlessinger, J., and Hubbard, S.R. (1996). Structure of the FGF Receptor Tyrosine Kinase Domain Reveals a Novel Autoinhibitory Mechanism. Cell *86*, 577–587.

Morris, S.W., Kirstein, M.N., Valentine, M.B., Dittmer, K.G., Shapiro, D.N., Saltman, D.L., and Look, A.T. (1994). Fusion of a kinase gene, ALK, to a nucleolar protein gene, NPM, in non-Hodgkin's lymphoma. Science *263*, 1281–1284.

Munshi, S., Kornienko, M., Hall, D.L., Reid, J.C., Waxman, L., Stirdivant, S.M., Darke, P.L., and Kuo, L.C. (2002). Crystal structure of the Apo, unactivated insulin-like growth factor-1 receptor kinase. Implication for inhibitor specificity. The Journal of Biological Chemistry *277*, 38797–38802.

Murphy, L.O., and Blenis, J. (2006). MAPK signal specificity: the right place at the right time. Trends in Biochemical Sciences *31*, 268–275.

Murphy, L.O., MacKeigan, J.P., and Blenis, J. (2004). A Network of Immediate Early Gene Products Propagates Subtle Differences in Mitogen-Activated Protein Kinase Signal Amplitude and Duration. Mol. Cell. Biol. *24*, 144–153.

Nakagawara, A., Arima-Nakagawara, M., Azar, C.G., Scavarda, N.J., and Brodeur, G.M. (1994a). Clinical significance of expression of neurotrophic factors and their receptors in neuroblastoma. Progress in Clinical and Biological Research *385*, 155–161.

Nakagawara, A., Arima-Nakagawara, M., Scavarda, N.J., Azar, C.G., Cantor, A.B., and Brodeur, G.M. (1993). Association between high levels of expression of the TRK gene and favorable outcome in human neuroblastoma. The New England Journal of Medicine *328*, 847–854.

Nakagawara, A., Azar, C.G., Scavarda, N.J., and Brodeur, G.M. (1994b). Expression and function of TRK-B and BDNF in human neuroblastomas. Molecular and Cellular Biology *14*, 759–767.

Nolen, B., Taylor, S., and Ghosh, G. (2004). Regulation of protein kinases; controlling activity through activation segment conformation. Molecular Cell *15*, 661–675.

O'Brian, C.A., and Ward, N.E. (1991). Stimulation of the ATPase activity of rat brain protein kinase C by phospho acceptor substrates of the enzyme. Biochemistry *30*, 2549–2554.

Obermeier, A., Bradshaw, R.A., Seedorf, K., Choidas, A., Schlessinger, J., and Ullrich, A. (1994). Neuronal differentiation signals are controlled by nerve growth factor receptor/Trk binding sites for SHC and PLC gamma. The EMBO Journal *13*, 1585–1590.

Otwinowski, Z., and Minor, W. (1997). Processing of X-ray diffraction data collected in oscillation mode. Method Enzymol *276*, 307–326.

Parast, C.V., Mroczkowski, B., Pinko, C., Misialek, S., Khambatta, G., and Appelt, K. (1998). Characterization and kinetic mechanism of catalytic domain of human vascular endothelial growth factor receptor-2 tyrosine kinase (VEGFR2 TK), a key enzyme in angiogenesis. Biochemistry *37*, 16788–16801.

Paudel, H.K., and Carlson, G. (1991). The ATPase activity of phosphorylase kinase is regulated

in parallel with its protein kinase activity. The Journal of Biological Chemistry *266*, 16524–16529.

Paul S Mischel, J.A.U.S.E.S.G.S.C.B.G.G.A.Z. (2002). Nerve growth factor signals via preexisting TrkA receptor oligomers. Biophysical Journal *83*, 968.

Pike, L., Eakes, A., and Krebs, E. (1986). Characterization of affinity-purified insulin receptor/kinase. Effects of dithiothreitol on receptor/kinase function. The Journal of Biological Chemistry *261*, 3782.

Plaza-Menacho, I., Barnouin, K., Goodman, K., Martínez-Torres, R.J., Borg, A., Murray-Rust, J., Mouilleron, S., Knowles, P., and McDonald, N.Q. (2014). Oncogenic RET Kinase Domain Mutations Perturb the Autophosphorylation Trajectory by Enhancing Substrate Presentation In trans. Molecular Cell *53*, 738–751.

Postigo, A., Calella, A.M., Fritzsch, B., Knipper, M., Katz, D., Eilers, A., Schimmang, T., Lewin, G.R., Klein, R., and Minichiello, L. (2002). Distinct requirements for TrkB and TrkC signaling in target innervation by sensory neurons. Genes Dev. *16*, 633–645.

Rebagay, G., Yan, S., Liu, C., and Cheung, N.-K. (2012). ROR1 and ROR2 in Human Malignancies: Potentials for Targeted Therapy. Front Oncol *2*, 34.

Red Brewer, M., Choi, S.H., Alvarado, D., Moravcevic, K., Pozzi, A., Lemmon, M.A., and Carpenter, G. (2009). The Juxtamembrane Region of the EGF Receptor Functions as an Activation Domain. Molecular Cell *34*, 641–651.

Sadowski, I., Stone, J.C., and Pawson, T. (1986). A noncatalytic domain conserved among cytoplasmic protein-tyrosine kinases modifies the kinase function and transforming activity of Fujinami sarcoma virus P130gag-fps. Molecular and Cellular Biology *6*, 4396–4408.

Schlessinger, J. (2003). Signal transduction. Autoinhibition control. Science *300*, 750–752.

Segal, R.A., Bhattacharyya, A., Rua, L.A., Alberta, J.A., Stephens, R.M., Kaplan, D.R., and Stiles, C.D. (1996). Differential utilization of Trk autophosphorylation sites. The Journal of Biological Chemistry *271*, 20175–20181.

Sharma, S.V., Bell, D.W., Settleman, J., and Haber, D.A. (2007). Epidermal growth factor receptor mutations in lung cancer. Nat Rev Cancer *7*, 169–181.

Shen, J., and Maruyama, I.N. (2011). Nerve growth factor receptor TrkA exists as a preformed, yet inactive, dimer in living cells. FEBS Letters *585*, 295–299.

Shen, J., and Maruyama, I.N. (2012). Brain-derived neurotrophic factor receptor TrkB exists as a preformed dimer in living cells. J Mol Signal *7*, 2.

Sheng, Z., and Charbonneau, H. (1993). The baculovirus Autographa californica encodes a protein tyrosine phosphatase. The Journal of Biological Chemistry *268*, 4728–4733.

Shibayama, E., and Koizumi, H. (1996). Cellular localization of the Trk neurotrophin receptor family in human non-neuronal tissues. The American Journal of Pathology *148*, 1807–1818.

Sievers, F., Wilm, A., Dineen, D., Gibson, T.J., Karplus, K., Li, W., Lopez, R., McWilliam, H., Remmert, M., ding, J.S.O., et al. (2011). Fast, scalable generation of high-quality protein multiple sequence alignments using Clustal Omega. Mol Syst Biol *7*, 1–6.

Sopko, R., and Perrimon, N. (2013). Receptor tyrosine kinases in Drosophila development. Cold Spring Harb Perspect Biol *5*.

Soppet, D., Escandon, E., Maragos, J., Middlemas, D.S., Raid, S.W., Blair, J., Burton, L.E., Stanton, B.R., Kaplan, D.R., and Hunter, T. (1991). The neurotrophic factors brain-derived neurotrophic factor and neurotrophin-3 are ligands for the trk B tyrosine kinase receptor. Cell *65*, 895–903.

Sossin, W.S. (2006a). Tracing the evolution and function of the Trk superfamily of receptor tyrosine kinases. Brain Behav Evol *68*, 145–156.

Sossin, W.S. (2006b). Tracing the evolution and function of the Trk superfamily of receptor tyrosine kinases. Brain Behav Evol *68*, 145–156.

Sours, K.M., Xiao, Y., and Ahn, N.G. (2014). Extracellular-Regulated Kinase 2 Is Activated by the Enhancement of Hinge Flexibility. Journal of Molecular Biology.

Squinto, S.P., Stitt, T.N., Aldrich, T.H., Davis, S., Blanco, S.M., RadzieJewski, C., Glass, D.J., Masiakowski, P., Furth, M.E., and Valenzuela, D.M. (1991). trk B encodes a functional receptor for brain-derived neurotrophic factor and neurotrophin-3 but not nerve growth factor. Cell *65*, 885–893.

Stephens, P., Edkins, S., Davies, H., Greenman, C., Cox, C., Hunter, C., Bignell, G., Teague, J., Smith, R., Stevens, C., et al. (2005). A screen of the complete protein kinase gene family identifies diverse patterns of somatic mutations in human breast cancer. Nat. Genet. *37*, 590–592.

Stephens, R.M., Loeb, D.M., Copeland, T.D., Pawson, T., Greene, L.A., and Kaplan, D.R. (1994). Trk receptors use redundant signal transduction pathways involving SHC and PLC-[gamma]1 to mediate NGF responses. Neuron *12*, 691–705.

Suzuki, T., Bogenmann, E., Shimada, H., Stram, D., and Seeger, R.C. (1993). Lack of High-Affinity Nerve Growth Factor Receptors in Aggressive Neuroblastomas. J. Natl. Cancer Inst. *85*, 377–384.

Takagi, T., Taylor, G.S., Kusakabe, T., Charbonneau, H., and Buratowski, S. (1998). A protein tyrosine phosphatase-like protein from baculovirus has RNA 5'-triphosphatase and diphosphatase activities. Proceedings of the National Academy of Sciences of the United States of America *95*, 9808–9812.

Tanaka, K., Mohri, Y., Nishioka, J., Kobayashi, M., Ohi, M., Miki, C., Tonouchi, H., Nobori, T., and Kusunoki, M. (2009). Neurotrophic receptor, tropomyosin-related kinase B as an independent prognostic marker in gastric cancer patients. J. Surg. Oncol. *99*, 307–310.

Tartari, C.J., Gunby, R.H., Coluccia, A.M.L., Sottocornola, R., Cimbro, B., Scapozza, L., Donella-Deana, A., Pinna, L.A., and Gambacorti-Passerini, C. (2008). Characterization of some molecular mechanisms governing autoactivation of the catalytic domain of the anaplastic lymphoma kinase. The Journal of Biological Chemistry *283*, 3743–3750.

Thiel, K.W., and Carpenter, G. (2007). Epidermal growth factor receptor juxtamembrane region regulates allosteric tyrosine kinase activation. Proceedings of the National Academy of Sciences *104*, 19238–19243.

Till, J.H., Becerra, M., Watty, A., Lu, Y., Ma, Y., Neubert, T.A., Burden, S.J., and Hubbard, S.R. (2002). Crystal Structure of the MuSK Tyrosine Kinase: Insights into Receptor Autoregulation. Structure *10*, 1187–1196.

Tomasson, M.H., Xiang, Z., Walgren, R., Zhao, Y., Kasai, Y., Miner, T., Ries, R.E., Lubman, O., Fremont, D.H., McLellan, M.D., et al. (2008). Somatic mutations and germline sequence variants in the expressed tyrosine kinase genes of patients with de novo acute myeloid leukemia. Blood *111*, 4797–4808.

Traverse, S., Seedorf, K., Paterson, H., Marshall, C.J., Cohen, P., and Ullrich, A. (1994). EGF triggers neuronal differentiation of PC12 cells that overexpress the EGF receptor. Current Biology *4*, 694–701.

Ubersax, J.A., and Ferrell, J.E., Jr (2007). Mechanisms of specificity in protein phosphorylation. Nature Reviews *8*, 530–541.

Ullrich, A., and Schlessinger, J. (1990). Signal transduction by receptors with tyrosine kinase activity. Cell *61*, 203–212.

Ushiro, H., and Cohen, S. (1980). Identification of phosphotyrosine as a product of epidermal growth factor-activated protein kinase in A-431 cell membranes. The Journal of Biological Chemistry *255*, 8363–8365.

Wang, J., Steinbacher, S., Augustin, M., Schreiner, P., Epstein, D., Mulvihill, M.J., and Crew, A.P. (2010). The crystal structure of a constitutively active mutant RON kinase suggests an intramolecular autophosphorylation hypothesis. Biochemistry *49*, 7972–7974.

Wang, T., Lamb, M.L., Block, M.H., Davies, A.M., Han, Y., Hoffmann, E., Ioannidis, S., Josey, J.A., Liu, Z.-Y., and Lyne, P.D. (2012). Discovery of disubstituted imidazo [4, 5-b] pyridines and purines as potent TrkA inhibitors. ACS Med. Chem. Lett. *3*, 705–709.

Wang, W., Marimuthu, A., Tsai, J., Kumar, A., Krupka, H.I., Zhang, C., Powell, B., Suzuki, Y., Nguyen, H., and Tabrizizad, M. (2006). Structural characterization of autoinhibited c-Met kinase produced by coexpression in bacteria with phosphatase. Proceedings of the National Academy of Sciences of the United States of America *103*, 3563–3568.

Ward, N.E., and O'Brian, C.A. (1992). The intrinsic ATPase activity of protein kinase C is catalyzed at the active site of the enzyme. Biochemistry *31*, 5905–5911.

Wei, L., Hubbard, S.R., Hendrickson, W.A., and Ellis, L. (1995). Expression, characterization, and crystallization of the catalytic core of the human insulin receptor protein-tyrosine kinase domain. The Journal of Biological Chemistry *270*, 8122–8130.

Winn, M.D., Isupov, M.N., and Murshudov, G.N. (2001). Use of TLS parameters to model anisotropic displacements in macromolecular refinement. Acta Cryst (2001). D57, 122-133 [Doi:10.1107/S0907444900014736] 1–12.

Wybenga-Groot, L.E., Baskin, B., Ong, S.H., Tong, J., Pawson, T., and Sicheri, F. (2001). Structural basis for autoinhibition of the Ephb2 receptor tyrosine kinase by the unphosphorylated juxtamembrane region. Cell *106*, 745–757.

Xiao, Y., Lee, T., Latham, M.P., Warner, L.R., Tanimoto, A., Pardi, A., and Ahn, N.G. (2014). Phosphorylation releases constraints to domain motion in ERK2. Proceedings of the National

Academy of Sciences *111*, 2506–2511.

Yang, J., Eyck, Ten, L.F., Xuong, N.H., and Taylor, S.S. (2004). Crystal structure of a cAMP-dependent protein kinase mutant at 1.26A: new insights into the catalytic mechanism. Journal of Molecular Biology *336*, 473–487.

Yauch, R.L., and Settleman, J. (2012). Recent advances in pathway-targeted cancer drug therapies emerging from cancer genome analysis. Curr. Opin. Genet. Dev. *22*, 45–49.

York, R.D., Yao, H., Dillon, T., Ellig, C.L., Eckert, S.P., McCleskey, E.W., and Stork, P.J.S. (1998). Rap1 mediates sustained MAP kinase activation induced by nerve growth factor. Nature *392*, 622–626.

Zhang, X., Gureasko, J., Shen, K., Cole, P.A., and Kuriyan, J. (2006). An Allosteric Mechanism for Activation of the Kinase Domain of Epidermal Growth Factor Receptor. Cell *125*, 1137–1149.

Zhang, Z.Y., Clemens, J.C., Schubert, H.L., Stuckey, J.A., Fischer, M.W., Hume, D.M., Saper, M.A., and Dixon, J.E. (1992). Expression, purification, and physicochemical characterization of a recombinant Yersinia protein tyrosine phosphatase. The Journal of Biological Chemistry *267*, 23759–23766.

Zhang, Z.-Y. (2003). Chemical and Mechanistic Approaches to the Study of Protein Tyrosine Phosphatases. Acc. Chem. Res. *36*, 385–392.

Zhuo, S., Clemens, J.C., Hakes, D.J., Barford, D., and Dixon, J.E. (1993). Expression, purification, crystallization, and biochemical characterization of a recombinant protein phosphatase. The Journal of Biological Chemistry *268*, 17754–17761.